PFC/RR-92-10

AN EVALUATION OF THE FEASIBILITY OF LIQUID METAL DIVERTORS

Chungpin Liao and Mujid S. Kazimi

July, 1992

Plasma Fusion Center
Massachusetts Institute of Technology
Cambridge, MA 02139, USA

This work was supported by the U.S. Department of Energy under DOE Contract No. DE-FG02-91ER-54110.

ABSTRACT

The divertor technology has become the focus of concern for prospective steady state tokamak reactors such as the International Thermonuclear Experimental Reactor (ITER). Namely, the imposed heat flux and particle flux conditions cast doubt on the feasibility of any solid surface divertor. Thus, the old idea of liquid metals (mainly lithium and gallium) as the divertor surface protective materials has been revived, and different concepts of liquid metal divertors have been proposed. The aim of this work is to evaluate the feasibility of the existing concepts from both the physics and engineering points of view.

A model is developed for the edge plasma which includes the important interaction mechanisms, such as the backscattered energy flux from the divertor plate, the plasma momentum loss due to the charge exchange process, and the correct form of the energy transmission coefficients across the plasma sheath. This model is applicable to all types of divertors. Its results show that the edge plasma temperature will be more than 100 eV for a two-null steady state ITER-like tokamak with tungsten divertors, higher than was estimated by the previous engineering models. This outcome turned out to be in agreement with the recent simulation reported by the ITER team using the much more complicated Braams code. This implies that for the imposed heat load of 70 MW the physical sputtering erosion rate of a 20 m^2 tungsten plate is about 0.56 mm/day (without taking into account nonuniform redeposition). Similarly, the erosion rate for a beryllium plate is estimated to be 2 mm/day.

The hydrogen build-up in the liquid metal surface is addressed in order to determine the liquid metal divertor recycling coefficient needed for the edge plasma modeling. It is concluded that liquid lithium is a good hydrogen getter due to the precipitation of solid hydride LiH. For the condition of 70 MW per the 20 m^2 plate, this leads to an expected hydrogen recycling time of several tens of minutes. Hence, if the liquid lithium can be efficiently refreshed, the divertor may be expected to operate in a low recycling mode. However, since such efficient tritium extraction technology is probably unavailable (at the rate of about one mole of tritium per second), the tritium inventory becomes a concern as it reaches several kilograms in the divertor system. In addition, changes of lithium properties due to hydride precipitation may also occur. Thus, liquid lithium is not a favorable material for the liquid metal divertor. On the other hand, liquid gallium does not have a similar problem owing to its low hydrogen solubility and the decomposition of hydrides within the temperature window of interest. The evaluated short hydrogen recycling time of the order of milliseconds indicates that the liquid gallium divertor is suitable for high recycling operation.

Simulation results show that dense ($2 \cdot 10^{19}$ m^{-3}) and relatively cool (57 eV) edge plasma can be reached at the gallium divertor (with two divertors for each null point). Evaluation of existing liquid metal concepts against the

issues of evaporation, sputtering, blistering erosion, unipolar arc erosion, MHD instability, heat transfer, and major disruption concludes that the liquid gallium droplet curtain divertor appears to be the most feasible concept. The protective film divertor concept (of film thickness 5 mm) suffers mainly from the problem of MHD instability when the film speed is higher than about 10 m/s which is needed to avoid the blistering erosion, even though the heat transfer requirement is a much lower speed of the order of 1 m/s.

It is pointed out, however, that there is uncertainty about insufficiency in helium ash removal even with a large pumping panel area and perfect vacuum pumps. A new vacuum pumping scheme is thus proposed, which not only meets the vacuum pumping requirement with much smaller pumping panel area, but also offers the means to control the divertor recycling coefficient.

ACKNOWLEDGEMENTS

This report is based on the thesis submitted by the first author to the MIT Department of Nuclear Engineering in partial fulfillment of the requirements for the degree of Doctor of Philosophy in Nuclear Engineering.

Our gratitudes are directed to several people who have offered valuable advice and timely help: Dr. Bruce Montgomery, for his advice on the research goals and raising of the tritium inventory issue; Dr. Brian LaBombard, for his advice and numerous discussions on almost all aspects of this work; Prof. John Meyer, for his valuable advice about both the hydrogen getter issue of the liquid metals and the blistering erosion problem; Dr. Bruce Lipschultz, for his penetrating questions whenever the first author gave a talk; Prof. Samuel Cohen at Princeton Plasma Physics Laboratory, for his comments on the edge plasma modeling results and the supply of much useful information; Dr. Dai Kai Sze at Argonne National Laboratory, for offering basic information about liquid gallium; and Dr. Barton Lane previously at Plasma Fusion Center of MIT, for help in constructing the collision operators of the Boltzmann equations.

The authors are also grateful for the help provided by others, particularly Mathias Koch, officemate of the first author, for useful discussions; also Elizabeth Parmelee, Janet Anderson, and Clare Egan, for their generous administrative assistance.

Table of Contents

List of Figures

List of Tables

CHAPTER I. INTRODUCTION

I.A. Divertors for ITER-like Continuous Reactors

Impurity control is of crucial importance in fusion tokamak devices, particularly for continuous plasma operation reactors like the proposed International Thermonuclear Experimental Reactor (ITER) [Post et al, 1991] (see Table I.1 for the ITER engineering parameters). Without this function, not only would the main plasma first wall not survive the severe charged particle bombardment and heat load, but more essentially, the main plasma would quench in seconds due to fuel dilution and synchrotron or bremsstrahlung radiation losses. However, even though playing such an important role, impurity control remains an unresolved technology issue up to this day.

Table I.1

Engineering Design Parameters of ITER

Major radius	$6\ m$
Minor radius	$2.15\ m$
Plasma current	$22\ MA$
Axis B field	$5\ T$
Fusion power	$1000\ MW$
Alpha power	$200\ MW\ (\sim 4 \cdot 10^{20}\ He\ atoms/s)$

The impurity control system must remove the helium ash and other impurities at a rate that allows efficient plasma operation, and the system itself must not be a significant impurity source. The major engineering requirements

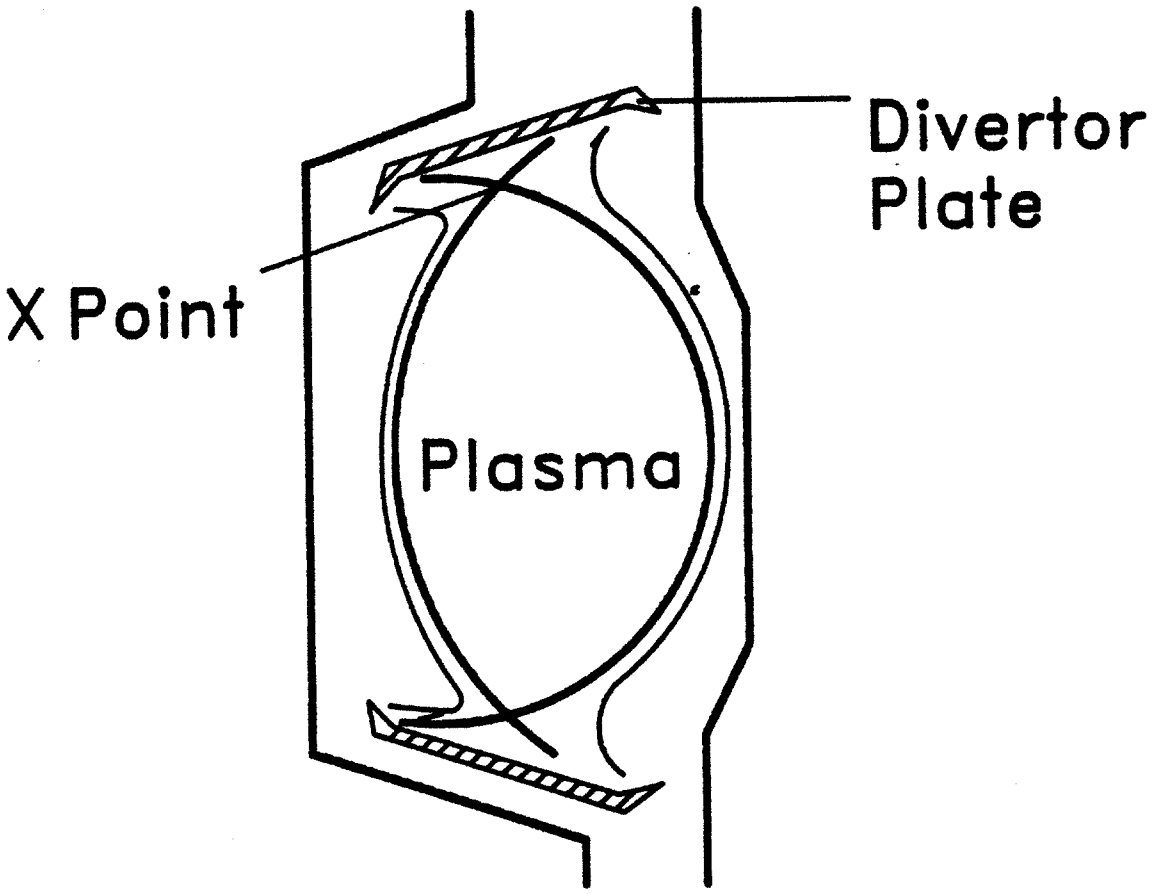

Figure I.1: Two-null operation of the ITER tokamak reactor

are that both the charged particle and the heat deposited on the impurity control surface must be effectively neutralized and removed, and that the lifetime of the system must be sufficiently long for high availability and economic operation. At present, it appears that the divertor has more potential than other devices to meet these requirements. In addition, a fusion reactor with divertors is said to be in an "H-mode" operation, which is found experimentally to have about twice the energy confinement time as of that of "L-mode" operation associated with a reactor using limiters as impurity control system. For a detailed comparison between the limiter and divertor concepts, see, Keilhacker et al, [1982 b].

The operation of a divertor is as follows. The plasma is diverted from the plasma edge by a coil that carries a current parallel to the plasma current. At a null point between the coil and the plasma center, the poloidal magnetic field is zero. The plasma outside this null point flows in the flux surface that encircles both the coil and main plasma and can thus be diverted away from the main plasma. The ITER design is proposed to have two null points [Post et al, 1991] (see, Figure I.1).

In the divertor chamber, the plasma flows along the field lines until it strikes the neutralizer plate. During flying, these charged particles approach the divertor plate at a very small grazing angle (less than 10°); however, when very close to the plate, they are oriented almost perpendicular to the plate by the plasma sheath action. The ions and electrons recombine on the plate, and are re-emitted (either immediately after impact or somewhat delayed) from the plate as neutral atoms or molecules. These neutral particles then travel either back down the divertor chamber and get ionized again or toward the vacuum pumping panels and are removed from the divertor system.

The newly proposed continuous plasma operation fusion reactor ITER [Post

et al, 1991] poses severe challenge to the feasibility of conventional stationery divertors. That is, in addition to the enormous divertor heat load (average at $4 \sim 6\ MW/m^2$, peaking at $15 \sim 20\ MW/m^2$) which leads to strict heat transfer requirements, there are two other features of the ITER edge plasma that make the applicability of any stationery divertor very difficult. Namely, the high edge plasma temperature (on the order of 100 eV) leads to serious surface sputtering problems. The large incident charged particle flux (on the order of $10^{23} m^{-2} s^{-1}$) may also result in embrittlement, bubble formation and blistering erosion of the stationery divertor plates.

It is thus believed that without the resolution of the divertor problem, the proposed ITER power reactor could not be built.

I.B. Motivation for Liquid Metal Divertors

I.B.a. Difficulties of solid metal divertors

Solid surface divertors (i.e., divertors with solid neutralizer plates) have long been proposed and experimented with (on pulse-type fusion experimental devices) to some extent for impurity control of tokamaks. Nevertheless, the conventional solid surface divertor, by its nature, faces two conflicting engineering design requirements. Namely, the plate needs to be thin to facilitate heat transfer; while on the other hand, it should be thick enough to withstand sputtering erosion. Usually, a compromise needs to be made depending on the pusle length, duty cycle of the plasma operation, and the planned lifetime of the specific test fusion device.

However, it will be demonstrated later in Chapter II that this is not the case for solid divertors associated with a steady state power reactor. Namely, with

whatever compromise in the divertor plate thickness, the feasibility of any solid surface divertors is very questionable. In other words, the erosion rate of the solid divertor plate based merely on the physical sputtering process by incident deuterons and tritons is already unacceptably high, even for the known most sustaining (but also high Z) solid material– tungsten. This is without taking into account the peak-to-average factor $3.4 \sim 5.2$ of the divertor heat load [Post et al, 1991] owing to possible asymmetry in heat exhaust between the two null points and great uncertainty in the plasma scrape-off layer thickness. Besides, there are other physical processes that can severely aggravate the situation, such as self-sputtering, embrittlement exfoliation, and blistering erosion due to the eruptions of hydrogen bubbles within the divertor plate during charged particle bombardment.

I.B.b. Self-cooling and self-annealing of liquid metals

Flowing liquid metals (particularly, lithium (Li) and gallium (Ga)) are considered possible candidates for the divertor plate materials due to their self-cooling and self-annealing properties. That is, unlike solid divertor plate materials, there is no design conflict between the heat transfer and the erosion protection. Liquid metals have fairly high heat capacity, and the flowing liquid metal flow itself is expected to carry away the divertor heat load more efficiently than the water coolant flowing within the solid surface divertors under the same ITER-like conditions. While passing through the divertor position, the liquid metal serves as divertor plate, which may be capable of recovering itself from the bombardment by the charged particles.

The physical properties of Li and Ga under conditions of interest are given in Table I.2,

Table I.2

Li and Ga Physical Properties

	lithium (Li)	gallium (Ga)
Atomic number Z	3	31
Mass number A	7	70
Melting temperature $T_m(^\circ C)$	186	29
Heat capacity c_p (J/kgK)	4190	380
Electrical conductivity σ $(1/\Omega - m)$	$2.8 \cdot 10^6$	$2.6 \cdot 10^6$
Mass density ρ (kg/m^3)	500	5720
Kinematic viscosity ν (m^2/s)	$8. \cdot 10^{-7}$	$3. \cdot 10^{-7}$
Surface tension σ_s (N/m)	0.365	0.700

I.B.c. Control of divertor recycling coefficient R

The divertor recycling coefficient R is defined as the probability for an average bombarding charged particle to be recycled back into the divertor plasma. From an engineering point of view, $R = 1 - \overline{p}f$, where $\overline{p}$ is the average probability for a re-emitted neutral particle from the neutralizer plate to escape into the divertor plenum without being ionized by the divertor plate-overlaying plasma and then being recycled; f is the average probability that a neutral particle which escaped into the divertor plenum will be pumped out of the divertor system.

The operation of solid surface divertors under ITER steady state conditions would always be in the high recycling regime (i.e., $R \geq 0.99$). This is because the edge plasma temperature is very high (on the order of 100 eV, to be discussed in Chapter II) such that the probability $\overline{p}$ for the average recycled neutral particle to escape from the divertor plate-overlaying plasma is very low.

Thus, even with efficient vacuum pumping (e.g., f=100 %), R is still very close to unity. In fact, this is in favor of the lifetime of the solid divertor plate, since the recycled neutral particles consume plasma energy in the ionization and charge-exchange processes, which leads to lower edge plasma temperature, and consequently, lower plate erosion rate. However, as mentioned in the previous Section, even with high recycling operation, the physical sputtering erosion rate of a conventional solid divertor plate is still unacceptably high. This will be demonstrated later in Chapter II.

Nevertheless, high recycling divertor operation tends to stagnate the charged particle influx at the divertor throat (near the null point). That is, the heat exhaust is conveyed to the divertor plate predominantly through thermal conduction, rather than through thermal convection. This results in an undesirable dirty main plasma (i.e., high impurity fraction) which is likely to be thermally unstable. In the worse case, when there is anomalous heat load, the edge plasma temperature is further increased and thus the ionization mean free paths of helium ash and impurities are shortened. Consequently, the insufficiency in the helium removal rate would very possibly cause the main plasma to disrupt and eventually to quench.

Compared with the seemingly unfitting solid surface divertors, there are some positive expectations for the liquid metal divertors. First, if the liquid metal divertor is operated with similarly high recycling, the corresponding edge plasma temperature might be lower than that associated with the solid metal (especially with tungsten) divertors. This is based on the fact that the selected liquid metals are not as massive as tungsten (in terms of the atomic number), such that not as much heat flux is reflected back into the divertor plasma.

Second, fresh liquid metals can often act as hydrogen getters (or, ion burial

materials). Adsorption of the gas exhaust by fresh liquid metal divertors may facilitate the low recycling operation. In fact, there is experimental evidence on TFTR tokamak (with proper arrangement of the neutral beam injection scheme) that pre-discharge cleaning (i.e., outgas conditioning) the bumper limiter can make the main plasma clean for some period of time during which the plasma energy confinement time is greatly enhanced (about two times that without the limiter conditioning) [see, e.g., Dylla et al, 1987]. This plasma operational parameter domain was later termed the "supershot regime". It is hoped that low recycling plasma operation at divertor position may also lead to this desired result for the steady state power reactor.

I.B.d. Availability of liquid metal vapor protection

Since liquid metals can evaporate at low temperature, there is speculation that the vapor cloud in front of a liquid metal plate may serve as another protection layer of the divertor system. In addition, this accumulated vapor cloud may enhance density and temperature gradients near the divertor plate, which may possibly reduce sputtering rate and block the flight of liquid metal plate atoms into the main plasma [see, e.g., Dolan, 1982].

I.C. Introduction to Reference Liquid Metal Divertor Concepts

There are several existing liquid metal divertor concepts (see Table I.3). Among them, the protective film and the droplet shower are more mature and have been modeled and tested to some extent mainly in the Soviet Union [see, e.g., Reed, 1989; Mazul, 1986].

It is also worth mentioning that US scientists seem to prefer lithium as the

working fluid, while Russian scientists appear to prefer gallium.

Table I.3

Reference Liquid Metal Divertor Concepts

Concept	Liquid Metal	Figure	Reference
injected protective film	Li or Ga	Figure III.1	[Mazul, 1986]
flowing protective film	Li or Ga	Figure III.2	[Morley et al, 1991]
stationery pool	Li or Ga	Figure III.3	[IAEA, 1986]
droplet beam	Li	Figure III.4	[Werley, 1989]
droplet curtain	Ga	Figure III.5	[Murav'ev, 1989]

I.D. Concerns of Liquid Metal Divertors

The feasibility of applying liquid metals as an alternative to the solid divertor plate materials should be examined based on the following issues:

a. evaporation depletion and contamination

b. sputtering erosion and contamination

c. blistering erosion and contamination

d. heat transfer and pumping requirement

e. MHD equilibrium

f. MHD stability

g. tritium inventory and permeation

h. helium ash removal

i. liquid metal renewal

j. material compatibility

k. effects of major disruptions

It is speculated that since liquid metals evaporate, in the near vacuum (in terms of neutral gas) divertor environment the liquid metal vapor pressure may be too large to be confined within the divertor region. That is, even though the ionization mean free path of these evaporated atoms is fairly short compared with the divertor size, the developed gradient in neutral liquid metal vapor pressure near the divertor plate eventually will cause transport of these atoms into the main plasma chamber and subsequent contamination of the main plasma.

Physical sputtering of the divertor plate by deuterons and tritons may lead to similar but more serious problems. Namely, since the sputtered atoms generally have considerable energy (unlike the evaporated atoms which possess only energy corresponding to the divertor plate temperature), if the sputtered flux is high enough, the resultant vapor pressure is expected to be larger than that caused by evaporation.

Under the expected fairly high flux of charged particles ($\sim 10^{23}\ atoms/m^2$) at ITER conditions, if the liquid metal has low hydrgen (i.e., deuterium or tritium) solubility then it is quite likely that most implanted hydrogen will accumulate to form bubbles within the liquid metal divertor plate, just like the case with solid metal plates. Then, each bubble would keep growing until it floats and bursts. This may cause serious erosion of the liquid metal plate, in addition, the erupted liquid metal droplets will pollute the divertor chamber.

The large heat capacity of liquid metals is in favor of the divertor heat transfer. However, this benefit can be justified only after the liquid metal operational temperature range is found to be wide and the liquid metal pumping power requirement can be met without difficulty.

For the liquid metal protective film divertor concept, there is suspicion

that the desired film thickness and flow speed (to meet, for example, the heat transfer requirement) may not be available due to the MHD effects. Namely, the corresponding MHD equilibrium condition may not exist. Even if such equilibrium does exist, there are still questions about how the flow thickness evolves and whether there will be dry spots and flooding regions (i.e., fast growth in film thickness which causes stagnation of the film flow) if the initial film thickness is not chosen properly.

Whether the equilibrium film flow can be fulfilled further depends on the film MHD stability with respect to any external perturbations. The MHD stability for a pumped liquid metal free surface flow with constant flow rate under actions of coplanar toroidal field, sheath negative pressure and particle bombarding pressure, has never been investigated. There is speculation that the effect of sheath pulling action on the negatively charged liquid metal plate may result in the Rayleigh-Taylor type instabilities [see, INTOR Concept Innovation, 1986] and thus may cause the rip-off of liquid metal film from the guiding plate. However, there is also suspicion that the bombarding particle pressure may dominate the above sheath pulling action, so that Rayleigh-Taylor type instability does not occur [LaBombard, private communication, 1991]. Thus, analytic effort is required to investigate the film MHD behavior under divertor plasma environment.

As mentioned earlier that liquid metals are often conceived as ion burial materials. If this is also true under the steady state ITER conditions (to be investigated in Chapter IV), then the tritium inventory becomes a safety concern, unless efficient tritium extraction technology is available to keep the tritium inventory low within the liquid metals. In this respect, the maximum allowed tritium inventory on ITER reactor site is set to be about 2 kg [Cohen,

private communication, 1991].

It is likely that the ITER divertor edge plasma temperture may be higher than expected even with liquid metal divertors, since there are uncertainties in the evaluation of the recycling coefficient R, in the symmetry of partitioning of heat load between the two null points, in the scrape-off layer thickness, etc. [Post et al, 1991]. Therefore, the resultant divertor recycling coefficient R may be very high, essentially unity. In other words, almost all re-emitted neutrals are ionized immediately by the plate-overlaying plasma and recycled repeatedly close to the divertor plate, such that only very few helium particles can escape to the divertor plenum in order to be pumped out of the tokamak. This insufficient helium removal rate can cause poisonous effects on the main plasma and can eventually quench the plasma.

I.E. Approach and Outline of This Work

This work can roughly be divided into two parts, the model construction for the plasma-liquid metal interactions, and the engineering evaluations of the liquid metal divertor concept. The edge plasma modeling is very important since it serves to give a correct basis for the engineering evaluations. In fact, it is believed that the reason the seriousness of the ITER divertor problem had not attracted wide early attention can be attributed largely to the inadequacy in the existing edge plasma models. Namely, they are either unrealistically optimistic or too cumbersome to use (e.g., the complete Braams & DEGAR code takes about 30 days (including human handshaking time) to obtain a steady state result [Cohen, private communication, 1991]).

Unfortunately, some detailed work on the ITER divertor plate design was based on the existing over-optimistic result of edge plasma temperature (i.e., 40

eV rather than around 100 eV) [see, e.g., Brooks, 1990], which made the particle impact energy even below the tungsten sputtering threshold energy, such that the lifetime of the tungsten can be as long as seven years or so [Brooks, 1990]. Therefore, constructing a simple, but reasonably accurate edge plasma model for the engineering evaluations is an essential step in addressing the divertor feasibility question.

The approach and outline of the performed analyses of this work are as follows. In Chapter II, the theoretical construction of the edge plasma model will be carried out in details, and the status of the feasibility of solid surface divertors will be examined. In Chapter III, existing liquid metal divertor concepts will be illustrated in more details, particularly the droplet shower divertor concept [Murav'ev, 1989]. Then, since the edge plasma simulation is the cornerstone for the engineering evaluation of the liquid metal divertors, issues related to the input data for the liquid metal divertor plasma modeling will be addressed first in Chapter IV, such as the hydrogen getter issue (or, recycling coefficients) of liquid metals.

The engineering issues presented in Section I.D are investigated in details from Chapter IV to Chapter VIII. During the process of these analyses, the feasibility of reference divertor concepts will be examined according to the different engineering requirements. During this procedure, if a certain liquid metal divertor concept cannot meet one of the requirements, then the candidacy of that particular concept is suggested to be excluded at that point.

In Chapter VII, the problem of insufficient helium ash removal will be addressed. Finally, summary and conclusions will be presented in Chapter IX.

CHAPTER II. A MODEL FOR THE EDGE PLASMA

II.A. Introduction

There exists a number of fluid models for estimating the divertor edge plasma conditions. Ranging from crude 1-D models to fairly complicated multi-dimensional models, they serve primarily as tools for the evaluation of the divertor performance covering issues such as impurity control, helium exhaust, and heat removal in fusion tokamaks. In particular, the total heat flux transmitted to the divertor plate is a key element in these models. However, it is recognized that the estimates from these models are greatly dependent on the boundary conditions assumed.

Three shortcomings in these models can be pointed out. First, the energy flux associated with backscattered fast D-T neutral atoms has been either neglected or confused with the amount of power transmitted across the sheath. As will be shown in this work, this reflected energy flux is not negligible, but on the contrary, can dominate other major energy loss mechanisms such as ionization, radiation, and charge exchange processes, particularly in the case when the divertor neutralizer is made of a high Z material.

Second, the divertor plasma momentum loss caused by charge exchange events occurring between the recycled neutrals and the incident D-T charged particles has often been ignored. This effect is not negligible and tends to make the plasma density near the divertor plate lower than would be predicted without charge exchange.

Third, except in some works, for example, Harrison INTOR benchmark [Harrison, 1983], the values of the so-called electron and ion energy transmission

coefficients across the sheath, δ_e and δ_i, are often crudely assumed, rather than estimated from a self-consistent physics model.

In order to examine the impact of backscattered D-T atoms and subsequent charge exchange on the estimates of steady state divertor plasma conditions, a simple 1-D single fluid "two-point" model that includes these effects is developed. This model is analytically concise and yet accurate enough for engineering evaluation purposes, and applicable to any type of solid or liquid metal divertors.

Section II.B outlines the derivation of the 1-D, one fluid hydrodynamic equations from velocity moments of electron and ion Boltzmann equations. Ion-neutral and electron-neutral collisions are handled by a constructed collision model. Momentum and energy source terms arising from neutral collisions appropriately emerge in the single fluid description. Then the "two point" integration is employed to arrive at the divertor plasma model equations.

In Section II.C, standard formulas for the electron and ion transmission coefficients δ_e and δ_i are first given. Then, a distinction is made between the usual definition of $(\delta_e + \delta_i)$ and the effective energy transmission coefficient, δ, which includes backscattering neutral effects.

The divertor plasma conditions of both INTOR and ITER operating with tungsten and beryllium divertors are presented and discussed in Section II.D. Tungsten and beryllium divertors are chosen to represent the most sustaining materials among those of solid surface divertors. The prospect for achieving dense, cool plasmas (say, $n_e > 10^{20}\ m^{-3}$, $k_B T_e < 50\ eV$) near these neutralizer plates is shown to be dim, even for high recycling divertors. This latter result emphasizes the importance of including backscattering effects in divertor plasma models, which have mostly been ignored in existing models.

The edge plasma simulations for liquid metal divertors, however, will be

presented in Chapter V, i.e., after the modeling of the recycling coefficient R at liquid metal surfaces in Chapter IV. Finally, Section II.E summarizes the major points of this chapter.

II.B. Divertor Plasma Model and Particle, Momentum, Energy Source Terms

II.B.a. Boltzmann equations

The behavior of the electrons and D-T ions in the divertor plasma can be described by the evolution of their respective phase space distribution functions, f_e and f_i, according to the Boltzmann equations,

$$\begin{aligned}\frac{Df_e}{Dt} =& C_{ei} + C_{ee} \\ &+ n_0\, n_e < \sigma v >_{ion} \delta(\vec{v}) \\ &- n_0\, n_e < \sigma v >_{ion} [f_e(\vec{v}) - h(\vec{v})]\end{aligned} \tag{II.1}$$

$$\begin{aligned}\frac{Df_i}{Dt} =& C_{ie} + C_{ii} \\ &+ R_N\, n_0\, n_e < \sigma v >_{ion}\ g(\vec{v}) \\ &+ (1 - R_N)\, n_0\, n_e < \sigma v >_{ion}\ \delta(\vec{v} - \vec{v}_s) \\ &+ (1 - R_N)\, n_0\, n_i < \sigma v >_{cxs}\ [\delta(\vec{v}) - f_i(\vec{v})] \\ &+ R_N\, n_0\, n_i < \sigma v >_{cxf}\ [G(\vec{v}) - f_i(\vec{v})]\end{aligned} \tag{II.2}$$

in which $\frac{D}{Dt} \equiv \frac{\partial}{\partial t} + \vec{v} \cdot \nabla + \frac{e(\vec{E}+\vec{v}\times\vec{B})}{m} \cdot \frac{\partial}{\partial \vec{v}}$, and C_{ei}, C_{ee}, C_{ie} and C_{ii} are the elastic two-body collision operators, whose exact representations are not of concern here. Other terms on the right hand sides are sources and sinks, due to the interactions of electrons or ions with neutral particles, i.e., C_{e0}

and C_{i0}, respectively. R_N is the fast neutral D-T particle reflection coefficient from the divertor plate, and n_0 is the recycled neutral D-T particle density in the divertor plasma. The local density of fast neutrals is approximated as $R_N\ n_0$, while $(1-R_N)\ n_0$ approximates the local density of slow neutrals. (This approximation will be justified later when we integrate along the magnetic field to obtain a "two point" model.) The plasma density near the divertor plate is given by $n_e\ (= n_i)$, and $< \sigma v >_{ion}$ is the rate coefficient for the electron impact ionization. While $< \sigma v >_{cxf}$ and $< \sigma v >_{cxs}$ are the rate coefficients for hydrogen ions to have charge exchange with fast and slow neutrals, respectively.

When the neutralizer plate is saturated with the bombarding particles, a steady state is achieved and the incident particle flux reaching the divertor plate is balanced by the returning flux. Among the incident D-T charged particles, the fraction R_N is reflected immediately from the neutralizer plate as neutral hydrogen atoms, carrying a considerable fraction of the incident energy, with a certain velocity distribution $g(\vec{v})$, normalized to satisfy $\int g(\vec{v})d\vec{v} = 1$. Most of these fast neutrals reflect back into the divertor plasma and are subject to electron impact ionization and charge exchange with incident charged D-T particles.

The fraction $(1 - R_N)$ of the incident hydrogen charged particles is initially neutralized and implanted in the divertor plate surface, but after diffusion eventually recombines and leaves the plate surface as molecules. Like fast recycled neutrals, it is assumed that only a very small proportion (about 8% to 10%) of them escape from being ionized by the plasma overlaying the neutralizer plate and reach the pump plenum. Even after a first escape, most of these neutrals bounce back onto the divertor plasma and are ionized or charge exchanged. Only about 1% to 10% of the neutral flux that escapes

to the divertor plenum is pumped away. For simplicity, it is assumed that the majority of the slow molecules entering the plasma undergo a dissociation process ($H_2 \longrightarrow H + H$) immediately upon entering the plasma, and then go through the same processes as the fast neutral component.

A more detailed description of the physical contents of equations (II.1) and (II.2) can now be given. The first neutral source term in equation (II.1) accounts for the birth of electrons due to the ionization of all recycled neutral atoms (It is assumed that ionization of impurities does not contribute significantly to the electron population). These newly born electrons are expected to have much less energy than the ionizing electrons and hence are assumed to have zero velocity. The second term represents the shape change of the electron distribution function in velocity space due to all inelastic collisions with neutrals. Such collisions result in hydrogen atomic ionization and excitation, as well as molecular dissociation and dissociative excitation. The function $h(\vec{v})$ pedagogically represents the velocity distribution function for electrons after collision, and $h(\vec{v})$ has the property, $\int h(\vec{v})d\vec{v} = 1$. Thus, when integrating over velocity space, this term yields no net change in the density of electrons. Similarly, in equation (II.2), $G(\vec{v}) - f_i(\vec{v})$ represents the change of the ion velocity distribution function due to the fast charge exchange. Here again, $\int G(\vec{v})d\vec{v} = \int f_i(\vec{v})d\vec{v} = 1$.

The distinction between ionization source terms from fast and slow D-T neutrals in equation (II.2) is necessary, owing to the action of sheath acceleration. A recycled fast neutral carries energy comparable to that of an incident plasma ion, while a slow neutral carries only the relatively small Franck-Condon energy ($\frac{1}{2}mv_s^2 \approx 3 \sim 5$ eV).

In describing the change of the ion velocity distribution associated with

the charge-exchange process, some simplifying approximations have been made. Namely, even though the collisions resulting in charge exchange lead to no net change in the number of ions, if the new ion has negligible amount of energy (i.e., the Franck-Condon energy from the original slow neutral), the plasma loses the energy associated with the original ion. The plasma is assumed to lose no energy when an incident ion has charge exchange with a fast neutral. However, this is not the case for momentum, since an incident ion loses its parallel momentum (i.e., the momentum in the one-directional direction of interest here) whenever it has charge exchange with either a fast or slow neutral. This is because, on the average, fast neutrals emanate nearly perpendicular to the magnetic field [Harrison, 1983], and the direction of slow neutrals is immaterial in the momentum balance equation.

It is assumed that there is no net energy change in the bulk divertor plasma due to the dissociation process, since the required dissociative excitation energy ($\sim$ 8.9 eV, accounted for in the electron equation) roughly balances the Franck-Condon energy carried by the two dissociated hydrogen atoms.

II.B.b. Steady state, 1-D, hydrodynamic equations

A one dimensional model of the divertor [Galambos and Peng, 1984] is constructed by straightening the magnetic field lines from the null point (x_t) to the sheath edge near the neutralizer plate (x_p) (see Figure II.1). Note that the 2-D effects on the particle recycling have been taken into account in this model, as is obvious from the previous Boltzmann formulations. The steady state, 1-D, one fluid hydrodynamic equations describing the divertor plasma system can be obtained by taking velocity moments of equations (II.1) and (II.2), and then combining the electron and ion contributions:

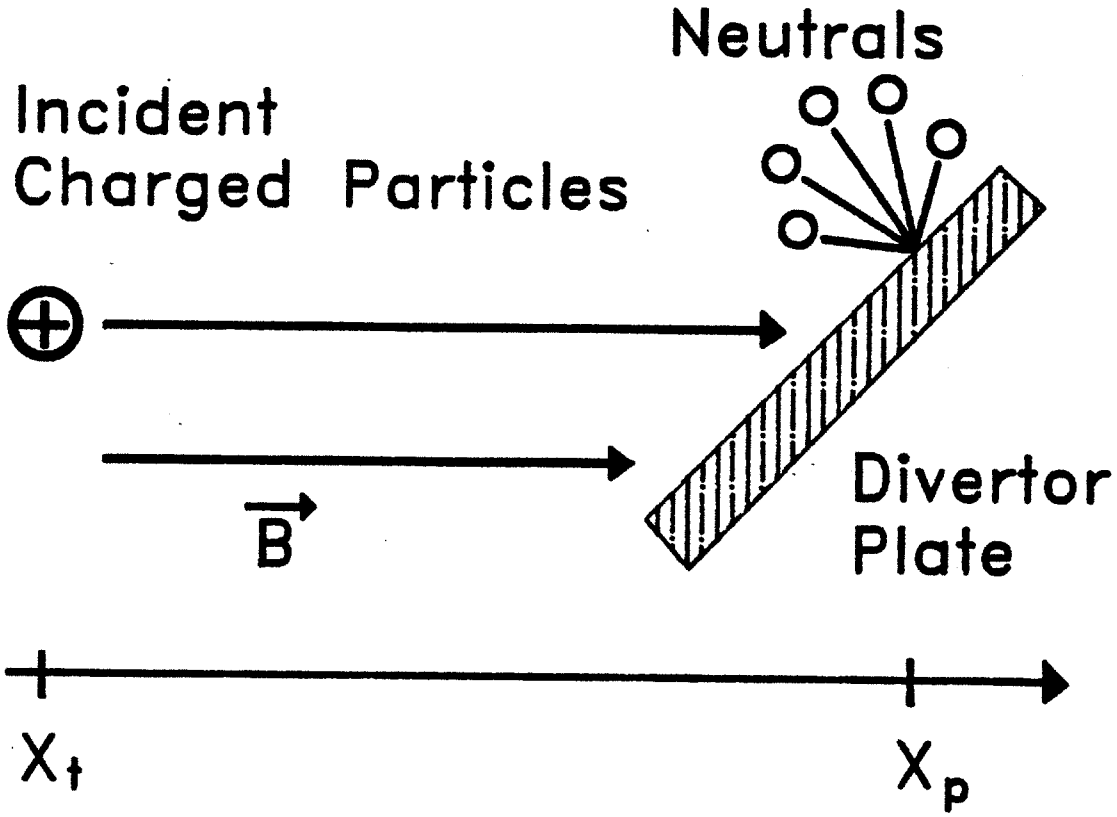

Figure II.1: The unwound one dimensional divertor geometry

continuity equation

$$\frac{d}{dx}(nv) = n_0\, n < \sigma v >_{ion} \equiv S_n \tag{II.3}$$

momentum equation

$$\begin{aligned}\frac{d}{dx}[mnv^2 + nT(1+r)] = &-(1-R_N)\, S_n\, f_{cxs} m\, v_p \\ &- R_N\, S_n\, f_{cxf} m\, v_p\end{aligned} \tag{II.4}$$

energy equation

$$\begin{aligned}\frac{d}{dx}[-\chi_0 T^{\frac{5}{2}} \frac{d}{dx} T + nv(\frac{5}{2}T(1+r) + \frac{1}{2}mv^2)] \\ = R_N\, n_0\, n < \sigma v >_{ion} \epsilon + S_e \\ = R_N\, S_n\, \epsilon + S_e \\ = S_E\end{aligned} \tag{II.5}$$

where n is the electron (ion) density, m is the mass of the average plasma ion, T is the electron temperature, and r is the ratio of ion temperature to electron temperature. In the energy equation, $\epsilon = \int dv\; g(v)\frac{1}{2}mv^2$ is the average energy carried into the plasma by each backscattered neutral, whose value is estimated in Subsection II.C.b. S_e accounts for the plasma power loss due to ionization, charge exchange, radiation processes, whose representation is given in Subsection II.B.d. The first term on the left hand side of the energy equation acounts for the electron thermal conduction, with χ_o the Spitzer conductivity coefficient. The second term acounts for convected energy.

During the derivation, several approximations have been made. First, the electron momentum contribution was neglected due to its light mass compared with that of the average ion. Second, for 1-D modeling, the parallel plasma momentum source from fast recycled neutrals (in the ion equation) was ignored due to the fact that backscattered neutrals tend to emanate in

a cosine angular distribution with respect to the divertor plate surface. The molecular dissociative process was also asssumed not to contribute to the parallel momentum since it is characterized by an isotropic distribution.

The dominant plasma momentum sink is due to charge-exchange occurring between the recycled neutrals and the incident D-T ions, leading to the definitions: $f_{cxs} \equiv \frac{<\sigma v>_{cxs}}{<\sigma v>_{ion}}$ and $f_{cxf} \equiv \frac{<\sigma v>_{cxf}}{<\sigma v>_{ion}}$. In equation (II.4), the approximation is made that charge exchange takes place predominantly near the divertor plate, i.e., $\bar{v} \approx v_p$. To close the equations, the boundary condition at the plasma-sheath interface is required:

$$Q_t + \int_t^p S_E dx = n_p v_p T_p \left(\delta_e + \delta_i\right) \qquad (II.6)$$

where Q_t is the prescribed input energy flux entering the divertor throat (in W/m^2) (parallel to the magnetic field); $\delta_{e,i}$ is the energy transmission coefficients for electrons or ions (defined as the ratio of the plasma heat flux transmitted across the sheath to kT times particle flux at x_p), n_p and n_t are the plasma densities near the divertor plate ($x = x_p$), and at the throat ($x = x_t$), respectively; T_p is the plasma electron temperature near the divertor plate; v_p is plasma fluid speed near the divertor plate, which is taken to be the ion acoustic speed due to Bohm sheath criterion [see, for example, Stangeby, 1984]; and r_p is ion-to-electron temperature ratio near the plate.

These equations are very similar in form to those derived by Galambos and Peng [1984], except they include a momentum sink (from charge exchange) rather than a momentum source (from ionization of backscattered neutrals), and they include an energy source term from charge exchange events. In addition, the assignment of the values for δ_e and δ_i will be different, as will be shown in

Subsection II.C.b. The hydrodynamic treatment is justified for plasma densities and temperatures of interest, since the typical mean free paths of all processes are short compared with the characteristic dimension of the divertor plasma.

II.B.c. Recycling coefficient and model formulas

The recycling coefficient, R, is defined as the ratio of the neutral D-T atom flux recycled back into the divertor plasma to the D-T ion flux impinging on the neutralizer plate under steady state conditions. Thus, defined from an engineering point of view, $R = 1 - \overline{p}f$, where $\overline{p}$ is the average ionization escape probability for neutrals passing through the plate-overlaying plasma, and f is the probability for the escaping neutrals to be subsequently pumped away. Since $\overline{p}$ is usually small (less than 10 %) resulting from the short ionization mean free path in fusion reactor divertors, the resultant R is always close to unity (i.e., high recycling), even though f can be made large.

Since at steady state the flux of particles into the divertor throat (parallel to the magnetic field), Γ_t, must be equal to the flux of non-recycled particles into the divertor plate, $(1 - R)\Gamma_p$, an alternate definition for R is,

$$R = \frac{(\Gamma_p - \Gamma_t)}{\Gamma_p} \qquad (II.7)$$

where Γ_p is the net D-T ion particle flux at the divertor plate.

The spatially conservative form of the hydrodynamic equations (II.3), (II.4), and (II.5) facilitates the use of the so-called "two point method". That is, to integrate the equations along the field line and evaluate the physical quantities only at two points x_t and x_p. Integrating (II.3) to (II.5) over the straightened field line and combining with the boundary condition (II.6), the following edge

plasma model emerges:

$$n_p = \left[\left(\frac{n_p}{n_T}\right)^{\frac{7}{3}} + 1\right]^{\frac{2}{7}} \left[\frac{n_t(1+r_t)(1+M_t^2)}{[2+(1-R_N)f_{cxs}R + R_N f_{cxf}R](1+r_p)}\right] \qquad (II.8)$$

$$T_p = \left[\left(Q_t + \int_t^p S_E dx\right)\left(\frac{m^{\frac{1}{2}}}{n_p(1+r_p)^{\frac{1}{2}}(\delta_e+\delta_i)}\right)\right]^{\frac{2}{3}} \qquad (II.9)$$

$$T_t = \frac{[2+(1-R_N)f_{cxs}R + R_N f_{cxf}R](1+r_p)\, T_p\, n_p}{(1+M_t^2)\,(1+r_t)\, n_t} \qquad (II.10)$$

with

$$n_T = \left(\frac{2\chi_0}{7Lu}\right)^{\frac{3}{7}} \cdot \frac{Q_t^{\frac{4}{7}}(1+\int_t^p S_E dx/Q_t)}{(\delta_e+\delta_i)}\left(\frac{m}{1+r_p}\right)^{\frac{1}{2}} \qquad (II.11)$$

in which L is the physical length of the straightened divertor plasma channel, and u is a measure of the fraction of energy input flux Q_t that is conveyed through thermal conduction in the divertor plasma channel, i.e., it is defined through

$$\frac{\left(\frac{2}{7}\right)\chi_0\left(T_t^{7/2} - T_p^{7/2}\right)}{L} = uQ_t \qquad (II.12)$$

which results in

$$u = 1 + \frac{1}{Q_t L}\int_t^p \left\{\int_t^x S_E dx' - nv\left[\frac{1}{2}mv^2 + \frac{5}{2}T(1+r)\right]\right\} dx \qquad (II.13)$$

In the divertor plasmas associated with the fusion reactors, u is essentially unity, which relieves the labor in modeling the profiles of S_E, n, v, and T for the

integration. While M_t is the fluid Mach number at the divertor throat, derived from the continuity and momentum equations:

$$M_t \equiv \frac{v_t}{C_{st}} = \left(\frac{a}{1-a}\right)^{\frac{1}{2}} \qquad (II.14)$$

where

$$a = \frac{n_p}{n_t} \frac{(1-R)^2}{\left[2 + (1-R_N) f_{cxs} R + R_N f_{cxf} R\right]} \qquad (II.15)$$

$$C_{st} = \left(\frac{T_t(1+r_t)}{m}\right)^{\frac{1}{2}} \qquad (II.16)$$

Also, by the definition of R, i.e., equation (II.7), we obtain from the continuity equation,

$$\int_t^p Sn\, dx = R\, n_p\, v_p \qquad (II.17)$$

where $v_p = C_{sp} \equiv \left(\frac{T_p(1+r_p)}{m}\right)^{\frac{1}{2}}$ is set as required by the Bohm sheath criterion [Stangeby, 1984]. Then, with the definition of R, the energy source flux $\int S_E dx$ can now be written as,

$$\int_t^p S_E dx = \int_t^p S_e dx + R\, R_N\, n_p\, v_p\, \epsilon \qquad (II.18)$$

It is obvious from the forms of equations (II.8) to (II.18) that these equations are highly nonlinear, despite the fact that they originate from the simple 1-D, two point integration. Therefore, numerical means is required to obtain the steady state solution. For given R, n_t and Q_t, physical quantities such as n_p, T_p, T_t, M_t, and subsequently the helium pumping rate, and sputtering erosion rate can be obtained.

II.B.d. Formulas used for the energy sink term

In constructing the representations for the energy loss mechanisms from the electron-neutral and ion-neutral collisions, several empirical formulas are adopted. The particle and energy reflection coefficients are approximated as $R_N = 0.19 - 0.237 \cdot log_{10}(E_0/EL)$, and $R_{Ei} = 0.06 - 0.22 \cdot log_{10}(E_0/EL)$, respectively, where E_0 is the incident D-T ion energy in eV, and $EL = \frac{(M_1+M_2)(Z_1Z_2)(Z_1^{2/3}+Z_2^{2/3})^{1/2}}{0.03255M_2}$ eV, with $M_{1,2}$, $Z_{1,2}$ the mass and atomic number of the incident particle and target atoms, respectively [Harrison, 1983].

The explicit structure of the energy sink term $\int_t^p S_e dx$ is as follows ($\int_t^p S_e dx = \int_t^p S_{ion} dx + \int_t^p S_{he} dx + \int_t^p S_{cx} dx + \int_t^p S_{sput} dx$):

<u>D-T neutrals ionization loss</u>

$$\int_t^p S_{ion} dx = -n_p v_p R \cdot \chi_i \qquad (II.19)$$

where $\chi_i = 17.5 + (5.0 + (37.5/T_p)) \cdot log_{10}(1 \times 10^{21}/n_p)$ eV, is the energy loss per ionization event [Harrison, 1983; Baehre and Steiner, 1990], and T_p is in eV. This empirical law is valid for T_p greater than about 10 eV with n_p ranging from $10^{19}\ m^{-3}$ to $10^{21}\ m^{-3}$.

<u>He impurity radiation loss</u>

$$\int_t^p S_{he} dx = -n_p v_p f_{hep} (1. + p12) R_{he} \chi_{he} \qquad (II.20)$$

where f_{hep} is the He flux fraction among the recycled neutral flux near the divertor plate, $p12$ is the probability for He^+ to become He^{++}, R_{he} is the He recycling coefficient, and $\chi_{he} = 15.0 + p12(70.0 + 3360.0/T_p)$ eV is the averaged energy radiated due to the presence of one He ion [Harrison, 1983]. In later simulations, $p12 = 0$ is used, by assuming there are not many deeper shell

ionizations.

charge-exchange loss

$$\int_t^p S_{cx} dx = -n_p v_p R \cdot (1 - R_N) f_{cxs} \left[\frac{3}{2} T_{ip} + \frac{1}{2} m v_p^2 \right] \qquad (II.21)$$

in which $< \sigma v >_{cxs}$ is the rate coefficient for the charge exchange between the incident D-T ions and the recycled slow neutrals, and $f_{cxs} \equiv \frac{<\sigma v>_{cxs}}{<\sigma v>_{ion}}$.

ionization loss due to sputtered plate atoms

$$\int_t^p S_{sput} dx = -R_{sput} \; n_p \, v_p \, Y \, u_0 \qquad (II.22)$$

where R_{sput} is the probability that a sputtered plate atom will enter the plasma, Y is the sputter yield, and u_0 is the ionization energy of the sputtered atom. In evaluating the sputter yield, Smith et al's formula [Smith et al, 1982] is employed. That is,

$$Y = \frac{C}{u_0} Z_1^{0.75} (Z_2 - 1.8)^2 \left(\frac{M_1 - 0.8}{M_2} \right)^{1.5} \frac{(E_0 - E_{th})}{[E_0 - E_{th} + 50 Z_1^{0.75} Z_2]^2} \qquad (II.23)$$

where C is a constant and is 2000 for hydrogen plasma, the sputter threshold energy is $E_{th} = u_0 \frac{(4M_1 + M_2)^2}{4M_1 M_2}$ in eV. The calculated sputter threshold energy for tungsten is 164 eV.

II.C. Sheath Physics and Energy Transmission Coefficients

II.C.a. Floating neutralizer

It is assumed that the neutralizer plate acts as if it is an unbiased (floating) Langmuir probe in the divertor plasma. In this case, electron and ion currents reaching the plate are equal in magnitude, so that the net current is zero. The floating potential ϕ_f can be expressed as [Stangeby, 1984],

$$\frac{e\phi_f}{kT_e} = 0.5\, ln\left[\left(2\pi\frac{m_e}{m_i}\right)\left(1+\frac{T_i}{T_e}\right)(1-r_e)^{-2}\right] \qquad (II.24)$$

where m_i is the average hydrogen ion mass, and $\phi_f < 0$ with respect to $\phi_{plasma} = 0$, and r_e is the secondary electron emission coefficient of the neutralizer plate.

The potential drop ϕ_f occurs in a thin sheath established between the plasma and the plate, whose thickness is on the order of the Debye length $\lambda_D \equiv (\frac{\epsilon_0 kT_e}{n_e e^2})^{\frac{1}{2}}$. The typical value for λ_D in a reactor-type edge plasma is about several hundred microns.

The existence of the potential drop ϕ_f has at least two consequences: 1) Ions are accelerated through the sheath and thus impact the divertor plate surface with an energy which is greater than that associated with the edge ion temperature T_i. This generally enhances the sputtering phenomena and does damage to the divertor plates. It also influences backscattering/retention/release of incident particles, and accordingly, the ability of the plate and the plasma to come into equilibrium with regard to the recycling of the hydrogen particles. 2) The sheath controls the rates at which particles and energy are removed from the plasma by the divertor plate. It is due to this reason that one needs to know the electron and ion energy transmission coefficients across the sheath for the modeling of the divertor plasma.

As revealed by equation (II.24), ϕ_f can be reduced by increasing T_i/T_e or by increasing the secondary electron emission r_e. In addition, the floating potential $e\phi_f$ is very sensitive to the divertor plate material, not only directly through r_e, but also indirectly through T_e, since T_e depends on the power balance which in turn depends on the backscattered fluxes, sputtering, impurity levels, etc. Note

also that equation (II.24) does not include the so-called "pre-sheath" potential.

The origin and importance of the "pre-sheath" potential can be described as follows. A plasma is quasi-neutral to a high degree (i.e., $n_e \approx n_i$). The sheath, by contrast, has a net positive charge population, since the plasma electrons tend to be repelled by the negative potential on the plate. The sheath thus acts to shield the plasma from this negative potential on the plate surface. However, the shielding effect is not perfect due to the thermal motion of the edge plasma ions, and hence a small residual field (i.e., the "pre-sheath") penetrates deep into the plasma, all the way to the symmetry point between the inner and outer divertors of a tokamak (if there are inner and outer divertors associated with a null point; otherwise, it would be all the way to the other end of the scrape-off layer).

Though the potential drop in the pre-sheath is small, about $\frac{(1/2)kT_e}{e}$, it acts to draw ions from the plasma toward the sheath. This accelerating field is just enough to make the ion drift velocity at the plasma-sheath interface equal to the ion acoustic speed $C_s = [\frac{k(T_e+T_i)}{m_i}]^{\frac{1}{2}}$ in order for these ions to reach the divertor plate. This is the Bohm sheath criterion [see, e.g., Stangeby, 1984].

II.C.b. Energy transmission coefficients including backscattered neutrals

Next consider the energy transmission across the sheath. Figure II.2 illustrates the heat fluxes involved. The electron energy flux removed from the edge plasma (i.e., including the pre-sheath potential $\frac{1}{2}kT_e$) is [Stangeby, 1984],

$$Q_e = \left[\left(\frac{2kT_e}{1-r_e}\right)(1-R_{Ee}) - e\phi_f + \frac{1}{2}kT_e\right]\Gamma_p \qquad (II.25)$$

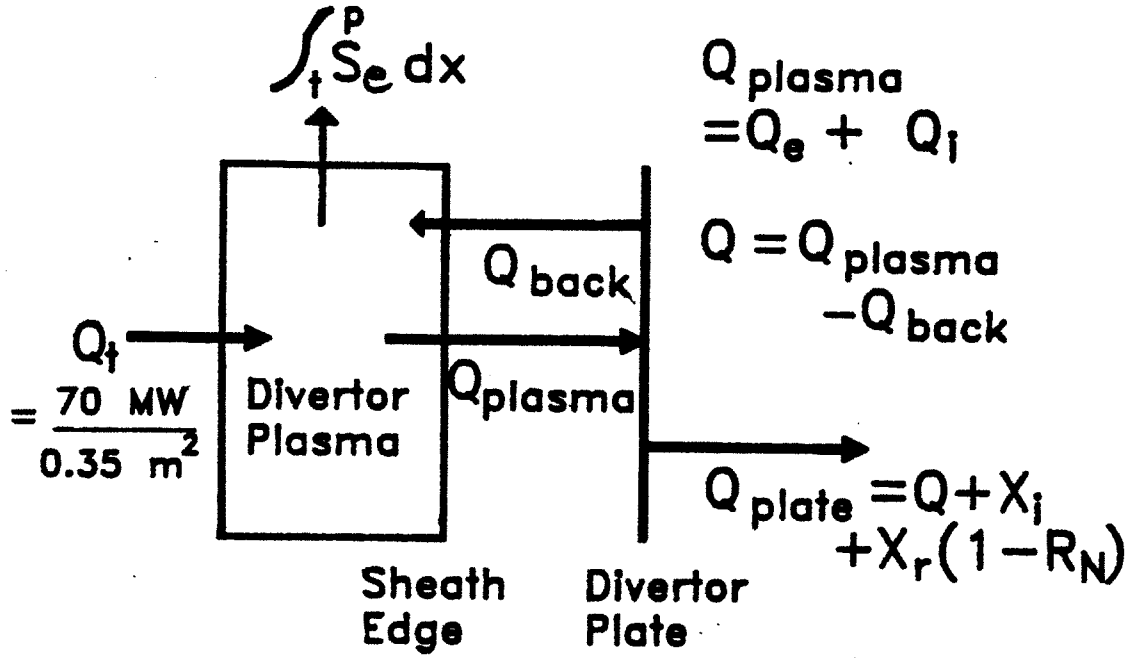

Figure II.2: Heat fluxes to the divertor plate

While ion energy flux is,

$$Q_i = 2kT_i\Gamma_p \tag{II.26}$$

It is generally found useful to define the so-called, "sheath energy transmission coefficient", which is the ratio of the energy flux to $(kT_e)\times$ (particle flux Γ_p). Thus, the electron energy transmission coefficient is (including the pre-sheath contribution):

$$\begin{aligned}\delta_e \equiv & \frac{Q_e}{kT_e(\Gamma_p)} \\ & = \left(\frac{2}{1-r_e}\right)(1-R_{Ee}) - \frac{e\phi_f}{kT_e} + \frac{1}{2}\end{aligned} \tag{II.27}$$

where T_e is evaluated near the plate, i.e., $T_e = T_p$. While the ion energy transmission coefficient is simply $\delta_i = 2r_p$. This implies that each electron carries more energy across the sheath edge than does each ion. However, for one electron starting in the plasma going towards the plate, the energy $-e\phi_f + \frac{1}{2}kT_e$ is conveyed from the electron to the ions. Therefore, ions impact the plate with more energy than electrons.

The *net* energy flux Q extracted from the plasma is given by [Stangeby, 1984]:

$$\begin{aligned}\frac{Q}{\Gamma_p} \equiv \delta \cdot kT_e = & [2kT_i - e\phi_f + \frac{1}{2}kT_e](1-R_{Ei}) \\ & + \frac{2kT_e}{1-r_e}(1-R_{Ee})\end{aligned} \tag{II.28}$$

which defines the effective heat transmission coefficient, δ.

Among the net transmitted energy flux, $[2kT_i - e\phi_f + \frac{1}{2}kT_e](1-R_{Ei})$ is carried by ions and $\frac{2kT_e}{1-r_e}(1-R_{Ee})$ is carried by electrons, where R_{Ee}, R_{Ei} are the electron and ion energy reflection coefficients from the divertor plate, respectively. Note that although Q is the net energy flux extracted from the

plasma, it is still *not* the energy flux received by the plate, but rather,

$$\frac{Q_{received-by-plate}}{\Gamma_p} = \frac{Q}{\Gamma_p} + \chi_i + \chi_r(1 - R_N) \qquad (II.29)$$

where χ_i is the ion recombination energy, and χ_r is the molecular recombination energy.

One may note that the plasma energy flux crossing the sheath edge does *not* equal the net energy flux reaching the floating plate. That is,

$$\delta_e + \delta_i \neq \delta \qquad (II.30)$$

This is because the plate returns considerable amount of energy to the plasma through the backscattered fast D-T neutrals, which is represented by the $R_N S_n \epsilon$ energy source term in equation (II.5). To be more specific, it is obvious from equations (II.28) and (II.29) that

$$\delta_e + \delta_i = \delta + \frac{1}{kT_e}[2kT_i - e\phi_f + \frac{1}{2}kT_e] \cdot R_{Ei} \qquad (II.31)$$

or equivalently,

$$\begin{aligned} Q_{plasma} = Q_e + Q_i &= Q + [2kT_i - e\phi_f + \frac{1}{2}kT_e] \cdot R_{Ei} \cdot \Gamma_p \\ &= Q + RR_N\Gamma_p\epsilon \\ &= Q + Q_{back} \end{aligned} \qquad (II.32)$$

Therefore, it can be inferred from equation (II.32), that $[2kT_i - e\phi_f + \frac{1}{2}kT_e]R_{Ei} \cdot \Gamma_p \cdot R$ is the energy flux associated with ions backscattered by the plate and deposited onto the divertor plasma as neutrals. Each backscattered neutral carries energy, $\epsilon = \frac{R_{Ei}}{R_N}[2kT_i - e\phi_f + \frac{1}{2}kT_e]$.

Note that even though it is mathematically correct to include Q_{back} into $Q_e + Q_i$ in the boundary condition (equation (II.6)), and thus retain only the

energy sink term $\int S_e dx$ in $\int S_E dx$ (in other words, use δ instead of $\delta_e + \delta_i$), the only possible choice for the energy source term in the energy equation (after spatial integration of equation (II.5)), is $\int_t^p S_E dx = \int_t^p S_e dx + Q_{back}$, as was shown by starting the derivation from the Boltzmann equations. The next section will show that the heat flux, Q_{back}, can be a significant fraction of the total heat entering the divertor, Q_t.

Another minor point worth some consideration is that it is not correct to use $\delta + (\chi_i + \chi_r(1-R))/kT_e\Gamma_p$ in the divertor plasma boundary condition [see, e.g., Harrison, 1983], since χ_i or χ_r is never the energy content of the edge plasma.

II.D. Simulation Results for Solid Surface Divertors

II.D.a. Comparison with INTOR Benchmark for tungsten neutralizer

For the numerical calculations, the following parameters are employed: (a) Secondary electron emission coefficient $r_e = 0.3$, (b) No electron backscatter, $R_{Ee} = 0$, (c) $T_e = T_i$, (d) Thermal conduction fraction $u = 1$, (e) Length of the divertor channel $L = 10\ m$, (f) Neutralizer plate area is 20 m^2, (g) Divertor channel cross-sectional area perpendicular to the magnetic field, $A_c = 0.35\ m^2$, (h) Heat load to one divertor is 37.5 MW. Numerical results obtained from solving equations (8) to (18) are compared with the existing INTOR benchmark [Harrison, 1983], and are illustrated in Table II.1 (Result A is for some nominal n_t, and Result B is for increased n_t).

The results reveal several important points. First, due to the effects of the backscattered energy flux and the momentum loss, the outcome appears to be much more conservative with regards to reaching the desired dense, cool edge

Table II.1

Comparison With INTOR Benchmark

	INTOR benchmark	Result A	Result B
R given	0.99	0.99	0.99
$n_t\ (m^{-3})$ given	$5.0{\cdot}10^{19}$	$5.0{\cdot}10^{19}$	$1.6{\cdot}10^{20}$
$n_p\ (m^{-3})$	$8.4{\cdot}10^{19}$	$1.89{\cdot}10^{19}$	$1.63{\cdot}10^{20}$
$T_t\ (eV)$	66.0	80.1	62.7
$T_p\ (eV)$	25.5	68.6	16.3
$A_c \int_t^p S_E\, dx\ (MW)$	—	4.5	4.2
ionization & rad. loss (MW)	—	2.1	7.4
He radiation loss (MW)	—	0.03	0.12
CX loss (MW)	—	5.0	4.3
$Q_{back}\ (MW)$	—	11.5	16.0
sputter ionization loss (kW)	—	5.0	0.

plasma for the tungsten plate divertor. This was also predicted by Ohyabu et al [1982] for INTOR. Second, even at such high recycling operation, n_p is not necessarily larger than n_t, as manifested by Result A. Only when certain critical value of n_t is exceeded will n_p be larger than n_t, as implied by Result A and Result B. This is because n_p is roughly proportional to n_t^3, which can be inferred from equation (II.8) (This relation was first scaled by Ohyabu et al [1982].). Consequently, as n_t increases, n_p grows faster than n_t.

Third, in Result B, for example, the backscattered power actually dominantes all loss mechanisms such that the net energy source term is *positive.* This positive value is of course smaller in magnitude than the energy transmitted across the sheath. Nevertheless, this means the achieved dense, cool edge plasma at such high n_t (not favorable for H mode operation, or may not even be accessible in reality) is *not* caused by ionization or charge exchange. Rather, it might be crudely explained as due to the fact that more charge carriers near the plate share the approximately fixed amount of heat load.

The sensitivity of the modeling results to the backscattered flux can be illustrated by Table II.2. The four cases presented span the following conditions: 1) Using the full model; 2) With no backscattered energy flux; 3) With no backscattered energy flux and no momentum sink; 4) With no backscattered energy flux, no momentum sink, using assumed energy transmission coefficients (e.g., $\delta_e = 6.5$, $\delta_i = 2.0$).

It is clear that too optimistic results can be obtained if the backscattered energy flux, momentum sink, and energy transmission coefficients are not properly handled.

Table II.2

Sensitivity of INTOR Divertor Results to Model Assumptions

	case 1	case 2	case 3	case 4
backscattered energy	yes	no	no	no
momentum sink	yes	yes	no	no
transmission coefficients	modeled	modeled	modeled	assumed
R given	0.99	0.99	0.99	0.99
$n_t\ (m^{-3})$ given	$5.0{\cdot}10^{19}$	$5.0{\cdot}10^{19}$	$5.0{\cdot}10^{19}$	$5.0{\cdot}10^{19}$
$n_p\ (m^{-3})$	$1.9{\cdot}10^{19}$	$2.2{\cdot}10^{19}$	$6.4{\cdot}10^{19}$	$7.3{\cdot}10^{19}$
$T_t\ (eV)$	80.1	70.0	63.2	62.9
$T_p\ (eV)$	68.6	51.6	24.6	21.6

II.D.b. Steady state ITER divertor results for tungsten neutralizer

The relevance of the ITER tungsten divertor calculation is restricted by the fact that both physics and engineering parameters are still evolving. However, for a crude estimate, all parameters are assumed the same as those for INTOR except that now the plate heat deposition is taken to be 70 MW. That is, the incident heat flux on the divertor plate is 3.5 MW/m^2, without accounting for the peak-to-average ratio caused by the variation of the scrape-off layer thickness, asymmetry of heat load etc. A "physics safety factor" of 3.4 for the outer plate and 5.2 for the inner plate were suggested by the ITER team [Post et al, 1991]. The results for three cases with varying throat plasma densities are presented in Table II.3. The value of Q_t can be evaluated to be 70 MW/A_c = 200 MW/m^2, where A_c = 0.35 m^2 is the divertor channel area perpendicular to the magnetic field lines.

II.D.c. Steady state ITER divertor results for beryllium neutralizer

The edge plasma results for beryllium divertor under steady state ITER conditions is presented in Table II.4. It can be noted that even though the edge plasma temperature is less than that at the tungsten divertor, the calculated physical sputter yield (Y = 0.1) of the beryllium divertor plate is about one order of magnitude greater than that at the tungsten plate. Estimate of the beryllium erosion rate based on physical sputtering is about 70 cm/yr for a 20 m^2 beryllium divertor plate. In addition, according to an interpolation of existing data by Roth et al [1989], the beryllium self-sputter yield can even

Table II.3

Numerical Results for ITER Tungsten Divertor With Varying n_t

	ITER 1	ITER 2	ITER 3
R (given)	0.99	0.99	0.99
n_t (m^{-3}) (given)	$5.0{\cdot}10^{19}$	$8.0{\cdot}10^{19}$	$1.0{\cdot}10^{20}$
n_p (m^{-3})	$1.7{\cdot}10^{19}$	$3.2{\cdot}10^{19}$	$4.6{\cdot}10^{19}$
T_t (eV)	116.1	90.3	82.5
T_p (eV)	108.4	73.4	58.1
$A_c \int_t^p S_E \, dx$ (MW)	4.9	8.1	9.6
ionization & rad. loss (MW)	2.3	3.4	4.3
He radiation loss (MW)	0.03	0.05	0.06
CX loss (MW)	10.9	9.6	9.0
Q_{back} (MW)	18.2	21.1	22.9
sputter ionization loss (MW)	0.0095.	0.0045	0.0
plate sputter yield	0.014	0.004	0.0

Table II.4

Numerical Results for ITER Beryllium Divertor With Varying n_t

	ITER 1	ITER 2	ITER 3
R (given)	0.99	0.99	0.99
n_t (m^{-3}) (given)	$5.0{\cdot}10^{19}$	$8.0{\cdot}10^{19}$	$1.0{\cdot}10^{20}$
n_p (m^{-3})	$2.0{\cdot}10^{19}$	$4.5{\cdot}10^{19}$	$7.4{\cdot}10^{19}$
T_t (eV)	94.4	78.7	76.0
T_p (eV)	79.6	47.1	33.6
$A_c \int_t^p S_E \, dx$ (MW)	-15.6	-13.7	-13.9
ionization & rad. loss (MW)	2.3	3.8	5.1
He radiation loss (MW)	0.03	0.06	0.08
CX loss (MW)	13.8	12.9	12.9
Q_{back} (MW)	1.1	3.2	4.4
sputter ionization loss (MW)	0.08	0.15	0.19
plate sputter yield	0.1	0.1	0.1

exceed unity. Hence, it is quite unlikely that beryllium can be employed as divertor plate material under the ITER-like power reactor conditions.

II.D.d. Sensitivity studies

Sensitivity of the modeling results to the possible uncertainties in the physics and engineering parameters is domonstrated via the variations of the heat load and the recycling coefficient. The former simulates the possible effect of enhanced radiation in the main plasma or the edge plasma at divertor throat, and is illustrated in Table II.5. The latter simulates the possible recycling of particles to regions other than the original one, and is presented in Table II.6. The enhancement of radiation power is shown to cause considerable increase in plate plasma temperature. While variation of the recycling coefficient does not affect the modeling results very much. However, as R is increased, the plate plasma density decreases and the plate plasma temperature increases, while the plate plasma pressure remains roughly constant. This confirms the trend discovered by Galambos and Peng [1984].

These results for the ITER tungsten divertor appear to be pessimistic in terms of achieving the goal of dense, cool edge plasmas. For the desired low impurity operation in the major tokamak chamber, it is likely that n_t will be around $5.0 \cdot 10^{19}\ m^{-3}$. Thus, the high edge plasma temperature is expected to cause material compatibility and sputtering, unipolar-arcing erosion (of divertor wall) problems. The sputtering erosion rate of the tungsten plate can be crudely estimated as follows. Since $Y\Gamma_{p\perp} \cdot A = (dx/dt) \cdot A\rho$, where A is the divertor plate area, using $Y = 0.014$ as obtained above for $R = 0.99$, and $\Gamma_{p\perp} \equiv n_p v_p \cdot (Ac/A) \approx 4 \times 10^{20}\ m^{-2}s^{-1}$, the erosion rate can be found to be $(dx/dt) \approx 20\ cm/yr$. Note that this serious consequence is only due to the

Table II.5

Numerical Results for ITER Tugsten Divertor With Varying Q_t

	case 1	case 2	case 3	case 4
$Q_t \times A_c$ (MW) (given)	50	60	70	80
R (given)	0.99	0.99	0.99	0.99
n_t (m^{-3}) (given)	$5.0{\cdot}10^{19}$	$5.0{\cdot}10^{19}$	$5.0{\cdot}10^{19}$	$5.0 \cdot 10^{19}$
n_p (m^{-3})	$1.79{\cdot}10^{19}$	$1.74{\cdot}10^{19}$	$1.70{\cdot}10^{19}$	$1.67 \cdot 10^{19}$
T_t (eV)	94.7	105.7	116.1	126.1
T_p (eV)	85.2	97.2	108.4	119.00

Table II.6

Numerical Results for ITER Tungsten Divertor With Varying R

	case 1	case 2	case 3	case 4
$Q_t \times A_c$ (MW) (given)	70	70	70	70
R (given)	0.79	0.89	0.94	0.99
n_t (m^{-3}) (given)	$5.0{\cdot}10^{19}$	$5.0{\cdot}10^{19}$	$5.0{\cdot}10^{19}$	$5.0 \cdot 10^{19}$
n_p (m^{-3})	$1.89{\cdot}10^{19}$	$1.79{\cdot}10^{19}$	$1.74{\cdot}10^{19}$	$1.70 \cdot 10^{19}$
T_t (eV)	109.7	113.0	114.6	116.1
T_p (eV)	100.6	104.7	106.5	108.4

assumed uniform (on 20 m^2 plate) physical sputtering by deuterons and tritons, not including the self-sputtering. Similarly, the erosion rate for the beryllium plate is around 70 cm/yr. The effect owing to the unipolar arc (caused mainly by the high edge plasma temperature) will be discussed in Chapter V.

The situation will be much worse, of course, if the peak-to-average safety factor is to be taken into account. In other words, even if the heat transfer requirements can be met (i.e., 70 MW per divertor plate), the feasibility of employing any solid metal neutralizers in ITER-like power reactors is questionable due to the intolerable erosion rate of divertor plates.

II.E. Summary and Conclusions of Chapter II

Improvements in divertor edge plasma modeling are suggested, namely, the proper inclusion of the backscattered energy flux contribution, the momentum loss, and the adoption of formulas for the energy transmission coefficients from standard plasma sheath analysis. For illustration, a self-consistent derivation of a simple 1-D, one fluid hydrodynamic model is performed, starting from the Boltzmann equations.

Numerical calculations reveal the fact that with these modifications, the results for INTOR are considerably different from those of the INTOR benchmark [Harrison, 1983]. The unavailability of a dense, cool edge plasma and also the plasma density scaling between the divertor throat and near the plate, as predicted by Ohyabu et al [1982], are confirmed.

Calculations for the ITER case turn out to be pessimistic for continuous reactor operation, even without taking into account the peak-to-average heat load condition. Namely, the physical sputtering rates of 2.0 mm/day and 0.56 mm/day are predicted for the beryllium and tungsten divertor plates,

respectively. Hence, protective layers of low Z materials and/or optimistic behavior of self-redeposition will be needed for the solid divertors to survive. The feasibility of employing any solid metal neutralizer plates thus appears to be questionable according to the modeling results of this work.

CHAPTER III. REFERENCE CONCEPTS OF LIQUID METAL DIVERTORS

III.A. Protective Film Divertor

Since the lifetime of a solid metal divertor plate is limited mainly by erosion, it seems most natural to apply a self-renewable liquid metal film over the original solid plate to achieve the possible goal of an ever-lasting divertor. In order to carry away the divertor heat load two options can be taken. One is self-cooled film divertor, i.e., the liquid metal film is pumped at high enough speed such that it is capable of conveying the deposited heat away without extra coolant within the solid backing plate. The other is coolant-cooled film divertor, in which the liquid metal is circulated slowly only to protect the backing plate. Typical poloidal film divertor configurations are illustrated in Figure III.1 (injection type film divertor) and in Figure III.2 (film flowing down an inclined chute).

Most concerns associated with the film divertor concept focus on whether the heat transfer can be properly managed without having too much MHD (magnetohydrodynamic) pressure losses, and whether the protective film would be ripped off from the backing plate if severe plasma-liquid metal interaction is taking place, as well as whether there would be abrupt variations of the film thickness such that there are dry spots or flooding regions on the backing plate. The injection type film divertor is expected to have more problems. Namely, if the heat transfer requires the circulation speed of the self-cooled liquid metal to exceed certain value, then it is likely that the injected liquid metal will be projected into the plasma rather than being flown over the guiding plate as a film.

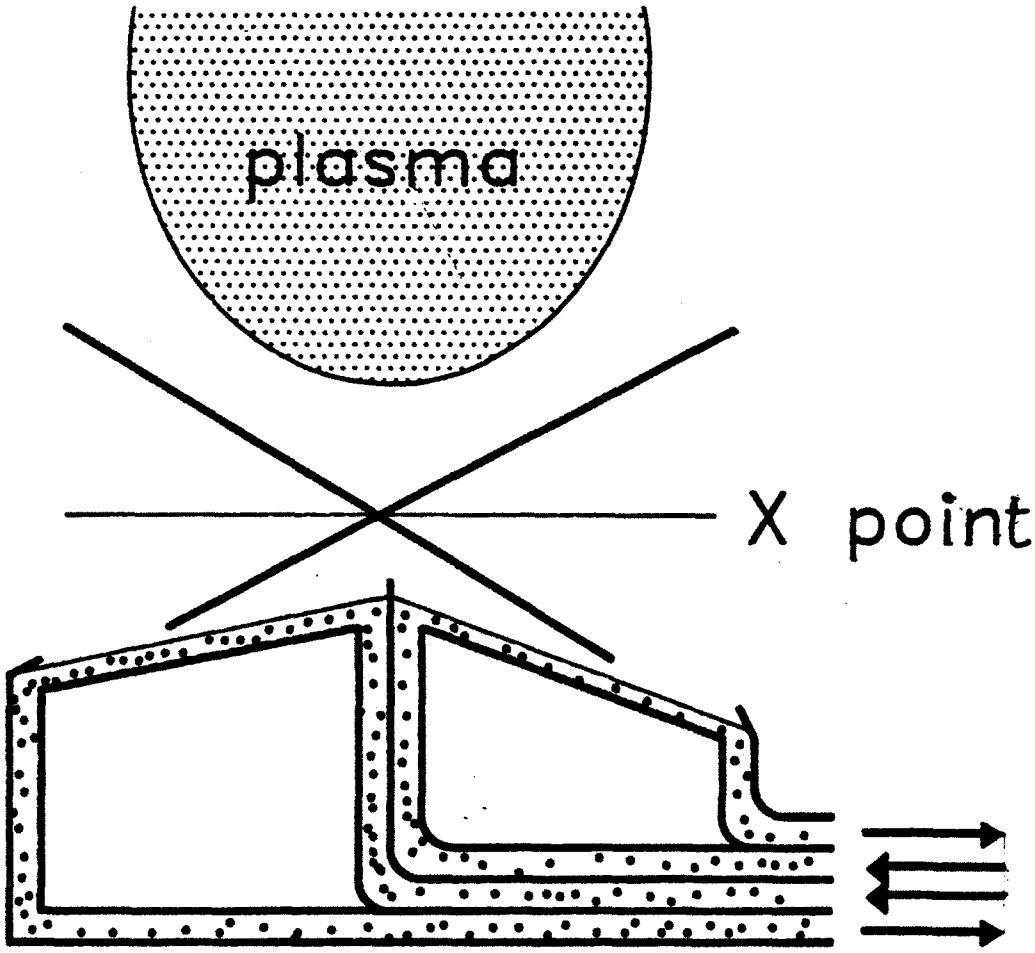

Figure III.1. Injection type film divertor

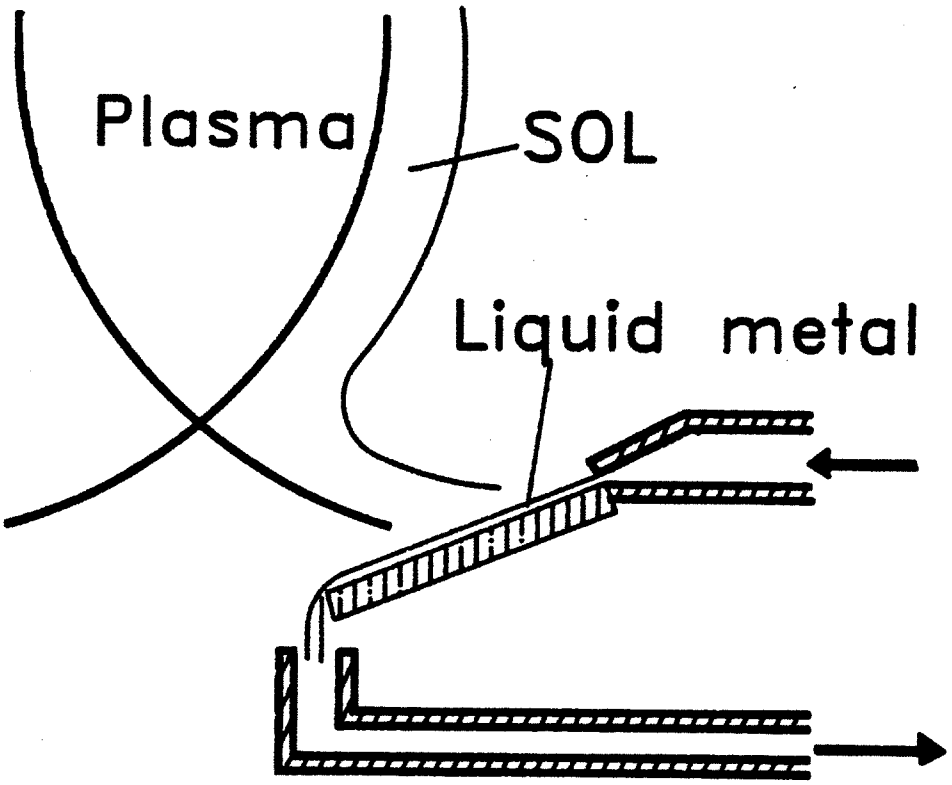

Figure III.2. Liquid metal film flowing down an inclined chute

From the above reservations about the heat transfer and MHD pressure losses, it may seem that the coolant-cooled, slowly flowing liquid metal film divertors are more favorable. However, there is speculation that in this case the hydrogen bubble formation and subsequent eruptions (due to the large bombarding charged particle flux of an ITER-like reactor [Post et al, 1991]) may cause serious contamination problems in both the main plasma and the divertor chamber.

III.B. Liquid Metal Pool Divertor

The pool type divertor is essentially a variation of the previous coolant-cooled, slowly flowing film divertor. That is, now the liquid metal is kept motionless within a basin with imbedded coolant tubes (see Figure III.3). However, if there are blistering erosion and contamination problems associated with the coolant-cooled film divertors, they surely will also occur in the case of pool type divertors. Another concern with this concept is that if the working liquid metal is a hydrogen (D+T) getter, then the accumulated tritium inventory within the divertor system can well exceed the maximum permissible limit set by the safety considerations. This issue will be explored further in Chapter IV.

III.C. Lithium Jet Droplet Beam Divertor

A divertor concept with two high speed ($160\ m/s$) beams ($0.14\ m \times 0.86\ m$) of liquid lithium (Li) droplets passing through the divertor regions below and above the main plasma is proposed by Werley [1989] (see Figure III.4). The lithium droplets are formed by forcing turbulent-jet flow of liquid lithium through a nozzle array. The lithium leaving each nozzle breaks up into droplets, and the resulting droplet beam enters the magnetic field, passes through the divertor

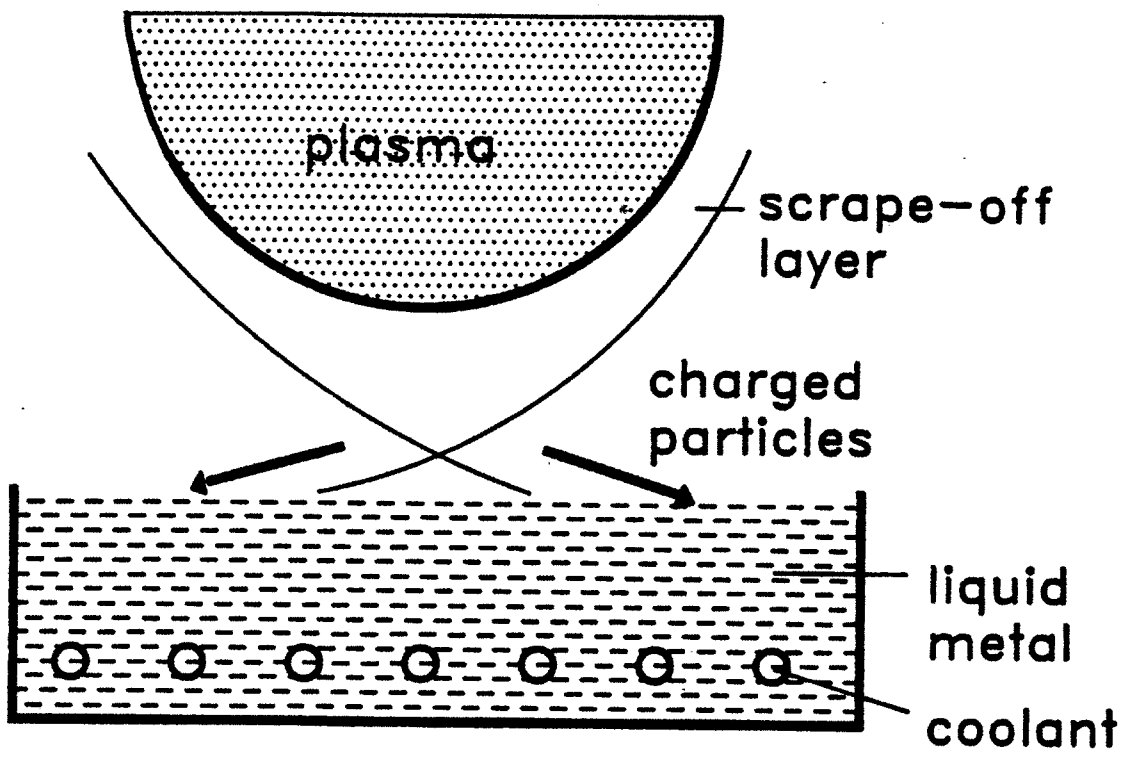

Figure III.3: Pool type liquid metal divertor

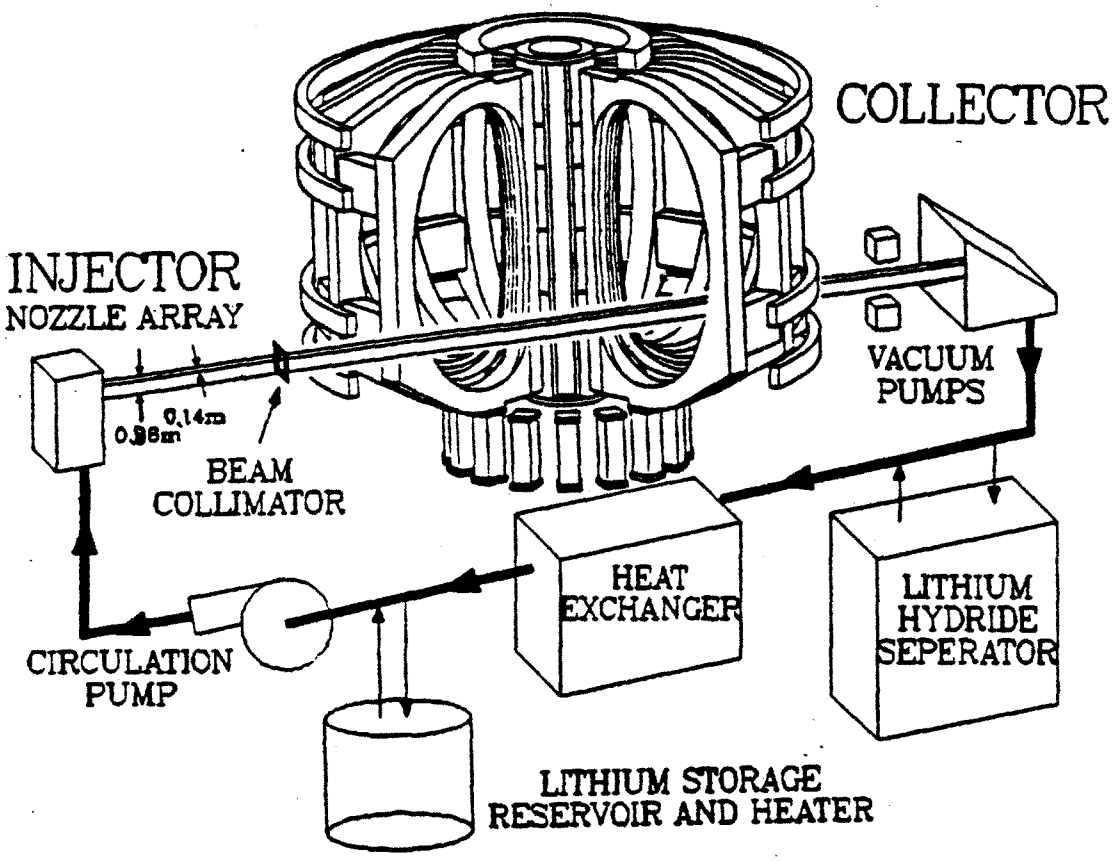

Figure III.4: Lithium jet droplet beam divertor [Werley, 1989]

Table III.1

Parameters for a Liquid Lithium Droplet Beam Divertor

[Werley, 1989]

beam width	$0.14\ m$
beam height	$0.86\ m$
beam length	$30\ m$
length of collection zone	$5.5\ m$
droplet diameter	$5\ mm$
droplet speed	$160\ m/s$
lithium jet break-up length	$2\ m$
MHD droplet speed reduction	$0.011\ m/s$
MHD sideward deflection	$\sim 0\ m$
gravitational deflection	$0.043\ m$
lithium inlet temperature	$211°C$
lithium outlet temperature	$336°C$
average temperature increase per droplet	$28.2°C$
peak lithium vapor pressure	$4 \times 10^{-6}\ Torr$
gross physical sputtering rate	$4.5\ mm/yr$
gross evaporation rate	$1.2\ mm/yr$
extended lithium surface area	$69\ m^2$
lithium mass flow rate	$1520\ kg/s$

positions, accumulating diverted plasma particles and thermal energy, and then leaves the tokamak and is collected in a tank. The droplet formation and collection are carried out external to the tokamak in a region of low magnetic field so that MHD-induced pressure drops associated with the circulation of a conducting fluid is negligible. The collected liquid lithium is circulated through a heat exchanger and a lithium-hydride (LiH) separator (e.g., molten salt extraction [Finn, 1988]) before being returned to the injector nozzle.

The operational parameters of the lithium droplet beam divertor is given in Table III.1.

The liquid lithium droplet beam divertor was claimed to have the following merits [Werley, 1989]:

a. uses low Z liquid metal,
b. has small overall size with effectively extended lithium surface,
c. has negligible MHD effects and pressure drops,
d. removes impurities,
e. requires low power to circulate the lithium,
f. has efficient helium ash and hydrogen removal capability (since Li is treated as hydrogen getter),
g. exhibits low recycling divertor operation (due to hydride formation) compatible with lower hybrid current drive, H-mode plasma confinement and no flow reversal in the edge plasma,
h. has no thermal or pressure stress problems associated with conventional solid divertor plates,
i. eliminates the possibility of having dry spots on the divertor plate,
j. is insensitive to plasma shifts,

k. protects solid structures from the plasma thermal energy for those disruptions that deposit energy preferentially into the divertor while simultaneously being rapidly re-established after a major disruption.

However, there are major defects in this design concept. First, in Werley's calculation, the assumed edge plasma particle flux incident on the droplet beam divertor, i.e., $\sim 10^{20}\ m^{-2}s$ was too small. In fact, from the edge plasma simulation of this work (see Chapter II), the bombarding particle flux parallel to the magnetic field should be $\sim 10^{24}\ m^{-2}s$ instead, which makes the particle flux on the 5 m^2 droplet beam divertor (i.e., the part of the droplet beam area that grazes the incident charged particle flux) about $\sim 10^{23}\ m^{-2}s$, (i.e., three orders of magnitude greater than that assumed by Werley [1989]). Therefore, even if the liquid lithium is a hydrogen getter (which forms hydrides LiH) under the steady state ITER divertor conditions, the lithium is expected to saturate in very short time and accordingly the afore-mentioned benefits of having low recycling divertor operation really cannot be achieved, unless there is very efficient and economic liquid lithium renewal technology. However, at such hydrogen incident rate of about one mole per second for one divertor, it appears that the availability of such technology is questionable. As a matter of fact, even with the underestimated particle flux, it was pointed out by Werley [1989] that the feasibility for separating lithium hydrides at the required rate and to the required concentration is not known. On the other hand, if high recycling operation is preferred, then there may still be a problem in having excessive tritium inventory, as will be discussed in Chapter IV.

Second, the lithium droplet formation process depicted in Figure III.4 is not advisable. Namely, lithium should not be used in the air, since the oxidation reaction can result in serious fire hazard. Accordingly, employment of empirical

relations [Chen and Davis, 1964; Phinney, 1973] for fluid jet atomization in the air by Werley [1989] is not appropriate. Further, in order to ensure the vacuum confinement of the parts of the droplet beam (of considerable jet break-up length) external to the tokamak, enclosing tubes need to be built. While the part of the beam within the tokamak ($\sim 30\ m$) is expected to make the installation of many diagnostic devices and other supporting equipments very difficult. Hence, it can be anticipated that there will be many engineering problems in applying such divertors (if lithium is an usable divertor plate material) at top and bottom of the ITER-like two-null main plasma.

Third, the reception of the high speed droplet beam at the end tank can be a difficult task. That is, the spattering of the liquid lithium can be so serious as to contaminate the vacuum environment and subsequently to cause damage to the main plasma.

III.D. Gallium Droplet Curtain (Shower) Divertor

III.D.a. Droplet formation—the jet droplet flow generator

The gallium (Ga) droplet curtain divertor concept was compiled by Murav'ev [1989] as a major representation of Russian divertor designs for ITER tokamak reactor (see Figure III.5). The proposed droplet divertor each consists of 48 sections in such a way that a continuous curtain along the toroidal circumference is formed. Associated with each magnetic null point there are two curtain divertors (inner and outer). In each section, a so-called "jet droplet flow generator (JDFG)" is responsible for breaking up 3 layers of parallel liquid gallium jets into a 3-layered droplet curtain. The first single layer is designed to be able to meet the ITER divertor requirements, other two layers are for

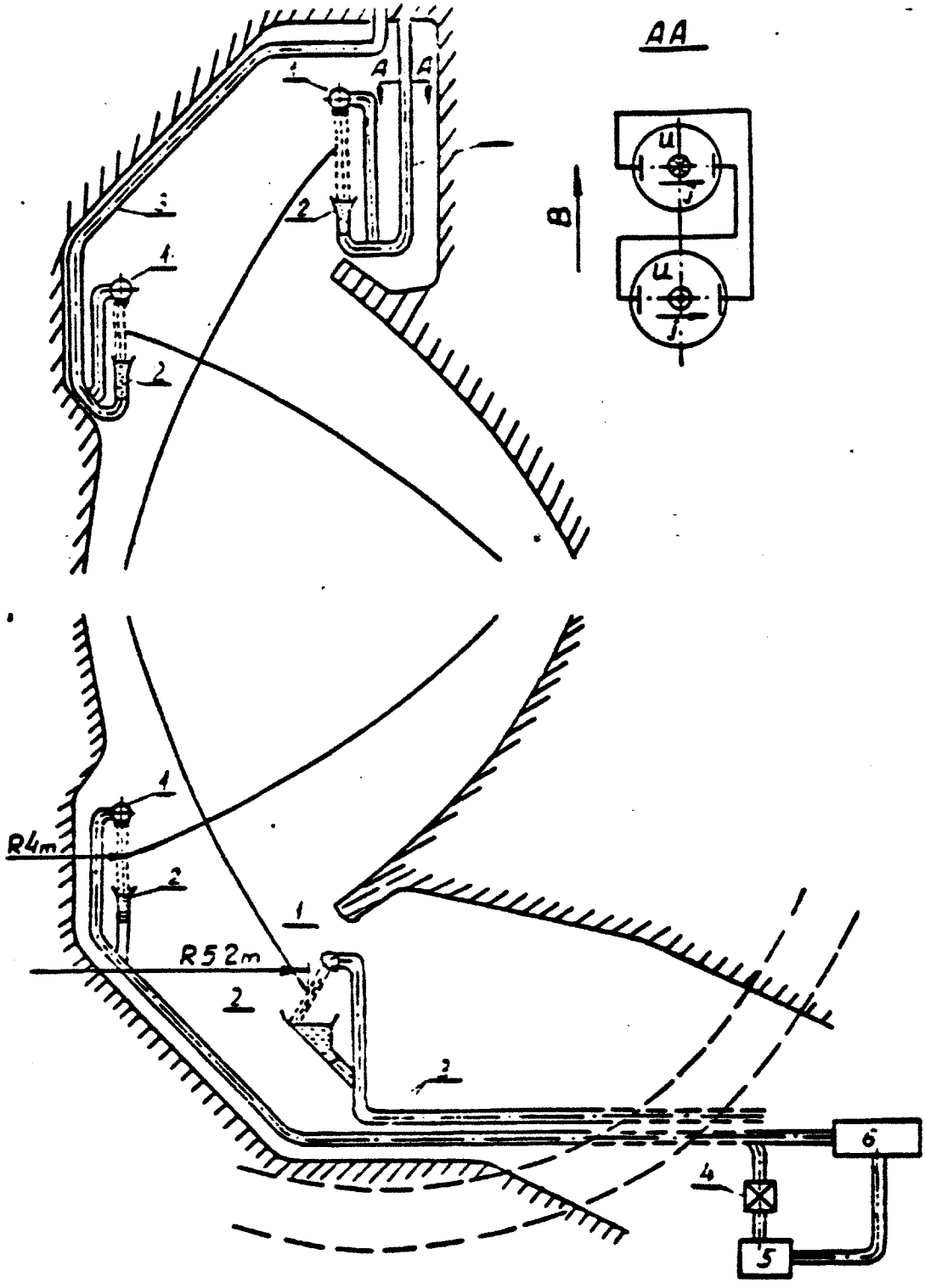

Figure III.5: Liquid Ga droplet curtain divertors in ITER tokamak

[Murav'ev, 1989]

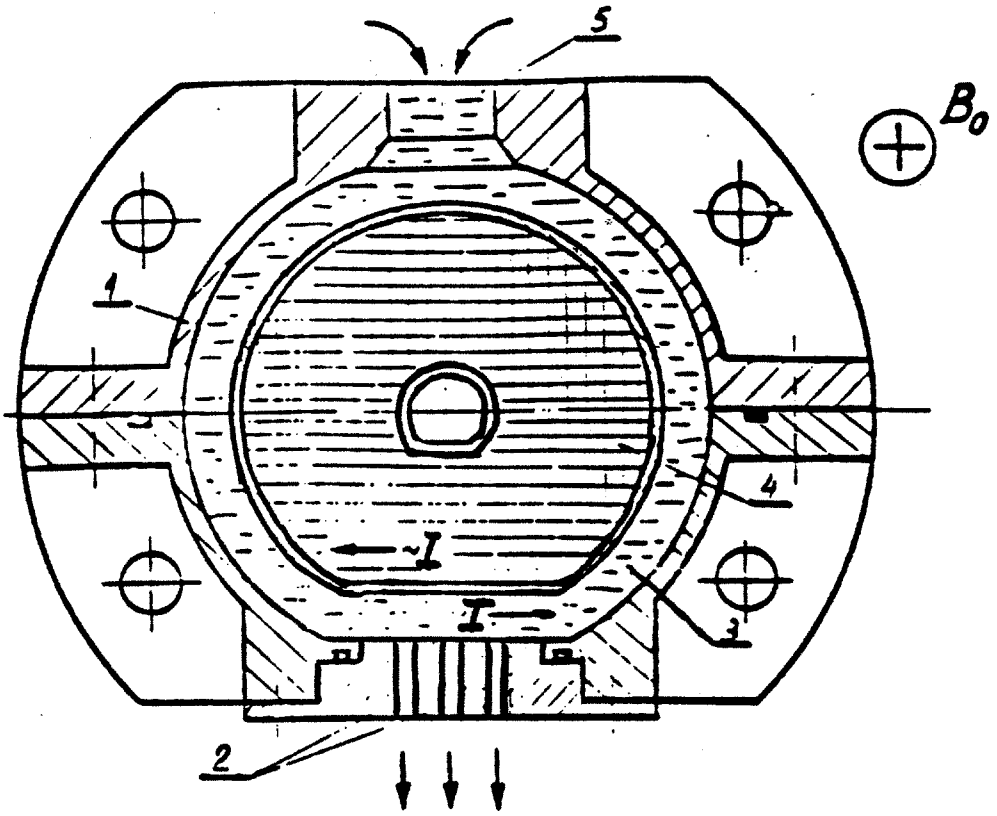

Figure III.6: Jet droplet flow generator (JDFG)

[Murav'ev, 1989]

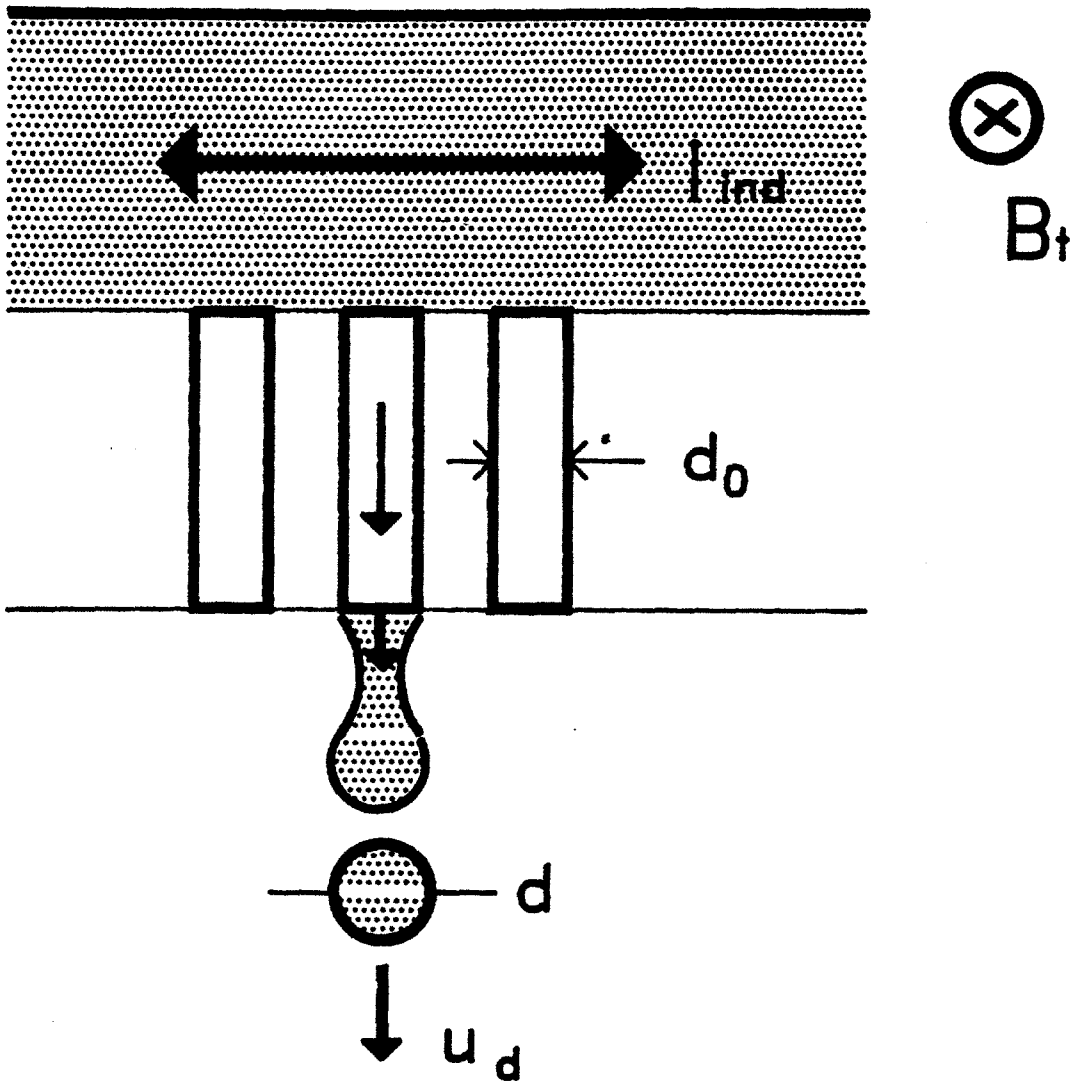

Figure III.7: Gallium plenum and jet tubes in the JDFG

engineering safety margin. In the following analysis, only the first single layer will be used in estimating the JDFG engineering parameters for simplicity.

The JDFG device works according to the Rayleigh jet instability theory [Rayleigh, 1878], and was varified experimentally to be able to decompose gallium eutectic (67 % Ga, 20.5 % In, 12.5 % Sn) jets into droplets of diameter 2.5 mm [Murav'ev, 1989]. Note that Ga-eutectic was initially used as a test material owing to its below room temperature melting point. However, it is not much preferred currently due to the fact that it has higher Z than pure Ga and that pure Ga has melting point only slightly above the room temperature.

The way the JDFG functions is described briefly as follows (see Figure III.6): First, within the JDFG an AC current is induced by the solenoidal inductor at the center of JDFG. Then, this induced AC current interacts with the toroidal magnetic field, which results in wave perturbation in the liquid gallium plenum above the heads of parallel gallium jets (see Figure III.7). This excited wave then propagates down the gallium jet tubes and starts the breakup instability which eventually leads to atomization of jets at some distance below the tube outlets. The relation between the droplet diameter d and the tube inner diameter d_0 can be derived from (see Figure III.7),

$$\lambda\pi\left(\frac{d_0}{2}\right)^2 = \frac{4}{3}\pi\left(\frac{d}{2}\right)^3 \qquad (III.1)$$

where λ is the perturbation wavelength on the liquid gallium jet, which is equal to 4.508 d_0 for the most probable jet breakup instability [Rayleigh, 1878]. Thus, we have

$$d = 1.89 d_0 \qquad (III.2)$$

The minimum induced current density j_{ind} (in the tokamak radial direction) required to have jet breakup is found experimentally [Murav'ev, 1989] to be scaled by the minimum electromagnetic Euler constant Eu, which is the ratio of the electromagnetic force to the inertial force, i.e.,

$$Eu = \frac{j_{ind} B_t d_0}{\rho u_0^2} \geq 0.1 \qquad (III.3)$$

where B_t is the local toroidal magnetic field strength, u_0 is the jet speed. For $\rho \approx 5720\ kg/m^3$, $B_t \approx 3.6\ T$, $u_0 = 10\ m/s$, $d = 2.5\ mm$ ($d_0 = 1.3\ mm$), the minimum induced current density is about $1.2 \times 10^7\ A/m^2$. For the Ga plenum height $h_g \approx 5d_0$, and the length of each section along the toroidal direction $L_g = 0.6\ m$, the induced current in each section can be calculated to be about $50\ kA$. While the inductor frequency ν_{ind} can be calculated by

$$\nu_{ind} = \frac{u_0}{\lambda} \qquad (III.4)$$

and thus is $\nu_{ind} \approx 1.7\ kHz$.

III.D.b. Curtain opaqueness

In order to determine the opaqueness of the droplet curtain with respect to the grazingly incident charged particles, the distance between jets t_t and that between falling droplets t_l (both center to center) (see Figure III.8) need to be determined. Derivation steps were omitted in [Murav'ev, 1989], and are presented here. The evaluation of t_l can be inferred directly from Figure III.9. That is, along $-y$ direction in Figure III.8 we have,

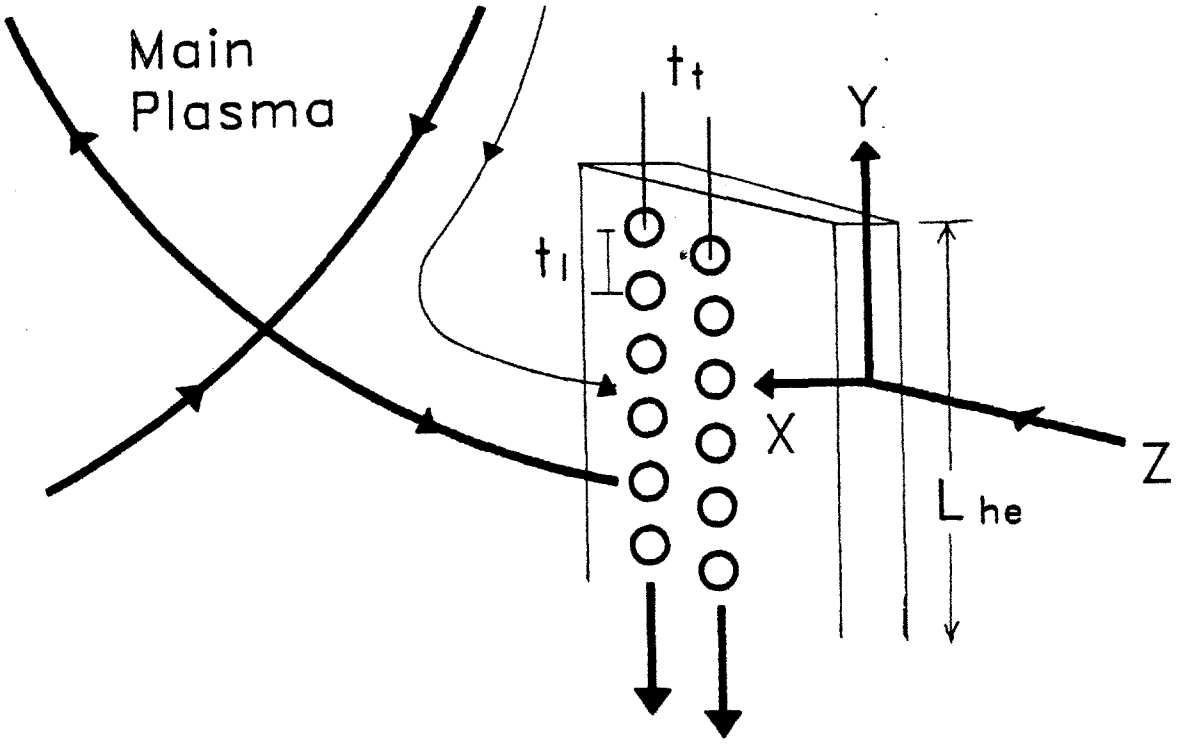

Figure III.8: Topology of the liquid Ga droplet curtain divertor

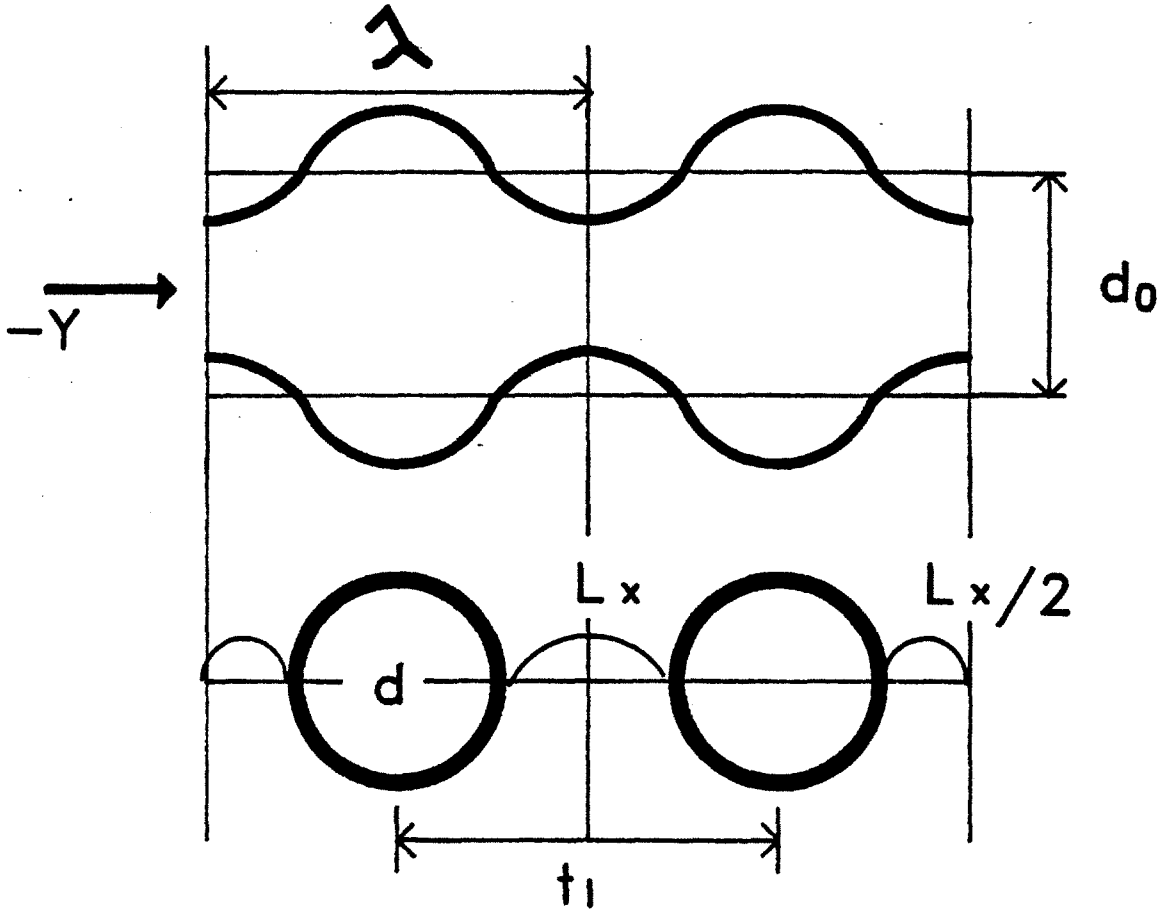

Figure III.9: Mechanism of the Ga jet decomposition

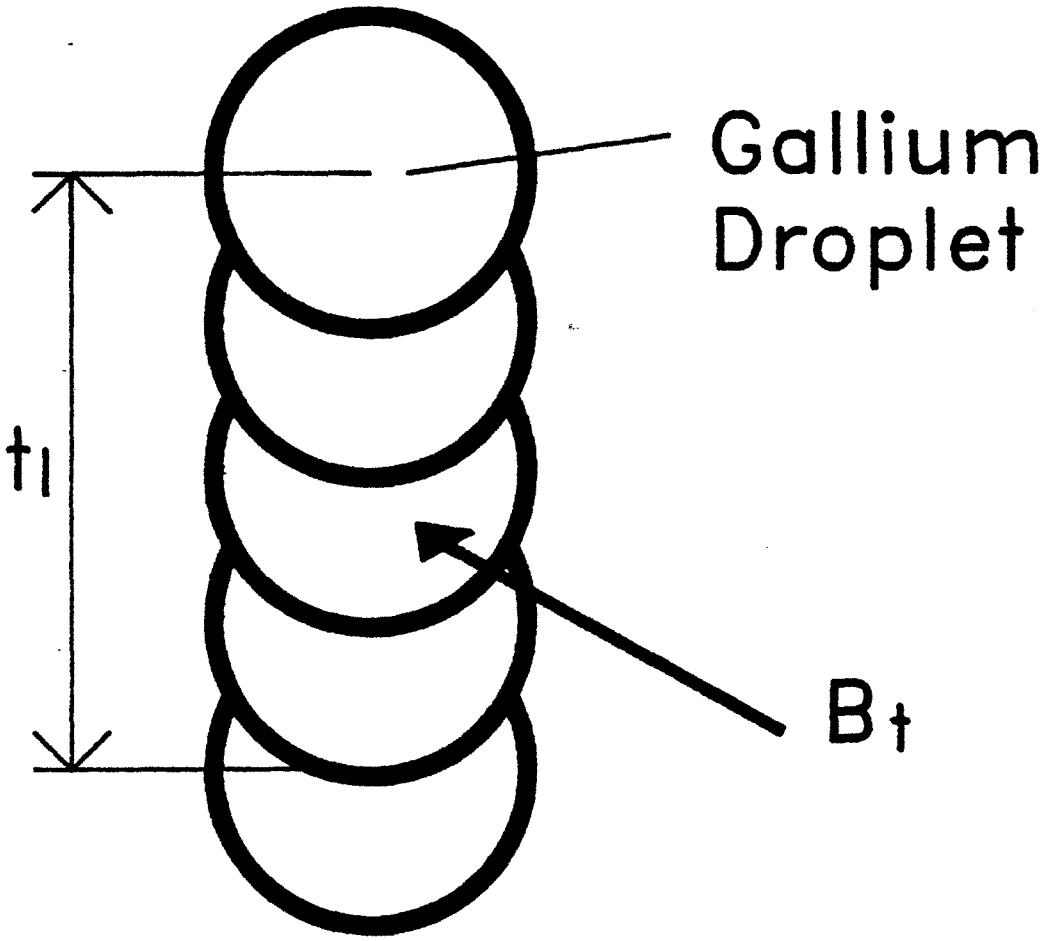

Figure III.10: Synchronization of adjacent Ga jets

for curtain opaqueness

$$2\lambda = 2d + 2L_x \qquad (III.5)$$

or

$$\begin{aligned} L_x &= \lambda - d \\ &= 4.508d_0 - 1.89d_0 \\ &= 2.6108d_0 \\ &= 1.38d \end{aligned} \qquad (III.6)$$

where d is the gallium droplet diameter, d_0 is the jet tube diameter, and λ is the perturbation wavelength caused by the electromagnetic excitation. Note in deriving equation (III.6), both the Rayleigh result $\lambda = 4.508d_0$ [Rayleigh, 1878] and equation (III.2) are used.

Therefore,

$$t_l = L_x + d = 4.508d_0 = \lambda = 5.95\ mm \qquad (III.7)$$

The grazingly incident charged particles fly mainly along the toroidal magnetic field (i.e. almost parallel to the z direction in Figure III.8). Thus viewing along the z direction (see Figure III.10), the number of droplet jets in z direction N_l required for complete curtain opaqueness with respect to one incident charged particle along the magnetic field can be estimated by assuming that these droplet jets are synchronized so that each differs the next one by $d/2$ in the instantaneous droplet positions. That is,

$$N_l = \frac{t_l}{(d/2)} \approx 5 \qquad (III.8)$$

i.e., five adjacent droplet jets in toroidal direction can achieve complete

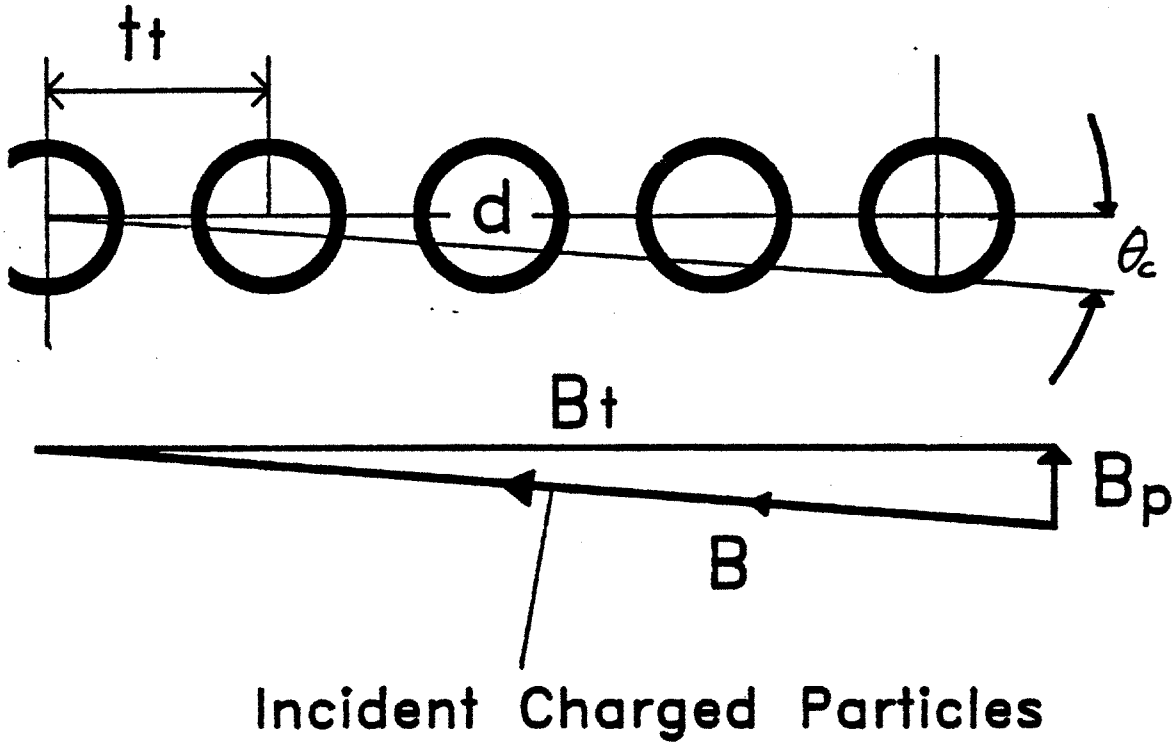

Figure III.11: Determination of the distance between adjacent Ga droplet jets

opaqueness for one incident particle flying along the magnetic field. Then, from this result and the ratio of the poloidal (B_p) to toroidal (B_t) magnetic field strengths, the upper limit for the distance between droplet jets along z direction can be decided. If γ is the angle between the total magnetic field and the toroidal magnetic field, then γ must be smaller than or equal to θ_c in Figure III.11 to ensure the curtain opaqueness. Since $\tan\theta_c = d/(4t_t)$, this implies that $B_p/B_t \equiv \tan\gamma \leq d/(4t_t)$ (Note that the derivation in [Murav'ev, 1989] is incorrect). Or,

$$t_t \leq \frac{B_t}{B_p}\frac{d}{4} \qquad (III.9)$$

Under the steady state ITER divertor conditions, t_t can be evaluated to be $t_t \approx (5/4)d = 3.1\ mm$.

Since the distance between the droplet jets (each with inner diameter of $d_0 = 1.3\ mm$), is very short (i.e., $t_t = 3.1\ mm$) there is a concern that the minimum tube thickness required against hoop stress may not allow such JDFG configuration. An assessment can be made by assuming the tube material to be some alloyed stainless steel or other materials (which do not interact appreciably with gallium under about $200°C$). If the engineering maximum allowed hoop stress σ_h is set to be several hundred MPa/m^2 for the tube material, the minimum tube wall thickness t_w can be estimated by,

$$2\sigma_h t_w = pd_0 \qquad (III.10)$$

where p is the pressure inside the tube and is approximated by the pressure drop of about 2.5 MPa for one divertor [Murav'ev, 1989], then the minimum required

tube wall thickness t_w is only several μm. Hence, with the jet holes made by drilling through a bulk material, the JDFG device is expected to be structurally robust. While other engineering aspects of this curtain divertor concept will be examined in the subsequent chapters.

CHAPTER IV. LIQUID METAL-HYDROGEN INTERACTIONS

IV.A. Introduction

In order to carry out engineering evaluations of the liquid metal (particularly, lithium (Li) and gallium (Ga)) divertors, knowledge of the edge plasma conditions is required. One crucial physical quantity needed in the divertor plasma modeling (developed in Chapter II) is the recycling coefficient R, which is closely related to the liquid metal-hydrogen interactions.

However, the fusion-related liquid metal data are hardly available. This makes the evaluation of the recycling coefficient R rather difficult and thus questions about the performance of liquid metal divertors left unresolved. For instance, if liquid metals are hydrogen getters (i.e., they are saturated by hydrogen only after a considerable period of time) under the steady state ITER conditions, then these divertors operate in a low recycling mode. This is because all implanted charged particles do not come out of the liquid metal during the period in which the flowing liquid metal is exposed to the charged particle bombardment. Even though this leads to the common perception that the desired dense, cool edge plasmas may not be achievable, cleaner main plasmas may be accomplished.

In addition, if liquid metals are hydrogen getters, then controlling the hydrogen concentration within the liquid metal divertors would in principle offer flexibility in controlling the divertor recycling coefficient. However, under such operational condition, the accumulated tritium inventory is a concern unless efficient tritium removal technology is available to keep the tritium quantity below a certain desirable value (i.e., the recycling coefficient cannot be too high).

On the other hand, if the liquid metals are not hydrogen getters (i.e., they are

saturated with deuterons and tritons in very short time), then the liquid metal divertors would be in high recycling operation (i.e., essentially one implanting ion will cause immediately the emission of one neutral particle). This would lead to denser, cooler edge plasmas (in favor of divertor plate protection) at the expense of having dirtier main plasmas (i.e., higher impurity concentration) and consequently more radiation losses and shorter energy confinement time.

In this Chapter, effort will be devoted to the evaluation of the liquid metal divertor recycling coefficient R to pave ground for the calculation of edge plasma conditions in Chapter V. Nevertheless, at this point the question about the possibility of controling the recycling coefficient (as mentioned above and more in Subsection I.B.c) can be answered.

The organization of this Chapter is as follows. In Section IV.B the operational temperature range for the liquid metals of interest will be determined. Then, hydrogen transport within liquid metals and the related tritium issue will be presented in Section IV.C. Based on this ground the hydrogen getter issue will be attacked in Section IV.D. Finally, summary and conclusions are to be given in Section IV.E.

IV.B. Liquid Metal Operational Temperature Range and Neutral Pressure

It is often stated [see, e.g., Yang, 1977; Lavrent'ev, 1989] that the operational temperature range for a specific liquid metal divertor is between the melting point (which is rather insensitive to the ambient pressure) and the boiling temperature associated with the divertor chamber pressure of about 10^{-5} to 10^{-4} $Torr$ (i.e., 1.3 mPa to 13 mPa). However, this is not correct. First, it is ambiguous to use the term "divertor chamber pressure". In fact, within the

divertor chamber the plasma pressure is on the order of one $Torr$ rather than 10^{-5} to 10^{-4} $Torr$. Second, even if the "boiling temperature" is exceeded, the liquid metal neutralizer will not boil. This is because the bombarding particle pressure on the liquid metal neutralizer surface prevents it from boiling at the normal temperature. Third, the boiling itself does not define the maximum operational temperature, since it really does not matter for liquid metals to boil.

The correct statement should be: the operational temperature range for a specific liquid metal divertor is between the melting point and the temperature at which the liquid metal vapor pressure is equal to the maximum allowed neutral pressure within the divertor chamber, which is about 10^{-5} to 10^{-4} $Torr$. While the origin for this neutral pressure limit will be disclosed as follows.

As far as radiation losses in the main plasma is concerned, the maximum permissible impurity concentration for ignition of a D-T plasma can be calculated from an energy balance. Taken from Jensen, Post, and Jassby [1978], Figure IV.1 shows the maximum tolerable concentrations of various impurity species for attaining certain Q-values (i.e., ratio of the output fusion power to the input power) in a D-T plasma at 10 keV temperature. To reach $Q = 100$, for example (corresponding roughly to ignition), the concentration of heavy metal impurities has to be kept below 10^{-4}, while that of iron below 10^{-3}. However, to avoid excessive radiation losses during the early heating phase at temperatures around 1 keV, the iron concentration has even to be kept below 10^{-4} [Keilhacker and Lackner, 1982 a]. Light impurities do not significantly contribute to radiation losses and would therefore be tolerated in larger quantities. In that case, however, the problem is that they add a considerable number of electrons to the plasma and cause fuel dilution. For instance, a helium concentration of

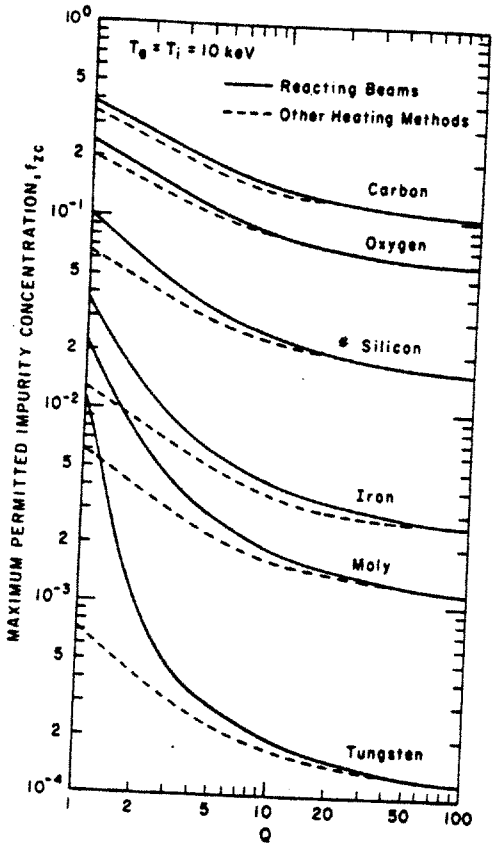

Figure IV.1: Maximum allowed impurity level in D+T plasma of fusion reactors [Jensen et al, 1978]

10 % reduces the fusion power density on the order of 10 %. Hence, it is safer to set the maximum tolerable concentration of all impurities to be around 10^{-5} to 10^{-4}.

From past experimental experience on fusion test devices [Tachon, 1984], impurities near the first wall can anomalously transport to the center of the main plasma and cause poisonous effects. Since the neutral pressure (mostly deuterium and triutium neutral atoms and molecules) near the first wall is on the order of one *Torr*, the maximum tolerable impurity pressure at the same location should, therefore, be kept below 10^{-5} to 10^{-4} *Torr*. Hence, in order to prevent downstream neutral gas near the divertor plate from transporting to the upstream main plasma edge, the maximum permissible neutral pressure in the divertor chamber is set to be about 10^{-5} to 10^{-4} *Torr* (see Figure IV.2).

The maximum permissible operational temperatures thus found for the lithium and gallium divertors are $325°C$ and $750°C$, respectively. Table IV.1 lists the operational temperature window for the lithium and gallium.

IV.C. Hydrogen Transport and Tritium Inventory Within Liquid Metals

IV.C.a. Hydrogen transport

In order to investigate the hydrogen getter issue of the liquid metals (necessary for the edge plasma simulations at liquid metal divertors), the "hydrogen recycling time", $\tau_{1/2}$, from liquid metals needs to be evaluated. It is defined as the time it takes for the re-emitted hydrogen flux (counted in terms of atoms) from the slowly moving (compared to the bombarding particle speed) liquid metal divertor to equal half of the implanting charged particle (D+T)

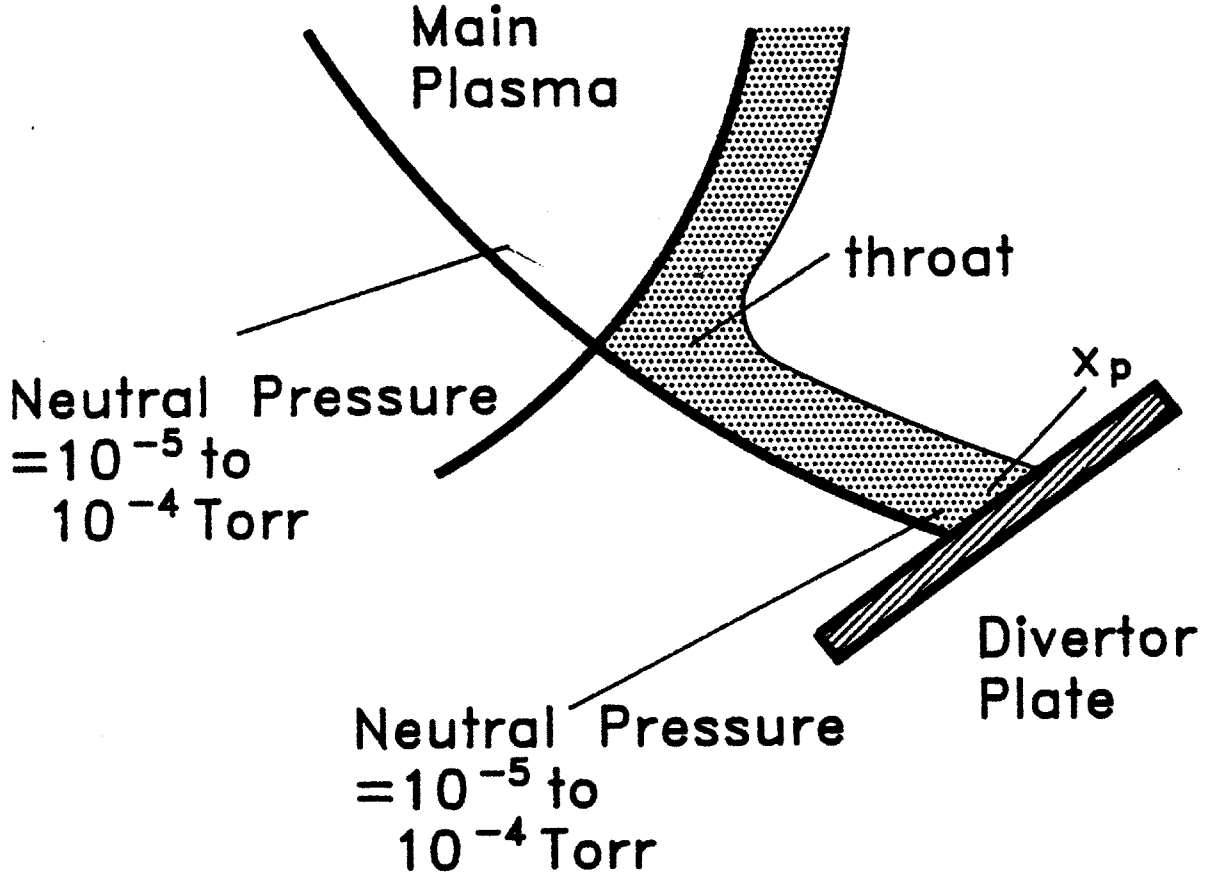

Figure IV.2: Maximum allowed neutral pressure near the divertor plate

Table IV.1

Li and Ga operational temperature window

	lithium (Li)	gallium (Ga)
Melting temperature T_m	$186°C$	$29°C$
Maximum temperature T^*_{max}	$325°C$	$750°C$
Boiling temperature at 1 atm	$1342°C$	$2205°C$

$*$ Maximum temperature corresponds to saturation at pressure of 10^{-4} $Torr$.

flux. A simplified, analytic theory for hydrogen transport within any material by Doyle [1982] is capable of fulfilling this purpose and thus will be briefly presented below. The recycle time can be calculated based on this theory once the value of the "hydrogen molecular recombination coefficient" K_f on the liquid metal neutralizer surface is known (to be evaluated in Section IV.D). In addition, this theory also gives analytic expressions for the important quantities such as the hydrogen concentration profile within the liquid metal and the steady state tritium permeation flux through the liquid metal divertor.

For the implanted hydrogen (D+T) to be released from a liquid metal neutralizer it must first diffuse to the surface and then combine with another surface hydrogen atom to form a molecule. The release of hydrogen in the liquid metal neutralizer will therefore be rate limited by either the diffusion process or the recombination process, depending on which one is the bottle-neck process. Some transport parameter (i.e., W) found by Doyle [1982] will give this natural classification of hydrogen release behavior among different liquid metals.

The concentration C of hydrogen in a divertor neutralizer of thickness x_0 can be determined by solving Fick's law:

$$\frac{\partial}{\partial t}C = D\frac{\partial^2 C}{\partial x^2} + J_{im}\delta(x - R_a) \qquad (IV.1)$$

where t is the time, x is the depth measured from the plasma side surface of the neutralizer plate, D is the hydrogen diffusion coefficient within the liquid metal, and J_{im} is the implanting hydrogen particle source flux which is assumed to penetrate into the liquid metal with a range R_a. Equation (IV.1) must be solved under the boundary conditions that at the plasma side,

$$J_f = K_f C_f^2 \qquad (IV.2)$$

and at the back side,

$$J_b = K_b C_b^2 \qquad (IV.3)$$

where J is the hydrogen particle flux out of a surface, K is the hydrogen molecular recombination coefficient on the liquid metal surface, and C here is the surface hydrogen concentration; the subscripts f and b refer to the plasma side and back side of the liquid metal neutralizer plate, respectively. Note that additional terms that could have been added to equation (IV.1) to include effects of hydrogen trapping and detrapping due to defects are ignored for simplicity. A solution can now be analytically found for both the steady state and the time varying case.

steady state solution

The solution to equation (IV.1) for $\frac{\partial}{\partial t}C = 0$ is a linear function of x and has a discontinuous first derivative at $x = R_a$. In other words, the concentration profile consists of two straight lines (see Figure IV.3): one line starts at C_f at the plasma side and increases to C_p at $x = R_a$, the other line starts from C_p at $x = R_a$ and decreases to C_b at the back side. It is also clear that at steady state, if $Ra \ll x_0$ (which is true for the case of interest, since $R_a \sim 10\ nm$ and $x_0 \sim 5\ mm$), then

$$J_{im} = J_f + J_b = K_f C_f^2 + K_b C_b^2 \qquad (IV.4)$$

and

$$J_f = K_f C_f^2 = D\frac{\partial}{\partial x}C|_{x=0} \approx \frac{D(C_p - C_f)}{R_a} \qquad (IV.5)$$

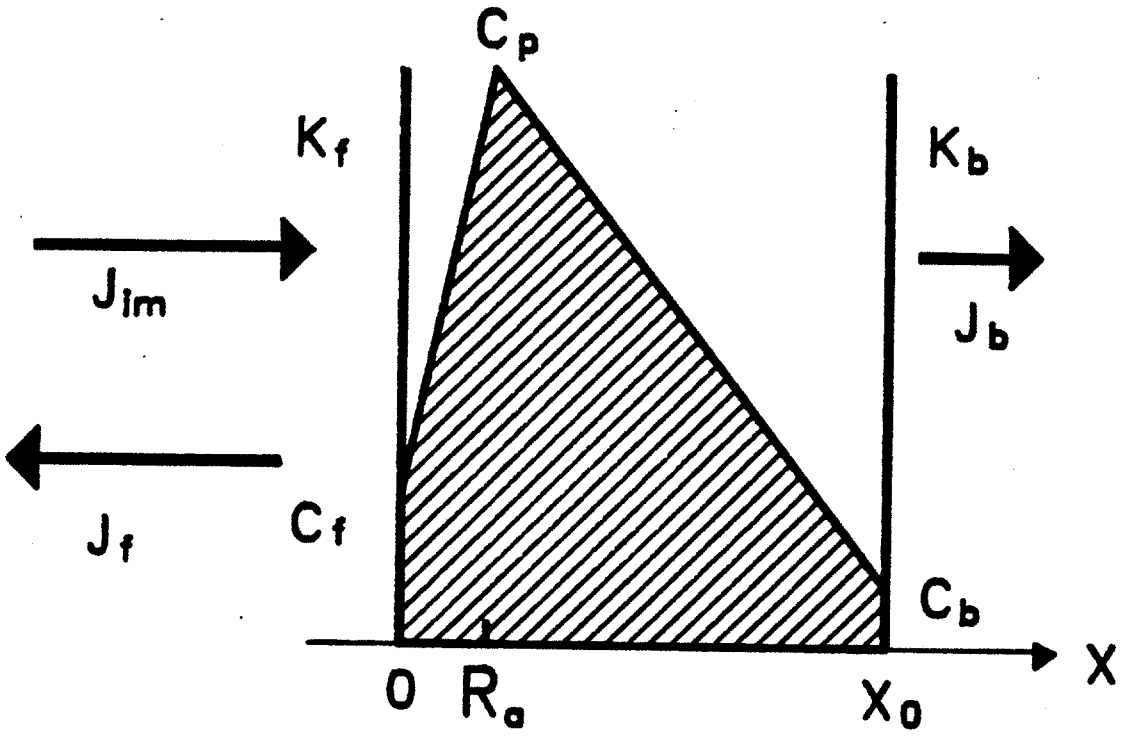

Figure IV.3: Hydrogen transport within the liquid metal

$$J_b = K_b C_b^2 = -D\frac{\partial}{\partial x}C|_{x=x_0} \approx \frac{D(C_p - C_b)}{x_0} \qquad (IV.6)$$

By defining the following parameters:

$$u = \left(\frac{K_f}{J_{im}}\right)^{\frac{1}{2}} C_f \qquad (IV.7)$$

$$v = \left(\frac{K_b}{J_{im}}\right)^{\frac{1}{2}} C_b \qquad (IV.8)$$

$$\alpha = \frac{R_a}{x_0} \ (\ll 1) \qquad (IV.9)$$

$$\gamma = \left(\frac{K_f}{K_b}\right)^{\frac{1}{2}} \qquad (IV.10)$$

$$W = \frac{R_a (J_{im} K_f)^{\frac{1}{2}}}{D} \qquad (IV.11)$$

we can obtain from equations (IV.4) to (IV.6),

$$v^2 \approx \frac{\alpha(1 + 1/W)}{1 + (1 + \gamma^2)\alpha(1 + 1/W)} \qquad (IV.12)$$

Through equation (IV.12), the steady state solution can be expressed as,

$$C_f = \left(\frac{J_{im}}{K_f}\right)^{\frac{1}{2}} (1 - v^2)^{\frac{1}{2}} \qquad (IV.13)$$

$$C_p = \left(\frac{J_{im}}{K_f}\right)^{\frac{1}{2}} \gamma \left[\left(\frac{W}{\alpha\gamma}\right) v^2 + v\right] \qquad (IV.14)$$

$$C_b = \left(\frac{J_{im}}{K_f}\right)^{\frac{1}{2}} \gamma v \qquad (IV.15)$$

Three distinct types of steady state hydrogen distributions result, depending on the value of W [Doyle, 1982]. For $W > 1$, the profile is highly peaked

at $x = R_a$ and the two surface concentrations can be assumed negligible. This behavior is characteristic of diffusion-limited hydrogen transport for both surfaces (see Figure IV.4(a)). For $\gamma^2\alpha < W < 1$, it is found that $C_p \approx C_f$ and $C_b \approx 0$, indicating hydrogen recombination-limited behavior on the plasma side and diffusion-limited behavior on the back side (see Figure IV.4(b)). If $W < \gamma^2\alpha$, the hydrogen concentration profile becomes uniform, characteristic of recombination-limited kinetics at both surfaces (see Figure IV.4(c)). Hence, from the representation of W (equation (IV.11)), it is obvious that the hydrogen transport behavior within a liquid metal depends not only on the liquid metal property (such as K and D) but also on the divertor situation associated with a specific fusion tokamak reactor (such as the implanting charged particle flux).

The re-emitted particle flux and the permeating flux at steady state can also be calculated. That is, from equations (IV.13) and (IV.15),

$$J_f = J_{im}u^2 = J_{im}(1 - v^2) \qquad (IV.16)$$

$$J_b = J_{im}v^2 \qquad (IV.17)$$

time varying solution

A time dependent model for hydrogen release process was derived by Erents and McCracken [1969] and Doyle [1982], respectively. Their model is appropriate for reactive materials (such as lithium, titanium) provided correct parameters are employed [Baskes, 1980]. The relation between the implanted and reemitted hydrogen fluxes is given by

$$J_{reem} \equiv J_f = J_{im} \cdot erfc\left[\frac{1}{2\sqrt{\theta}}\right] \qquad (IV.18)$$

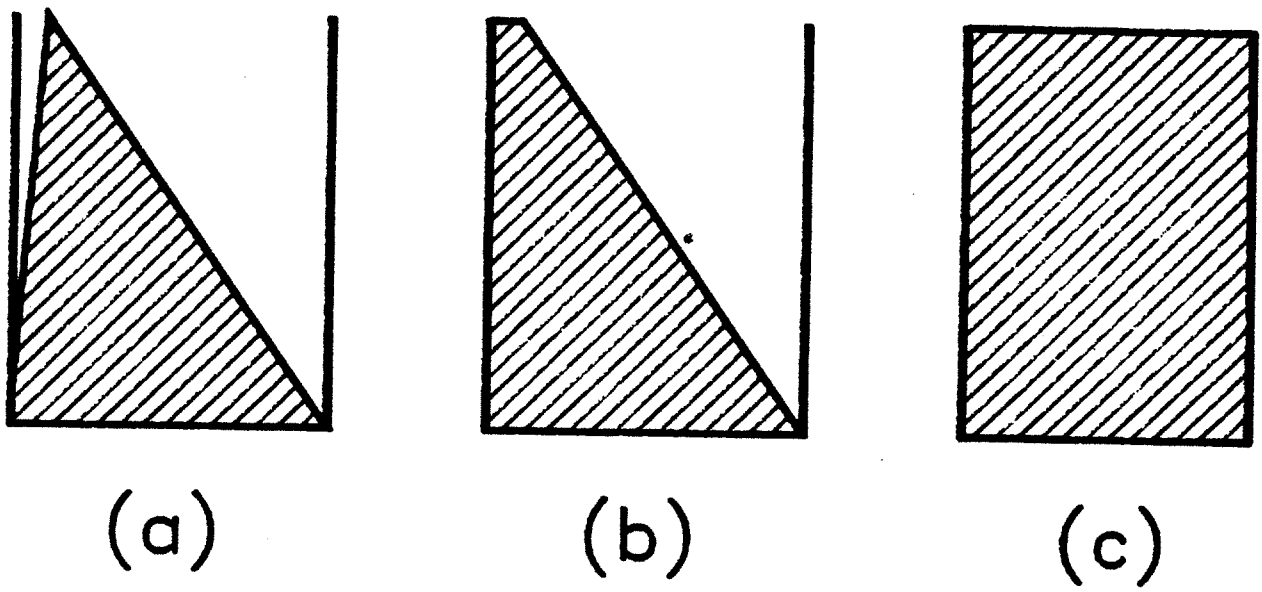

Figure IV.4: Hydrogen concentration profile within the liquid metal

(a) diffusion limited on both sides

(b) recombination limited on front side;
diffusion limited on back side

(c) recombination limited on both sides

where $\theta = t/(R_a^2/D)$ if the release process is diffusion-limited; as compared to $\theta = t/(D/K_f J_{im})$ if it is recombination-limited. In the equation, $erfc(x) = 1 - erf(x)$ is the compensated error fuction, and $erf(x) = \frac{2}{\sqrt{\pi}} \int_0^x e^{-t^2} dt$. R_a is the stopping range of hydrogen within lithium ($\sim 10^{-8}$ m), D is the hydrogen diffusion coefficient in lithium (in m^2/s), and K_f is the surface molecular recombination coefficient for hydrogen (in m^4/s). In Section IV.D, hydrogen recycling time at a liquid metal neutralizer will be inferred indirectly from an existing experiment by utilizing equation (IV.18).

IV.C.b. Tritium Inventory and safety

Tritium inventory within the liquid metal neutralizer can be easily evaluated from equations (IV.13) to (IV.15) once the surface hydrogen molecular recombination coefficient K_f for the specific liquid metal is known. Namely, for a D-T plasma the tritium concentration within the liquid metal will be about half of the average hydrogen concentration. As mentioned before, however, if the specific liquid metal is a hydrogen getter, then the resultant tritium inventory may become large enough to be a safety concern.

The question is how much tritium is allowed within the liquid metal divertor system. This remains an unsettled issue. However, with the proposed total tritium inventory of about 6 kg for the ITER reactor [Raeder et al, 1991], it appears reasonable to accept the value of 2 kg suggested by the ITER particle and power control group [Cohen, private communication, 1991] for the liquid metal divertor system. The relevant question now is whether the liquid metal is a hydrogen-getter or not.

IV.D. Are Liquid Metals Hydrogen-Getters ?

IV.D.a. Lithium H getter and tritium inventory

Liquid metals, particularly Li, are often considered as hydrogen getters (or ion burial materials) due to their ability to form hydrides [McCracken and Erents, 1969]. However, it is suspected that this may not be true under the ITER divertor condition. The investigation of this issue is made difficult by the scarcity of data on liquid metal interactions with hydrogens under fusion condition, even for the better known material Li. For example, the hydrogen recombination coefficient cannot be obtained directly from Baskes formula [Baskes, 1980] since there is great uncertainty (of several orders of magnitude) in assigning the so-called "sticking factor" α in the formula (see, for example, [Langley, 1984]), which is related to the cleanliness of the surface, and in our case, should be extended to include the property of the formed hydrides.

In the following, therefore, effort is devoted to infer crudely, from experimental data, the hydrogen molecular recombination coefficient K_f for a lithium surface. With this, the hydrogen residence time within the liquid lithium can be calculated and accordingly, the hydrogen recycling coefficient R for a Li divertor, required for edge plasma modeling, can be estimated. The recycling coefficient R is the probability that an incident charged particle on the divertor plate will be recycled and ionized in the plasma. The value of R for a large tokamak like ITER is expected to be about 0.99.

An experiment of hydrogen bombardment of liquid lithium was conducted by McCracken and Erents [1969], in which a 50 μA (or $10^{20}\ m^{-2}s^{-1}$) beam of 20 keV deuterium ions D^+ was directed perpendicularly towards a small cup of liquid lithium at various temperatures, in $10^{-9}\ Torr$ ($1.3 \cdot 10^{-7}\ Pa$) vacuum.

Due to the fact that not all the implanted hydrogen atoms form hydrides (solid LiH, melting point $680°C$) with lithium ions, some hydrogen atoms can escape from the lithium target. The fraction of the beam re-emitted from the surface during bombardment is inferred from the partial pressure rise in the target chamber measured with a quadrupole mass spectrometer. Their results in terms of trapping efficiency are illustrated in Figure IV.5. The trapping efficiency $\eta(t)$ at each instant is defined as the ratio of the number of deuterons trapped within lithium at that time to the total number of bombarding deuterons after starting the experiment.

Note that the beam flux they used ($10^{20}\ m^{-2}s^{-1}$) is much smaller than the one in the ITER divertor case ($\sim 10^{23}\ m^{-2}s^{-1}$) such that their lithium is far from being filled with hydrogen during the whole experiment. In addition, due to the light mass of lithium, backscattering is a negligible effect in their experiment. In addition, the sputtering effect is also negligible [McCracken and Erents, 1969]. Had their experiment been conducted for long enough time, the trapping efficiency would have eventually approached zero.

For the following derivation, no effort is made to distinguish between deuterium and tritium ions. The reference case is chosen for a lithium temperature of 300 $°C$, since the working temperature window for lithium divertors is between the melting point of 186 $°C$ and the saturation temperature of 325 $°C$ (corresponding to the 10^{-5} to $10^{-4}\ Torr$ (1.3 mPa to 13 mPa) lithium vapor partial pressure).

The hydrogen trapping by lithium can be described by

$$1 - \frac{N_{reem}}{N_{inci}} \equiv \eta(t)$$

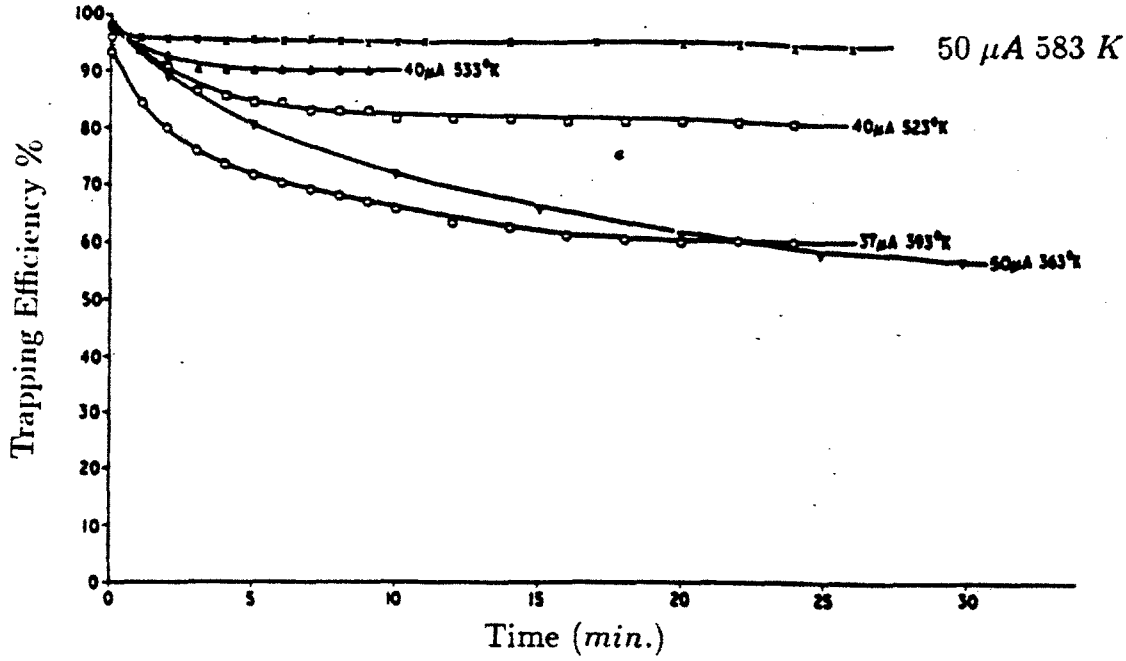

Figure IV.5: Hydrogen trapping efficiency vs time in liquid lithium [McCracken and Erents, 1969]

or

$$N_{reem}(t) = [1 - \eta(t)] \cdot N_{inci}(t) \qquad (IV.19)$$

where η is the trapping efficiency, $N_{inci}(t) = J_{im}tA$ is the accumulated number of implanted hydrogens, with J_{im} the fixed implanted hydrogen particle flux, A the lithium target area; and $N_{reem}(t) = \int_0^t J_{reem}(t')dt'A$ is the accumulated number of re-emitted hydrogen neutrals. While the relation between the implanted and reemitted hydrogen fluxes is given by equation (IV.18),

$$J_{reem} \equiv J_f = J_{im} \cdot erfc\left[\frac{1}{2\sqrt{\theta}}\right] \qquad (IV.18)$$

where $\theta = t/(R_a^2/D)$ if the release process is diffusion-limited; as compared to $\theta = t/(D/K_f J_{im})$ if it is recombination-limited. In the equation, $erfc(x) = 1 - erf(x)$ is the compensated error fuction, and $erf(x) = \frac{2}{\sqrt{\pi}} \int_0^x e^{-t^2} dt$. R_a is the stopping range of hydrogen within lithium ($\sim 10^{-8}$ m), D is the hydrogen diffusion coefficient in lithium (in m^2/s), and K_f is the surface molecular recombination coefficient for hydrogen (in m^4/s). Differentiating equation (IV.19) with respect to t, and neglecting $\frac{\partial}{\partial t}\eta$ (by choosing appropriately long time after the onset of particle bombardment), then combining with equation (IV.18), we obtain:

$$\eta(t) = erf\left[\frac{1}{2\sqrt{\theta}}\right] \qquad (IV.20)$$

Under ITER divertor condition, if the hydrogen release process by lithium is diffusion-limited, then according to Doyle's formula [Doyle, 1982], the steady state hydrogen concentration at the stopping depth, C_p, is (from equation (IV.14)),

$$C_p = \left(\frac{J_{im}}{K_f}\right)^{\frac{1}{2}} \left[\frac{W}{\alpha}v^2 + v\right] \qquad (IV.21)$$

where $W = R_a(J_{im}K_f)^{\frac{1}{2}}/D$, $v^2 = \alpha(1+1/W)$, $\alpha = R_a/x_0$, and x_0 is the thickness of the liquid lithium, the calculated C_p will be several orders of magnitude greater than the lithium number density, which is unrealistic. Therefore, similar to solid hydrogen getters such as titanium, niobium, zirconium, and erbium, the hydrogen reemission process in lithium is recombination-limited.

Matching equation (IV.20) with McCracken and Erents' data in Figure IV.5, i.e., $D/(K_f J_{im}) \approx 2000\ s$ for the reference temperature and for their experiment, we obtain $D/K_f \approx 2.3{\cdot}10^{23} m^{-2}$. The diffusion coefficient D can be extrapolated from Alire's experimental result [Alire, 1976] in which liquid lithium is enclosed in a niobium capsule with temperature range of 500 $°C$ to 800 $°C$, i.e.,

$$D(m^2/s) = 1.3 \cdot 10^{-3} e^{-1.7314{\cdot}10^{-19}/k_B T(^0K)} \qquad (IV.22)$$

in MKS unit. At 300 $°C$, $D = 4. \cdot 10^{-13}\ m^2/s$. The corresponding coefficient K_f is expected to be a function of only the temperature for a given liquid metal, as implied by Baskes formula [Baskes, 1980].

The hydrogen recycling time $\tau_{1/2}$ is defined as the time when the re-emitted hydrogen flux equals half of the incident flux, i.e., $K_f C_{1/2}^2 = \frac{1}{2} J_{im}$, where $C_{1/2}$ is the corresponding uniform hydrogen concentration (m^{-3}), characteristic of the recombination-limited hydrogen release process. For a Li film divertor of thickness $h = 5\ mm$ for example, the recycling time can be estimated as $\tau_{1/2} = \frac{C_{1/2}Ah}{J_{im}A} \approx O(10\ min)$ under steady state ITER conditions. It is only when the lithium is filled with hydrogen that the lithium divertor will operate

in a high recycling mode.

However, there are uncertainties associated with this calculation, and therefore the result should only be treated as a rough estimate. In particular, the calculated hydrogen concentration C seems very high. At steady state (implanted flux equals re-emitted flux), $J_{im} = K_f C^2 \approx 10^{23} m^{-2} s^{-1}$ (inferred from later modeling results), C is found to be of the same order as the lithium number density (i.e., $\sim 10^{29}\ H/m^3$). This implies that the pure Li property used above may be deceiving. In addition, by this stage, hydrogen bubbles should have formed within the lithium, since the hydrogen solubility in lithium at 300 $^\circ C$ is less than 1 % of the lithium number density [Borgstedt and Mathews, 1987]. In other words, molecular hydrogen recombination alone can no longer explain the hydrogen release process. Also, large amounts of solid LiH precipitation may have changed the state of the liquid lithium.

Other than the afore-mentioned problems, it is not desirable to operate the self-cooled lithium divertor in high recycling mode (i.e., when Li is filled with hydrogen) due to the resultant large tritium inventory. For example, the amount of tritium within a 5 m^2, 5 mm thick Li film reaches 10 kg at steady state conditions. Therefore, high recycling lithium divertors, applicable for a slowly moving lithium film over a solid plate, would be appealing only if the film can be made very thin (tens of microns) and thus tritium is limited to smaller quantities. On the other hand, an efficient external tritium separation process (if it exists) would limit the amount of tritium, and would also lead to low recycling conditions at the divertor plate. However, the availability of such technology is highly questionable, since the incoming rate of charged particles is as large as one mole per second.

The fact that lithium divertors have tritium inventory concern under steady

state ITER conditions also excludes the possibility of applying the lithium jet droplet beam divertor concept (see Figure III.4) and the lithium pool type divertor concept (see Figure III.3).

IV.D.b. Ga divertors

Gallium, on the other hand, has negligible hydrogen solubility when in contact with hydrogen gas [Galaktionowa, 1980]. In addition, its thermally most stable hydride, Ga_2H_6, is liquid at low temperature and decomposes at and beyond 130 $^\circ C$ into atomic hydrogen and Ga [Hurd, 1952]. Recall that the Ga divertor operational temperature range is between the melting point 29 $^\circ C$ and the temperature 750 $^\circ C$ corresponding to the allowed 10^{-5} to 10^{-4} $Torr$ (1.3 mPa to 13 mPa) Ga vapor pressure. Therefore, it is expected that the surface hydrogen molecular recombination coefficient K_f is fairly large, and thus the hydrogen concentration at the Ga surface is very low.

The hydrogen concentration at the stopping depth can be estimated as $C_p \approx J_{im}R_a/D \approx 10^{28}m^{-3}$ (see equation (IV.14)), if $D \sim 10^{-13}$ m^2/s as inferred from the data for Ga-eutectic (67% Ga, 20.5% In, 12.5% Sn) at around 400 $^\circ C$ [Begrambekov et al, 1987] and assumed applicable to the pure Ga. That is, unlike Li, the hydrogen release process is diffusion-limited in Ga. Since the volumetrically averaged hydrogen concentration is low, tritium inventory is not expected to be a concern for a self-cooled, high recycling gallium divertor.

The hydrogen recycling time at the Ga plate can be estimated as, $R_a^2/D \approx 10^{-3}s$ [Doyle, 1982]. This implies that the Ga plate stops absorbing hydrogen after a very short period of time. Thus, it is obvious that a Ga divertor is not suitable for low recycling operation under the steady state ITER-like power reactor conditions. In other words, there is simply no technology available that

can remove hydrogen from Ga at such efficiency as to make the Ga divertor operate in low recycling mode.

However, accumulation of hydrogen at the stopping depth may give rise to serious Ga film disruption and divertor chamber contamination due to the formation of hydrogen bubbles within the Ga and its subsequent eruptions. This issue will be addressed in Chapter V.

IV.E. Summary and Conclusions of Chapter IV

The main purpose of the this Chapter is to find the recycling coefficients (or more specifically, the hydrogen recycling time) of the liquid metal divertors, in order to facilitate the edge plasma modeling. It is discovered that lithium is hydrogen getter under steady state ITER conditions, namely, it takes fairly long time ($\sim O(10\ min)$) to saturate lithium with bombarding hydrogen ions. On the other hand, gallium is found not to be a hydrogen getter.

Thus, it appears that a lithium divertor might be operated either in low recycling mode to attain clean main plasma, or in varying recycling coefficient mode by controling the hydrogen concentration in lithium (which offers more engineering flexibility), if very efficient tritium removal technology is available (about one mole tritium per second from Li). However, since such technology does not exist, the lithium divertor (with fixed amount of lithium circulating) eventually will be operating in high recycling mode. Unfortunately, the resultant large tritium inventory makes this self-cooled high recycling lithium divertor undesirable. An alternative high recycling divertor concept might be a much thinner lithium film slowly moving over a coolant-cooled steel (or tungsten) plate. However, the change of lithium phase owing to hydrogen bombardment may be a concern. In addition, as will be shown in Chapter V, the blistering

erosion and subsequent contamination will pose threat to this concept too. It is also discovered that due to the excessive tritium inventory problem, the feasibilities of the lithium droplet beam divertor concept (see Figure III.4) and the lithium pool type divertor concept (see Figure III.3) are denied.

Gallium, on the other hand, is suitable for a self-cooled, high recycling divertor operation, without the concern of tritium inventory. This is because its hydrogen solubility is negligible and its hydride decomposes in the temperature range of interest. However, due to this same reason, unless special arrangement is made (see Chapter VII), the Ga divertor has to be operated in the naturally high recycling mode.

CHAPTER V. LIQUID METAL DIVERTOR PLATE EROSION AND MAIN PLASMA CONTAMINATION

V.A. Edge Plasma Simulation Results

From the conclusions of last Chapter, the liquid metal divertors of interest are the self-cooled, high recycling gallium (Ga) divertors (e.g., film, droplet curtain) and possibly a lithium film divertor with very thin lithium layer flowing slowly over a coolant-cooled steel (or tungsten) plate. The edge plasma modeling is carried out on these interested concepts in order to evaluate some aspects of their performance.

The general edge plasma model has been constructed in Chapter II. However, a point related to the liquid metals is worth mentioning here. That is, in constructing the representations for the energy loss mechanisms from electron-neutral and ion-neutral collisions, several semi-empirical formulas associated with solid materials are adopted. More specifically, the particle and energy reflection coefficients are approximated as

$$\begin{aligned} R_N &= 0.19 - 0.237 \cdot log_{10}(E_0/EL) \\ R_{Ei} &= 0.06 - 0.22 \cdot log_{10}(E_0/EL) \end{aligned} \qquad (V.1)$$

respectively, where E_0 is the incident D-T ion energy in eV, and

$$EL = \frac{(M_1 + M_2)(Z_1 Z_2)(Z_1^{2/3} + Z_2^{2/3})^{1/2}}{0.03255 M_2}\, eV \qquad (V.2)$$

with $M_{1,2}$ and $Z_{1,2}$ as the mass and atomic number of the incident particle and target atoms, respectively [Harrison, 1983].

The application of these relations to the liquid metals may be erroneous due to the liquid phase nature of the surface. This will require clarification

by future experiments. However, this approximation will be tolerable for our present purpose of estimation of liquid metal divertor performance.

The edge plasma simulation results are very general, independent of the type of liquid metal divertor such as protective film, droplet shower concept, etc. For the numerical calculations, the following parameters are employed: (a) Secondary electron emission coefficient $r_e = 0.3$, (b) No electron backscatter, $R_{Ee} = 0$, (c) The ion and electron temperatures are equal, $T_e = T_i$, (d) Thermal conduction fraction $u = 1$ (since high recycling), (e) Length of the divertor channel $L = 10\ m$, (f) Divertor channel cross-sectional area perpendicular to the magnetic field, $A_c = 0.35\ m^2$, (g) Heat load to one divertor (assuming one divertor per null point) is 70 MW under steady state ITER two-null plasma operation, (h) Helium sorption coefficient is zero, and the recycling coefficient of helium is 0.98.

Results of the simulation may not exactly reflect the situation of the final ITER reactor design due to the fact that both ITER physics and engineering parameters are still evolving. Numerical results thus obtained from solving the edge plasma model equations in Chapter II are compared with the case with tungsten divertor (the most sustaining among solid surface divertors) and illustrated in Table V.1. Note that the evaporation flux is specifically for a 2 mm thin film divertor as an example.

Note also that the employed recycling coefficient $R = 0.99$ is simply a typical example, in reality R can be higher or lower than this value. If it is the former case, then the helium ash removal will be a concern for ITER steady state operation. Namely, the main plasma will be quenched due to considerable radiation losses. This point will be further treated in Chapter VII.

The results in Table V.1 reveal that in terms of the capability to achieve

Table V.1

Comparison of Liquid Metal and Tungsten Plate Results

Under Steady State ITER Conditions

	Tungsten	Lithium	Gallium
R (given)	0.99	0.99	0.99
n_t (m^{-3}) (given)	$5.0{\cdot}10^{19}$	$5.0{\cdot}10^{19}$	$5.0{\cdot}10^{19}$
n_p (m^{-3})	$1.7{\cdot}10^{19}$	$2.0{\cdot}10^{19}$	$1.8{\cdot}10^{19}$
T_t (eV)	116.1	93.1	107.4
T_p (eV)	108.4	78.0	97.7
Γ_t $(m^{-2}s^{-1})$	$1.37{\cdot}10^{22}$	$1.55{\cdot}10^{22}$	$1.54{\cdot}10^{22}$
Γ_p $(m^{-2}s^{-1})$	$1.37{\cdot}10^{24}$	$1.55{\cdot}10^{24}$	$1.54{\cdot}10^{24}$
$A_c \int_t^p S_E\, dx$ (MW)	4.9	-16.2	-3.0
ionization & rad. loss (MW)	2.3	2.3	2.3
He radiation loss (MW)	0.03	0.06	0.06
CX loss (MW)	10.9	13.9	12.0
Q_{back} (MW)	18.2	0.1	11.4
sputter ionization loss (kW)	9.5	40.8	49.7
plate sputter yield	0.014	0.087	0.096
vapor pressure (Pa)	0.	$1.1{\cdot}10^{-4}$	$1.6{\cdot}10^{-14}$
evaporation rate $(m^{-2}s^{-1})$	—	$4.4{\cdot}10^{18}$	$2.1{\cdot}10^{8}$

Table V.2

Edge Plasma Results for Ga Droplet Shower (curtain) Divertor

Under Steady State ITER Conditions

(note: two divertor plates per null point)

R (given)	0.99
n_t (m^{-3}) (given)	$5.0 \cdot 10^{19}$
n_p (m^{-3})	$2.1 \cdot 10^{19}$
T_t (eV)	72.2
T_p (eV)	57.0
Γ_t $(m^{-2}s^{-1})$	$1.37 \cdot 10^{22}$
Γ_p $(m^{-2}s^{-1})$	$1.37 \cdot 10^{24}$
$A_c \int_t^p S_E \, dx$ (MW)	0.2
ionization & rad. loss (MW)	2.1
He radiation loss (MW)	0.06
CX loss (MW)	5.3
Q_{back} (MW)	7.3
sputter ionization loss (kW)	24.3
plate sputter yield	0.05
vapor pressure (Pa)	$1.6 \cdot 10^{-14}$

dense and cool edge plasmas, the saturated liquid metal divertors are better than tungsten divertors under the same ITER steady state conditions. This is mainly due to the fact that the selected liquid metals are not as massive as tungsten such that the backscattered powers to the divertor plasmas are not as significant. Nevertheless, the resultant edge plasma temperature may still be too high, which may cause material compatibility problems. Thus, employment of two liquid metal divertors, rather than one, for each null point, as in the droplet curtain divertor design [Murav'ev, 1989], may be more desirable. Results for this case, obtained by assuming that the divertor heat load now becomes 35 MW, is illustrated in Table V.2. Indeed, the temperatures at both the divertor throat and plate are reduced significantly, which results in a decrease of the physical sputtering yield by about a factor of two.

V.B. Evaporation and Availability of Vapor Shield

The most asked question with regard to the application of liquid metal divertors is the evaporation issue. From the results presented in Table V.1 and Table V.2, however, the liquid metal partial vapor pressures within the temperature range of interest are much lower than the acceptable vapor pressure of 10^{-4} $Torr$ (13 mPa), which may be recalled as being imposed by impurity level control (see Chapter IV, Section B). Besides, the average mean free path for these evaporated atoms is calculated to be only several millimeters before most of them suffer electron impact ionizations and are recycled back to the self-annealing liquid metal plate. Also, the possible depletion effect on the liquid metal plate caused by evaporation is negligible. That is, liquid metal evaporation is expected not to cause problems in the plate erosion or the main plasma contamination.

Since liquid metals evaporate, there is speculation that the vapor cloud in front of the liquid metal plate may provide another protection mechanism of the divertor system. Further, this accumulated vapor cloud may enhance density and temperature gradient forces near the divertor plate, which then reduces sputtering rate and blocks flight of liquid metal plate atoms into the main plasma [see, e.g., Dolan, 1982]. This issue can now be investigated.

The influence of this vapor cloud can be estimated from its stopping power of the flying charged particles or the backscattered flux. For this purpose, evaluation of the former will suffice. Take a lithium film divertor for example, which has much higher vapor pressure than Ga at the same temperature. The reduced energy EL (in eV) for the incident charged particles on the liquid metal vapor is given in equation (V.2). Since the incident energy ϵ_{in} is around 100 eV (in front of sheath edge), the so-called "Thomas-Fermi energy" (dimensionless) is $\epsilon_T = \epsilon_{in}/EL \approx 0.5$, which indicates that the relevant interaction is nuclear stopping [Behrisch, 1981]. The nuclear stopping power is defined as,

$$-\frac{dT}{dx} = n_{LM} S \qquad (V.3)$$

where $-\frac{dT}{dx}$ is in eV/cm, n_{LM} is the cloud liquid metal atomic number density, S is the nuclear stopping coefficient. The representation of S in $erg \cdot cm^2$ is given by [Behrisch, 1981]:

$$S = 4\pi a Z_1 Z_2 e^2 \left(\frac{M_1}{M_1 + M_2}\right) sn \qquad (V.4)$$

where $a = 0.468 \times 10^{-8}/(Z_1^{2/3} + Z_2^{2/3})^{1/2}$, e is in CGS unit (i.e. $e = 4.8 \times 10^{-10}$ esu), and sn is a correction variable and is about 0.3 at the Thomas-

Fermi energy of interest. S can be evaluated to be $3.2 \times 10^{-27}\ erg \cdot cm^2$. While n_{LM} is about $1.35 \times 10^{10}\ cm^{-3}$ from the lithium vapor pressure at $300°C$. Then, the stopping power can be estimated from equation (V.3) to be less than $3 \times 10^{-5}\ eV/cm$.

Therefore, it is obvious that the desired liquid metal protective vapor shield and other afore-mentioned good features do not exist under ITER steady state conditions. The situation under transient heat load due to major disruptions will be treated in Chapter VIII.

V.C. Sputtering

The formula used for evaluation of the physical sputtering effect on liquid metals is Smith et al's empirical formula [Smith et al, 1982], which fits experimental data for a wide range of atomic number Z among solid materials. The sputter yield Y (the average number of divertor plate atoms knocked out per incident charged particle) is,

$$Y = \frac{C_Y}{u_0} Z_1^{0.75} (Z_2 - 1.8)^2 \left(\frac{M_1 - 0.8}{M_2} \right)^{1.5} \frac{(E_0 - E_{th})}{[E_0 - E_{th} + 50 Z_1^{0.75} Z_2]^2} \qquad (V.5)$$

where C_Y is 2000 for H^+ ions, and is 400 for all other particles (here 2000 is used for more conservative estimation), u_0 is the liquid surface binding energy, and is approximated here as the liquid metal ionization energy; the sputter threshold energy is $E_{th} = u_0 \frac{(4M_1+M_2)^2}{4M_1M_2}$ in eV. For instance, the sputter threshold energy for lithium, gallium, and tungsten is 23 eV, 55 eV, and 164 eV, respectively.

The error associated with employing Smith et al's formula for the liquid metal targets is expected to be small due to the following facts: First, sputtering is an atomic scale process, which should not be too sensitive to the macroscopic

state of the target materials. Second, Smith et al's formula matches very well two theoretical formulas which are derived for general materials, i.e., formulas by Matsunami and Bohdansky (see, e.g., [Roth, 1984]), respectively. However, this sputtering issue of the liquid metals still awaits confirmation in the future liquid metal divertor experiments.

The edge plasma simulation results (see Table V.1) shows that the sputter yield of liquid metals is much larger than that of tungsten. This is because the selected liquid metal materials have lower masses and hence lower sputtering threshold energies. Even so, the average mean free path for the sputtered atoms is calculated to be at most several centimeters before most of them suffer electron impact ionizations or charge exchange and are recycled back to the self-annealing plate. The depletion and nonuniform redeposition of these sputtered atoms are thus not of concern for the flowing liquid metal divertors. (This is not the case for tungsten divertors.) In addition, the partial pressure of these sputtered atoms is evaluated to be at most on the order of 10^{-4} $Torr$ (13 mPa). Even if the sputtered atoms can be anomalously transported to the main plasma chamber, or, there is possible plasma flow reversal under high recycling condition, the selected liquid metals will not be as poisonous as the high Z tungsten.

V.D. Hydrogen Bubble Formation and Blistering Erosion

Accumulation of hydrogen at the stopping depth may give rise to serious liquid metal disruption and divertor chamber contamination due to the formation of hydrogen bubbles within the Ga and its subsequent eruption. In the following, only the Ga divertor will be considered, since the slowly flowing Li divertor (overlaying a coolant-cooled plate) will obviously have a blistering problem under the high particle flux condition.

The critical radius r_c of the bubble as it floats and then bursts can be estimated from a static balance of surface tension and buoyancy forces. The details of bubble shape calculations in this situation may be found in a paper by Wark [1933].

A simpler but analogous approach is adopted here (see Figure V.1). The horizontal plane that passes through the bubble center surface is denoted by A. The bubble shape above A is taken to be a hemisphere of radius r_c. The shape adjacent to A is taken to be a thin right circular cylinder of radius r_c. While it is true that momentum balances using this shape cannot be correct locally, the balances are satisfied on an integrated basis. p' denotes the pressure in the liquid metal outside the bubble, and p is the hydrogen pressure inside. The vertical downward force at the top of the bubble is $F = p'_A \pi r_c^2 - \rho g V$ [Wark, 1933], where V is the volume of the portion of the bubble being considered and is $V = (1/2)\ \frac{4}{3}\pi r_c^3$, and ρ is the liquid metal mass density. The vertical force balance on the bubble is, $F + 2\pi r_c \sigma_s = \pi r_c^2 p_A$. Horizontal equilibrium across the cylindrical shell is expressed by $p_A = p'_A + \frac{\sigma_s}{r_c}$. Combine these equations to obtain:

$$\frac{2\sigma_s}{r_c} \approx \frac{4}{3}\rho g r_c \qquad (V.6)$$

where $\sigma_s = 0.7\ N/m$ is the Ga surface tension, $\rho = 5720\ kg/m^3$ is the Ga mass density. Note that in equation (V.6) the effect of viscosity is not included. In this way, r_c can be calculated to be several millimeters.

In the following, all hydrogen is considered to be monatomic for simplicity, and effects of molecular hydrogen are taken to be negligible. The bubble growth can be modeled by,

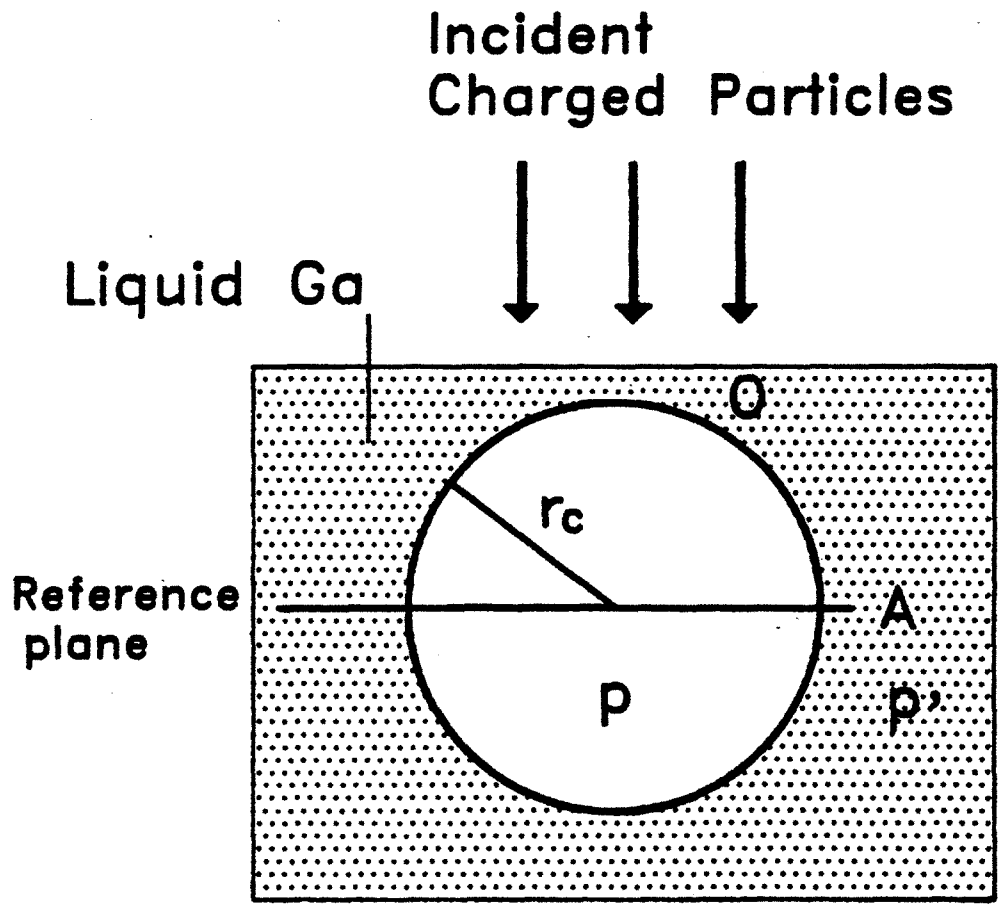

Figure V.1: A hydrogen bubble within the liquid metal

$$\frac{dp}{dt} = kT\frac{dn}{dt} = kT\frac{d}{dt}\frac{N}{V}$$
$$= \frac{kT}{V}\left(\frac{dN}{dt} - n\frac{dV}{dt}\right) \qquad (V.7)$$

where N is the instantaneous total number of hydrogen atoms within a bubble, $V = \frac{4}{3}\pi r^3$ is the bubble volume, $n = \frac{N}{V}$, and $p = nkT$ is the hydrogen pressure within the bubble, which is equal to $\frac{2\sigma_s}{r}$ in the static approximation. Therefore, $N = \frac{8\pi\sigma_s r^2}{3kT}$. Assuming $\frac{dN}{dt} \approx \pi r^2 J_{im}$, i.e., all implanted hydrogen is absorbed by the bubble, we get:

$$\frac{1}{r}\frac{dr}{dt} = \frac{3kT}{16\sigma_s}J_{im} \qquad (V.8)$$

Integration of equation (V.8) gives $r(t) = r_0 e^{t/\tau_d}$, where $\tau_d = \frac{16\sigma_s}{3kTJ_{im}} \approx 4\ ms$, and r_0 is the radius of the seeding bubble, and is recognized to be about 1 nm experimentally for a Ga-eutectic [Begrambekov et al, 1987]. If these numbers are adopted for pure-Ga, the time it takes for a bubble to grow to the critical size before eruption is about $0.02 \sim 0.06\ s$. This implies that the time period during which the circulating Ga plate is exposed to the charged particle bombardment should be made short enough, and as soon as the Ga fluid flows out of the exposure region, stirring or other separation procedure should be employed to enforce the liberation of hydrogen gas bubbles.

From this analysis it can be inferred that the afore-mentioned coolant-cooled slowly flowing lithium thin film divertor as well as the pool type divertor all suffer a more severe problem of blistering erosion, and hence will be excluded from the candidate ITER divertor list in the remainder of this work.

V.E. Unipolar Arc Erosion

One of the sources of contamination in plasma arises from the formation of arcs on divertor plates. Although arcs have been studied for over a century, the basic explanation for this phenomenon is still far from complete (see, e.g., [McCracken and Stott, 1979] and [Stangeby, 1984]). Experimentally, it is known that when a DC voltage is applied between two metal plates, about 1 cm apart, and with some gas present, a glow discharge is established characterized by anode-cathode voltages of several hundred to several thousand volts and currents of 10^{-12} to 10^{-1} A. The corresponding electron emission process is merely secondary electron emission caused by ion, photon and metastable atom impact on the usually cold cathode plate. Since the entire cathode tends to emit electrons, the current density is always low.

However, if there is an external circuit that permits the current to increase to about 1 A, then an entirely different phenomenon occur. Namely, suddenly the voltage required to sustain the discharge drops drastically to $\sim$ 10 V. In addition, the cathode emitting area collapses to a tiny spot, which results in current density of about $10^4 \sim 10^6$ A/cm^2. While this transition has been known experimentally for over a century and has been widely investigated, the basic processes are still not well understood. Usually, large quantities of the cathode material are eroded locally, typically $0.1 \sim 1$ atoms per emitted electron.

Since DC voltages are not generally applied between metallic components of fusion devices one might hope that such an undesirable process would not occur at the first wall, limiter or divertor. Unfortunately, this is not the case [McCracken and Stott, 1979] and arc tracks are widely observed in fusion devices and are associated with plasma contamination, especially for those at the first

wall and limiter. This type of arc is called the "unipolar arc", in which the metallic part serves as the cathode, while the edge plasma serves as the anode.

The unipolar arc phenomenon is illustrated in Figure V.2. Initially, the plate is at a floating potential ϕ_f (see Chapter II) and collects equal negative and positive particle currents. If an arc is triggered across the space-charge sheath between the plate and the plasma, the potential difference is reduced to the cathode voltage $\phi_c \approx -10\ V$. Since the repelling negative potential has dropped, more plasma electrons from the tail of the nearly Maxwellian probability density distribution of electrons (in velocity space) can now reach the plate. This additional electron current to the plate is balanced by the strongly localized emission of electrons from the arc cathode spot. Since the minimum current to sustain an arc is roughly 1 A, this implies that in order to collect this minimum arc circulation current, a minimum plate area is required. There is, therefore, speculation that breaking up (electrically) the surface of the plate into smaller subsurfaces may eliminate this undesirable phenomenon.

A crude quantitative explanation was given by Robson and Thonemann [1959] in terms of the plasma sheath theory and the empirical data on the arc voltage ϕ_c and the minimum arc current I_{min}. The float potential of the plate (before formation of an arc) is given by (in Chapter II),

$$\frac{e\phi_f}{kT_e} = 0.5\ ln\left[\left(2\pi\frac{m_e}{m_i}\right)\left(1+\frac{T_i}{T_e}\right)(1-r_e)^{-2}\right] \qquad (V.9)$$

where m_i is the average hydrogen ion mass, and $\phi_f < 0$ with respect to $\phi_{plasma} = 0$, and r_e is the secondary electron emission coefficient of the neutralizer plate. Both particle currents (i.e., ion and electron currents) from the plasma to the plate are given by,

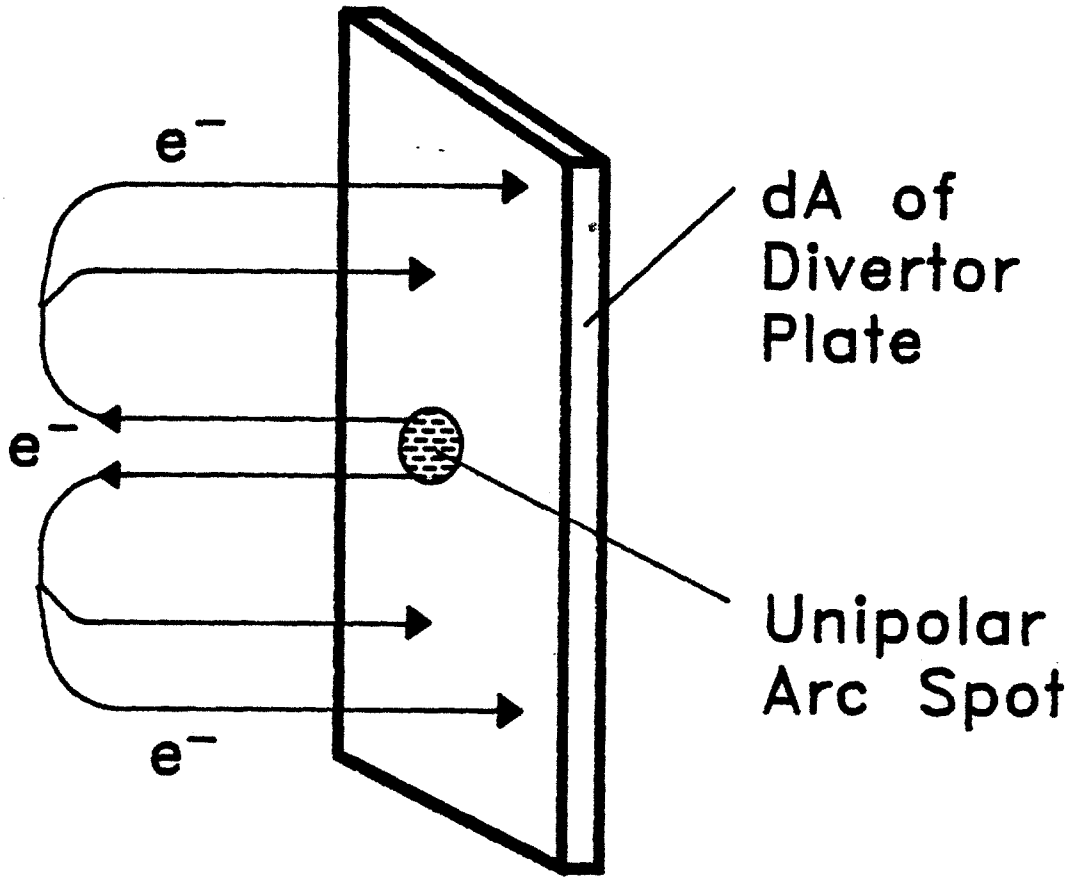

Figure V.2: Illustration of an Unipolar arc

$$-I^- = I^+_{sat} = J^+_{sat}A = \frac{1}{4}n_e\bar{v}eA\exp\left[\frac{e\phi_f}{kT_e}\right] \qquad (V.10)$$

where A is the area of the metal plate enclosing an arc spot, $\bar{v} = (8k_BT_e/\pi m_e)$ is the average speed of charged particles.

When the arc is initiated, the plate potential collapses to $\phi_c \approx -10\ V$ (i.e., no more $\phi = \phi_f \approx -3k_BT_e/e \approx -300\ V$ for ITER steady state divertor conditions). The ion (saturation) current remains essentially unchanged, but not the electron current. It becomes

$$I^- = \frac{1}{4}n_e\bar{v}eAe^{\frac{e\phi_c}{k_BT_e}} \qquad (V.11)$$

This makes the net current collected by the plate no longer zero. Instead,

$$I_{net} = \frac{1}{4}n_e\bar{v}eA\left[e^{\frac{e\phi_f}{k_BT_e}} - e^{\frac{e\phi_c}{k_BT_e}}\right] < 0 \qquad (V.12)$$

This is also the total electron current emitted from the arc spot.

Several indications can be drawn from equation (V.12). First, for the unipolar arc to occur $|\phi_f|$ must be larger than $|\phi_c| \approx 10\ V$. Therefore, from equation (V.9) it is clear that any plasma with temperature greater than about 3 eV supports unipolar arc. Second, for high density, high temperature plasma the minimum plate area required for the occurrence of unipolar arc is very small. For example, the edge plasma condition at an ITER tungsten or gallium divertor (i.e., $T_e \approx 100\ eV$, $n_e \approx 10^{19}\ m^{-3}$) implies the minimum required area is less than $10^{-6}\ m^2$. In other words, the problem of unipolar arc erosion is basically inevitable for any type of ITER divertors.

The minimum distance between arc tracks can be estimated conservatively as the square root of the minimum area, i.e., about several millimeters. This type of erosion is serious for the tungsten divertors under ITER reactor steady state conditions, as can be estimated by the following. As an upper bound assume that on one 20 m^2 tungsten divertor plate, about every 10^{-6} m^2 there is an arc centered in that small area (but occupies negligible area) with arc circulation current 1 A. Since the unipolar arc erosion rate for tungsten is around 0.032 *atoms/electron* [McCracken and Stott, 1979], the total tungsten yearly erosion rate per divertor is found to be nearly 40 tons. (Or about 10 cm thickness per year.) This is obviously an unrealistic number, since it required a total current equal to the total plasma current. However, the results can be taken as an indication that the unipolar arc may be a serious problem for the tungsten divertors.

However, it may not be so for the liquid metal divertors. That is, even though the number of atoms emitted per emitted electron at the arc spot is unknown, these emitted liquid metal atoms are expected to have very short range and are recycled back to the self-annealing liquid metal divertor surface. In case there are some small amount of emitted macroscopic particles, it is possible that the divertor chamber may be polluted, however, since this happens in the divertor region, direct contamination of the main plasma seems unlikely. Nevertheless, a concluding remark should not be made before future experimental proof is demonstrated.

In fact, for liquid metal divertors, the occurrence of unipolar arcs may result in favorable consequences due to the fact that the normal plasma sheath collapses into an "unipolar arc sheath" in which the plate voltage is only about 10 V (rather than around 150 V associated with the normal plasma sheath). This

means the physical sputtering, mainly enhanced by the acceleration of charged particles through normal sheath, is negligible. In other words, the average charged particle impact energy becomes less than the liquid metal sputtering thresholds (Ga: 55 eV; Li: 23 eV). (This is also true for tungsten divertor plate, however, other effects such as blistering erosion due to the large particle flux, or the arc erosion can still make its applicability very questionable.) Consequently, if this aspect of the unipolar arc phenomenon can be confirmed in the future experiments, the question of whether some fraction of the sputtered liquid metal atoms would leak into the main plasma chamber and cause detrimental effects, will become immaterial.

V.F. Summary and Conclusions of Chapter V

Based on the analytic edge plasma model developed in Chapter II, and the investigation of liquid metal-hydrogen interactions, a steady state edge plasma simulation is carried out for the liquid metal divertors in comparison with the tungsten divertor, under ITER steady state operational conditions. For a typical divertor recycling coefficient $R = 0.99$, the result shows that denser and cooler (but still very high temperature $\sim 100\ eV$) edge plasmas can be achieved by the liquid metal (Li and Ga) divertors than by the tungsten divertor. Note that, as a reminder, the Li divertor here refers to a very thin lithium layer (about hundreds of microns) slowly flowing over a coolant-cooled metal plate, since the thicker self-cooled Li divertor has tritium inventory problem. Note also that the recycling coefficient in reality may be different from the used $R = 0.99$. If $R > 0.99$ then problems may arise due to insufficient helium ash removal. However, since the edge plasma modeling results are not sensitive to the value of R as demonstrated in Chapter II, the engineering evaluations based on the

$R = 0.99$ edge plasma simulation results are still appropriate.

From the modeling results it is realized that in order to reduce the edge plasma temperature, the Russian droplet curtain divertor design seems more desirable. That is, instead of using a single long divertor for each null point (ITER is proposed to have two nulls, one on top, one at bottom), two shorter divertors are employed. This, according to the simulation results presented above, can reduce the edge plasma temperature to about 57 eV.

Some of the questions about the feasibility of applying liquid metals as divertor plate materials, i.e., evaporation and sputtering, turn out not to be serious ones. The liquid metal vapor pressures are far below the maximum neutral pressure in the divertor chamber limited by the impurity level control (see Chapter IV). For this same reason, it is also shown that there is no vapor shield in front of the divertor plate. While under the normal plasma sheath action (different from the unipolar arc sheath), the physical sputter yields of the liquid metals are larger than that associated with the tungsten. under the simulated steady state ITER edge plasma conditions. However, since the resultant neutral pressures are at most on the order of the maximum permissible neutral pressure ($\sim 10^{-4}$ $Torr$), these sputtered atoms are considered well confined near the divertor plate. In fact, it is expected that most of them will suffer electron impact ionization or charge exchange upon leaving the plate and are recycled back to the self-annealing liquid metal plate. If there is some fraction of these sputtered atoms that transport to the main plasma, the resultant detrimental effects are expected not to be as serious as those caused by the tungsten divertor.

The large bombarding charged particle flux of an ITER-like reactor poses severe threat on the lifetime of solid surface divertors through blistering erosion,

embrittlement and subsequent exfoliation. The concern relevant to the liquid metal divertors is the blistering erosion and divertor chamber contamination which result from the hydrogen bubble formation and eruptions within the liquid metals. It is found that if this phenomenon is to be avoided, the pumping speed of liquid metals will be very hard to achieve (i.e., on the order of 100 m/s), for a single long divertor at each null point. If two short divertors (each $10 \sim 20$ cm) are employed at each null point, then the pumping speed (about 10 m/s) can be achieved without difficulty, especially for the droplet curtain divertor concept. From this investigation, it is obvious that the slowly flowing Li divertor concept is not desirable. Therefore, in the subsequent Chapters, only Ga divertors will be discussed. For this same reason, any (stationary) pool type liquid metal divertors are expected to be not applicable.

Unipolar arc erosion appears to be a concern for the liquid metal divertors, particularly for the liquid Ga which is characterized by a low thermal conductivity (only about a quarter of that of tungsten). Indeed, it is estimated that this phenomenon will very likely occur at all ITER plasma contacting components, especially the divertors. Even though experimental data for the arc erosion rate of Ga is unavailable, it is expected that these emitted Ga atoms should have very short range under the high edge temperature environment and be recycled back to the self-recovering Ga plate. In case there is some emission of macroscopic particles, it is anticipated that even if the divertor chamber may be polluted by Ga droplets, the rendered detrimental effects on the main plasma may not be serious, since this does not occur close to the main plasma.

On the other hand, it may appear ironic that the occurrence of the unipolar arc phenomena be beneficial for the suppression of the physical sputtering on the divertor plates. Namely, when the unipolar arc is initiated, the divertor

plate voltage drops from about 150 V (under steady state ITER conditions) to 10 V. In other words, the normal plasma sheath is now replaced by the so-called "unipolar arc sheath". If this is proved to be true in future experiments, then the concern associated with the physical sputtering of divertor plates is essentially immaterial, for now the sputter threshold is no longer achieved by the average charged particles. As a comparison with the conventional solid surface divertors, even if this can be beneficial for the liquid Ga divertor, this is not the case for the tungsten divertor, since the latter still suffers severe threats from other physical processes such as the arc erosion and the blistering erosion.

CHAPTER VI. MHD FLOW AND HEAT TRANSFER

VI.A. Introduction

As concluded from last Chapter, liquid lithium is not considered as a favorable liquid metal divertor surface material. Therefore, from here on, only the liquid gallium (Ga) divertors will be discussed, particularly, the self-cooled Ga protective film divertor (see Figure III.2) and the self-cooled Ga droplet shower (curtain) divertor (see Figure III.5). In this Chapter, these two divertor concepts will be evaluated, respectively, according to their MHD (magnetohydrodynamic) behavior (including MHD equilibrium, stability and pumping power requirement) as well as their heat transfer capability.

As can be expected, the MHD effects pose more threat to the applicability of the protective film divertor than the droplet shower concept. This is because the continuous liquid metal film facilitates the flow of the induced current which in turn interacts with the imposed magnetic field and complicates the liquid metal flow behavior. For this reason, much of this Chapter will be devoted to the MHD effects associated with the self-cooled film divertor.

Investigations of the MHD behavior in this specific geometric and magnetic field configuration of the film divertor have only started recently. The equilibrium analysis was pioneered by Aitov et al [1987], and Murav'ev [1988]. While the stability analysis was only performed by Aitov et al [1988]. In the latter work, liquid metal surface tension was found to be a major factor that determines the MHD stable operational regime for the film divertors.

However, there are limitations in the afore-mentioned stability analysis [Aitov et al, 1988]. First, the equilibrium velocity profile employed in their stability

analysis is not consistent with the one obtained in the corresponding equilibrium analysis [Aitov et al, 1987]. That is, the equilibrium liquid metal flow rate used in this stability analysis is governed by the combined effects of the magnetic field strength, the chute inclination angle (gravity), and the chute width, rather than being controlled by the external pump (either to meet the heat removal requirement or to avoid blistering erosion). The equilibrium and stability analyses do not therefore correspond to the same situation.

Second, the liquid metal surface tension while an important force for short wavelength perturbations, is not expected to be significant in suppressing the long wavelength (compared with the film thickness of several millimeters) perturbations, as can be demonstrated later by the successive approximation of the perturbation equation. Accordingly, the stability criterion obtained by Aitov et al [1988] does not address this class of perturbations. In addition, when the magnetic field is removed, their result does not reduce to existing solutions for the unmagnetized case [Benjamin, 1957; Yih, 1963].

Third, the possible effects of the plasma charged particle bombardment and the sheath action on the free surface of the liquid metal film were not discussed. It has been suspected that sheath potential may cause Rayleigh-Taylor instability of the liquid metal film (see, for example, [Vladimirov, 1987]).

In order to understand the response of the pumped liquid metal film to perturbations around the equilibrium condition, an effort similar to Aitov et al [1987] [1988] is made, but taking into consideration the above mentioned points.

Section VI.B is devoted to the physics of plasma-film interaction and the derivation of the MHD model equations. The dominant force acting on the free surface of the film is identified.

In Section VI.C, the equilibrium solution is presented and the film thickness

evolution along the non-conducting chute is illustrated by an example of a gallium (Ga) film divertor associated with the ITER fusion reactor design [Post et al, 1991]. The feasibility of employing an electrically conducting chute is also discussed.

The stability criterion is obtained by a successive approximation technique in Section VI.D. Then, the heat transfer and MHD stability issues of the droplet curtain divertor concept are investigated and presented in Section VI.E. While the MHD pressure drop and the corresponding liquid metal pumping power requirement are estimated for both the film and droplet shower divertor concepts in Section VI.F. Finally, summary and conclusions are presented in Section VI.G.

VI.B. Plasma-Film Interaction and MHD Model Equations

VI.B.a. Combined effects of charged particle bombardment and sheath action

A liquid metal immersed in the divertor plasma develops a negative potential (i.e., the sheath potential) with respect to the divertor plasma. A so-called "plasma sheath" forms very near the film surface within which the ion density exceeds the electron density. The incident charged particles (electrons and ions) along the toroidal magnetic field reach this sheath edge at the ion acoustic speed in order to satisfy the Bohm sheath criterion [Stangeby, 1984]. Crossing the sheath potential drop, the ions are accelerated so that they strike the film surface at nearly normal incidence.

From the above picture, two types of pressures imposed by the plasma on the liquid metal free surface can be identified, namely, the particle bombarding pressure and the effective "negative pressure" exerted by the electrostatic field

which attempts to pull the negatively charged liquid metal surface into the plasma. In order to examine the possibility for film instability, the net surface pressure needs to be determined.

The ion dynamics at equilibrium within the sheath can be described by,

$$mv\frac{d}{dx}v = -e\frac{d}{dx}\phi(x) \qquad (VI.1)$$

where m, v, ϕ are the ion mass, ion velocity (in x direction), electric potential, respectively. x is in the direction perpendicular to the film surface. This implies that within the sheath,

$$\frac{1}{2}mv(x)^2 + e\phi(x) = const. \qquad (VI.2)$$

At the sheath edge, we define $v(x_s) = v_s$, $\phi(x_s) = 0$. Therefore, we have $v(x) = [v_s^2 - 2e\phi(x)/m]^{\frac{1}{2}}$, where v_s is the ion velocity at the sheath edge and is equal to the ion acoustic velocity, $[2k_BT/m]^{\frac{1}{2}}$, when $T_e = T_i = T$. In addition, the ion current density can be assumed to be uniform across the sheath, i.e.,

$$J_i = n_i(x)v_i(x) \approx n_s v_s \approx const. \qquad (VI.3)$$

The representation for the negative pressure (due to sheath pulling action) can be derived through Poisson's equation,

$$\begin{aligned}\frac{d^2}{dx^2}\phi(x) &= -\frac{e}{\epsilon_0}(n_i - n_e) \\ &\approx -\frac{e}{\epsilon_0}n_i \\ &= -\frac{e}{\epsilon_0}J_i[v_s^2 - \frac{2e\phi(x)}{m}]^{\frac{-1}{2}}\end{aligned} \qquad (VI.4)$$

where the electron contribution has been neglected for simplicity without introducing much error. Multiplying equation (VI.4) by $\frac{d}{dx}\phi$ and then integrating from sheath edge to x, the following result emerges,

$$(\frac{d}{dx}\phi(x))^2 = \frac{2J_i}{\epsilon_0} m v_s [(1 - \frac{2e\phi(x)}{mv_s^2})^{\frac{1}{2}} - (1 - \frac{2e\phi_s}{mv_s^2})^{\frac{1}{2}}] \qquad (VI.5)$$

where $(\frac{d}{dx}\phi)_s \approx 0$ is assumed. Utilizing equation (VI.3) and the fact that film potential $e\phi_w \approx -3k_BT$ for hydrogen plasmas with respect to $\phi_{plasma} \approx \phi_s \approx 0$, we have $(\frac{d}{dx}\phi)_w^2 \approx \frac{2n_s m v_s^2}{\epsilon_0}$. Therefore, the negative pressure on the film surface P_{Ew} can be evaluated as:

$$\begin{aligned} P_{Ew} &= \frac{\epsilon_0 E^2}{2} \\ &= \frac{\epsilon_0}{2}(\frac{d}{dx}\phi)_w^2 \\ &= n_s m v_s^2 \\ &= 2n_s k_B T \end{aligned} \qquad (VI.6)$$

where the negative pressure is equal to the electric energy density within the sheath, as can be derived by the technique of false displacement.

The particle bombarding pressures at the sheath edge and at film surface are $P_{ns} = n_s m v_s^2 = 2n_s k_B T$, and $P_{nw} = n_w m v_w^2$, respectively. Since $v_w^2 = v_s^2 - 2e\phi_w/m = 8k_BT/m$, and thus $n_w = J_i/v_w = n_s v_s/v_w = n_s/2$, where k_B is the Boltzmann constant, we have

$$P_{nw} = 4n_s k_B T \qquad (VI.7)$$

Together with equation (VI.6),

$$P_{nw} - P_{Ew} = P_{ns} = 2n_s k_B T > 0 \qquad (VI.8)$$

Therefore, the particle bombarding pressure dominates the pulling pressure, and there is no external free energy that can give rise to the Rayleigh-Taylor type of instabilities in the film flow system. In other words, plasma always tends to suppress perturbations on the film free surface. This also facilitates our treatment formally of the film MHD equilibrium and stability, since, from here on, the net effect of plasma on the film can simply be represented by a pressure P_a.

VI.B.b. Liquid metal film MHD model

The physical configuration of the liquid metal film system is illustrated in Figure III.2, in which the almost coplanar magnetic field B is approximately uniform along the non-conducting chute (or metal chute with non-conducting coating in contact with the liquid metal). The liquid metal flow can be divided into three parts, i.e., the core, Hartmann layers at side walls ($z = \pm b/2$), and Hartmann layer at chute bottom ($y = 0$). For the case of interest in which the Hartmann layer thickness $\sim \frac{1}{B}\sqrt{\frac{\rho\nu}{\sigma}}$ [Shercliff, 1965] is much smaller than the chute width b or the film thickness h, the film MHD model for non-conducting chute can thus be reduced to the treatment of the flow core with proper boundary conditions [Aitov et al, 1988]. The z dependence of quantities interested is not expected significant and hence will be neglected in the following. The model equations are:

continuity

$$\frac{\partial}{\partial x} j_x + \frac{\partial}{\partial y} j_y = 0$$
$$\frac{\partial}{\partial x} u + \frac{\partial}{\partial y} v = 0 \qquad (VI.9)$$

where $\vec{v} = (u, v, 0)$ and $\vec{j} = (j_x, j_y, 0)$ are assumed within the incompressible liquid metal flow core. Also, the low frequency MHD approximation has been made.

momentum

in the x direction (along the chute),

$$\frac{\partial}{\partial t} u + u \frac{\partial}{\partial x} u + v \frac{\partial}{\partial y} u = -\frac{1}{\rho} \frac{\partial}{\partial x} p + \nu \bigtriangledown^2 u + g \sin\theta + \frac{j_y B}{\rho} \qquad (VI.10)$$

in the y direction (perpendicular to the film surface),

$$0 \approx -\frac{1}{\rho} \frac{\partial}{\partial y} p - g \cos\theta - \frac{j_x B}{\rho} \qquad (VI.11)$$

where ρ is the liquid metal mass density, g is the gravitation acceleration, $j_{x,y}$ is the current density in x or y direction, B is the toroidal magnetic field strength, ν is the kinematic viscosity, and θ is the inclination angle of the chute.

boundary conditions

at $y = 0$

$$u = v = 0 \qquad (VI.12)$$

at $y = h(x,t)$

$$p = -\sigma_s \frac{\partial^2 h}{\partial x^2} + p_a \qquad (VI.13)$$

$$j_y = j_x \frac{\partial}{\partial x} h \qquad (VI.14)$$

$$\frac{\partial}{\partial x} v + \frac{\partial}{\partial y} u = 0 \qquad (VI.15)$$

where $h(x,t)$ is the thickness of the flowing film.

Both Maxwell's equations and Ohm's law are omitted in the model, since in this treatment the Lorentz force terms can be eliminated after the combination of equations (VI.10) and (VI.11). However, this implies that both Maxwell's equations and Ohm's law are satisfied.

In the continuity equation, incompressibility is assumed for the liquid metals. In the y component of the momentum equation, the so-called "shallow water approximation" is employed since from equation (VI.9), $v \sim \delta u$, where $\delta = h/L << 1$, and L is the characteristic length along the flow direction. For the film flow of interest, this only leads to an error of the order δ^2. equation (VI.13) accounts for the normal stress balance at the plasma-liquid metal interface. Equation (VI.14) means the normal component of the current density is always zero at the surface. Equation (VI.15) states that the shear stress at the free surface is negligible. Note that equations (VI.13) to (VI.15) are all accurate to $O(\delta)$.

In the strong toroidal magnetic field, the gradient of the film physical quantities along the field line (z axis) is much smaller than that along or perpendicular (y direction) to the flow. It is therefore convenient to integrate the model equations over the chute width b (along z axis) [Aitov et al, 1987],

i.e., $< \xi > \equiv \frac{1}{b}\int_{-b/2}^{b/2} \xi(x,y,z)dz$. This is accomplished by assuming the velocity profile $f(z)$ along the z axis to be $f(z) = 1 - \exp[Ha(|z/b| - 1/2)]$ [Aitov et al, 1987], where $Ha = Bb\sqrt{\sigma/\rho\nu}$ is the Hartmann number, and σ is the liquid metal electrical conductivity. The model equations can be averaged to become (neglecting the $< >$ notation for convenience):

$$\begin{aligned} \frac{\partial}{\partial x}j_x + \frac{\partial}{\partial y}j_y = 0 \\ \frac{\partial}{\partial x}u + \frac{\partial}{\partial y}v = 0 \end{aligned} \qquad (VI.16)$$

$$\frac{\partial}{\partial t}u + u\frac{\partial}{\partial x}u + v\frac{\partial}{\partial y}u = -\frac{1}{\rho}\frac{\partial}{\partial x}p + \nu\frac{\partial^2 u}{\partial y^2} - \Lambda u + g\sin\theta + \frac{j_y B}{\rho} \qquad (VI.17)$$

$$0 \approx -\frac{1}{\rho}\frac{\partial}{\partial y}p - g\cos\theta - \frac{j_x B}{\rho} \qquad (VI.18)$$

In equation (VI.17), the term $\nu\frac{\partial^2 u}{\partial x^2}$ has been neglected, and $\Lambda = (2B/b)\sqrt{\sigma\nu/\rho}$ is a measure of the resistance to film motion due to the Hartmann velocity profile at the chute side walls. Note that if each quantity is expressed in the form $\xi =< \xi > + d\xi$, in the above equations, terms involving $< d\xi d\xi >$ are discarded.

To further simplify the equations, integrate equation (VI.18) along the height (thickness) from y to h. We have,

$$p(x,y) = p_a(x) - \sigma_s\frac{\partial^2 h}{\partial x^2} + \rho g\cos\theta(h-y) + B\int_y^h j_x dy' \qquad (VI.19)$$

Plugging the last expression into equation (VI.17), and utilizing equations (VI.14) and (VI.16), the following result emerges,

$$\frac{\partial}{\partial t}u + u\frac{\partial}{\partial x}u + v\frac{\partial}{\partial y}u = \frac{\sigma_s}{\rho}\frac{\partial^3 h}{\partial x^3} - g\cos\theta\frac{\partial}{\partial x}h + g\sin\theta + \nu\frac{\partial^2 u}{\partial y^2} - \Lambda u + \frac{1}{\rho}\frac{\partial}{\partial x}p_a \qquad (VI.20)$$

Note that at this stage it is realized that the plasma effect enters the momentum equation (VI.20) in the form of derivative and is negligible in most locations along the chute compared with other terms in the same equation under the divertor conditions of interest.

For the accuracy of numerical calculation and the convenience of later successive expansion with respect to the small perturbation wave number of interest, it is beneficial to normalize the model equations. That is, with h_{in} and u_{in} as the controled initial thickness and speed of the liquid metal film, we have $h = \bar{h}h_{in}$, $x = \bar{x}h_{in}$, $y = \bar{y}h_{in}$, $u = \bar{u}u_{in}$, $v = \bar{v}u_{in}$, $t = \bar{t}t_*$, $\Lambda = \bar{\Lambda}\Lambda_* = \bar{\Lambda}t_*^{-1}$, where $t_* \equiv h_{in}/u_{in}$. The model equations after normalization are

$$\frac{\partial}{\partial \bar{t}}\bar{u} + \bar{u}\frac{\partial}{\partial \bar{x}}\bar{u} + \bar{v}\frac{\partial}{\partial \bar{y}}\bar{u} = -\frac{\cos\theta}{Fr^2}\frac{\partial}{\partial \bar{x}}\bar{h} + \frac{We}{Fr^2}\frac{\partial^3 \bar{h}}{\partial \bar{x}^3} + \frac{1}{Re}\frac{\partial^2 \bar{u}}{\partial \bar{y}^2} - \bar{\Lambda}\bar{u} + \frac{\sin\theta}{Fr^2} \qquad (VI.21)$$

$$\frac{\partial}{\partial \bar{x}}\bar{u} + \frac{\partial}{\partial \bar{y}}\bar{v} = 0 \qquad (VI.22)$$

$$\bar{u}(0) = \bar{v}(0) = 0 \qquad (VI.23)$$

$$\frac{\partial}{\partial \bar{x}}\bar{v} + \frac{\partial}{\partial \bar{y}}\bar{u} = 0 \qquad (VI.24)$$

where $Fr = (\frac{u_{in}^2}{gh_{in}})^{1/2}$ is the Froude number, $Re = \frac{q}{\nu}$ is the Reynolds number, with $q \equiv u_{in}h_{in}$ the fixed liquid metal flow rate per unit width of the chute, and $We = \frac{\sigma_s}{\rho g h_{in}^2}$ is the Weber number.

VI.C. MHD Equilibrium, Film Thickness Evolution and Heat Transfer

VI.C.a. Film MHD Equilibrium

For equilibrium calculation ($\frac{\partial}{\partial t}u = 0$), the surface tension term in equation (VI.21) can be neglected, since the third derivative of the film thickness along x axis is very small (i.e., several millimeter film thickness change per meter traveled). The $\frac{\partial}{\partial \bar{x}}\bar{v}$ term in equation (VI.24) can also be ignored since it is much smaller than $\frac{\partial}{\partial \bar{y}}\bar{u}$. Using equation (VI.22), the left hand side of equation (VI.21) can be written as $\frac{\partial}{\partial \bar{x}}\bar{u}^2 + \frac{\partial}{\partial \bar{y}}\bar{u}\bar{v}$. Then, after integrating equation (VI.21) from 0 to $\bar{h}$, applying equation (VI.24), and recognizing that $\bar{v}(h) = 0$, we have

$$\frac{\partial}{\partial \bar{x}}\int_0^{\bar{h}_0} \bar{u}_0^2 d\bar{y} + \bar{h}_0 \frac{\cos\theta}{Fr^2}\frac{\partial}{\partial \bar{x}}\bar{h}_0 + \frac{1}{Re}\frac{\partial}{\partial \bar{y}}\bar{u}_0(0) + \bar{\Lambda}\int_0^{\bar{h}_0}\bar{u}_0 d\bar{y} - \bar{h}_0\frac{\sin\theta}{Fr^2} = 0 \qquad (VI.25)$$

where the subscript "0" denotes the condition at equilibrium.

The parabolic velocity profile of $\bar{u}_0$ is assumed to be $\bar{u}_0(\bar{y}) = A_0\bar{y}^2 + B_0\bar{y} + C_0$ [Aitov et al, 1987]. After matching the boundary condition at the chute bottom and then plugging in $\int_0^{\bar{h}_0}\bar{u}_0 d\bar{y} = \frac{q}{u_{in}h_{in}} = 1$, where $q = u_{in}h_{in}$ is the chosen constant flow rate per unit chute width, the following is obtained,

$$\bar{u}_0(\bar{x},\bar{y}) = -\frac{3}{2\bar{h}_0(\bar{x})^3}\bar{y}^2 + \frac{3}{\bar{h}_0(\bar{x})^2}\bar{y} \qquad (VI.26)$$

Then, after substituting equation (VI.26) in equation (VI.25), the film thickness evolution equation emerges,

$$\frac{d\bar{h}_0(\bar{x})}{d\bar{x}} = \frac{\frac{\bar{h}_0^3}{Fr^2}\sin\theta - \bar{h}_0^2\bar{\Lambda} - \frac{3}{Re}}{\frac{\bar{h}_0^3}{Fr^2}\cos\theta - \frac{6}{5}} \qquad (VI.27)$$

where b is the chute width.

The stationery thickness $\bar{h}_{eq}$ is defined as the value of equilibrium thickness $\bar{h}_0$ at which the numerator of equation (VI.27) vanishes; while the critical thickness $\bar{h}_c$ is the value at which the denominator vanishes. The critical thickness is the point to avoid, since even operating near it may cause the flow to flood. That is, under fixed flow rate, the film thickness becomes so large that the flow speed reduces to the extent that the requirement of either the heat transfer or the blistering erosion is no longer met.

Furthermore, if $\bar{h}_{eq} > \bar{h}_c$, the equilibrium point is unstable, and the film thickness grows rapidly along the chute. Only when $\bar{h}_{eq} << \bar{h}_c$ all along the flow will the stationery point be an attracting one [Morley et al, 1991]. The operation of liquid metal film divertors of interest happens to fall in the latter category.

If the chute is electrically conductive, the net electromagnetic body force on the liquid metal film is no longer zero. The equilibrium thickness of the liquid metal film has to satisfy [Aitov et al, 1987]

$$h_{eq}g\sin\theta - \frac{3q\nu}{h_{eq}^2} - (\Lambda + \Lambda_\epsilon)q = 0 \qquad (VI.28)$$

where $\Lambda_\epsilon = \frac{2\epsilon_w B^2\sigma}{\rho}$ (note that the expression in Aitov et al's work [1987] $\Lambda_\epsilon = 2\epsilon_w B^2\sigma$ is wrong). Λ_ϵ is the conducting chute effect, where $\epsilon_w \equiv \frac{\sigma_w b_w}{\sigma b}$

is the so-called "wall conductance ratio", in which σ_w, b_w are the electrical conductivity and the thickness of the side walls of the conducting chute.

In general, Λ_ϵ (due to the net $J \times B$ effect) is several orders of magnitude greater than Λ (due to the Hartmann layer effect), for ordinary metal substrates. Thus, a conducting chute will lead to an equilibrium film thickness of several tens of centi-meters, and is not desirable. It may appear that employing a conducting chute of larger width can reduce the equilibrium film to the desired thickness. Indeed, it is. However, the resultant chute width becomes too large (several tens of meters) to be favored in the divertor system. Therefore, in the following analysis, only the film divertors with non-conducting chutes will be considered.

VI.C.b. Liquid gallium film heat transfer

The heat transfer capability of the self-cooled liquid Ga divertors of interest can be evaluated as follows. In order to carry away the ITER divertor heat load (70 MW per divertor, if assuming one divertor per null point), the following power balance equation needs to be satisfied:

$$P_d \approx \rho(h_{in} \cdot 2\pi R_c) u_{in} c_p \Delta T$$

where P_d (=70 MW) is the power dumped on the divertor plate, ρ and c_p are the mass density and the heat capacity of gallium within the temperature range of interest, R_c is the major radius of the divertor position, and ΔT is the temperature window for gallium operation (about $600°C - 50°C = 550°C$). It can be calculated that the inlet speed of the Ga film (5 mm thick) needed to convey the divertor heat load is less than 0.5 m/s. Nevertheless, in order to take into account the effect of nonuniform heat load, it may be safer to

set the liquid metal speed at about 1 m/s. Therefore, it is obvious that the heat transfer requirement on the Ga film pumping speed can be met without difficulty. An example of the Ga film thickness evolution, which meets the heat transfer requirement, is illustrated in Figure VI.1 through numerical integration of equation (VI.27).

VI.D. Film MHD Stability

In the unmagnetized environment, the liquid metal film of interest is always hydrodynamically unstable. This can be deduced from the classical result that the film flow is unstable when $Re > \frac{5}{6}\cot\theta$, and that Re of interest is much larger than unity. However, it is suspected that the toroidal magnetic field at divertor position may stabilize these perturbations to the flowing liquid metal film. An analytic work on MHD stability is thus carried out.

The driving free energy for the possible instability is the equilibrium velocity profile $\bar{u}(\bar{y})$, characteristic of the Helmholtz type hydrodynamic instabilities. The unmagnetized case for gravity driven flows over inclined chutes has already been solved [Benjamin, 1957; Yih, 1963]. The case of interest is for the pumped film flows with coplanar magnetic field.

Perturbing each physical quantity ξ around the equilibrium value in the MHD model equations, i.e., $\xi = \xi_0 + \xi_1$, where $|\xi_1| << |\xi_0|$, gives the linearized equations,

$$\frac{\partial}{\partial\bar{t}}\bar{u}_1 + \bar{u}_0\frac{\partial}{\partial\bar{x}}\bar{u}_1 + \bar{v}_1\frac{\partial}{\partial\bar{y}}\bar{u}_0 = -\frac{\cos\theta}{Fr^2}\frac{\partial}{\partial\bar{x}}\bar{h}_1 + \frac{We}{Fr^2}\frac{\partial^3\bar{h}_1}{\partial\bar{x}^3} + \frac{1}{Re}\frac{\partial^2\bar{u}_1}{\partial\bar{y}^2} - \bar{\Lambda}\bar{u}_1 \qquad (VI.29)$$

$$\frac{\partial}{\partial\bar{x}}\bar{u}_1 + \frac{\partial}{\partial\bar{y}}\bar{v}_1 = 0 \qquad (VI.30)$$

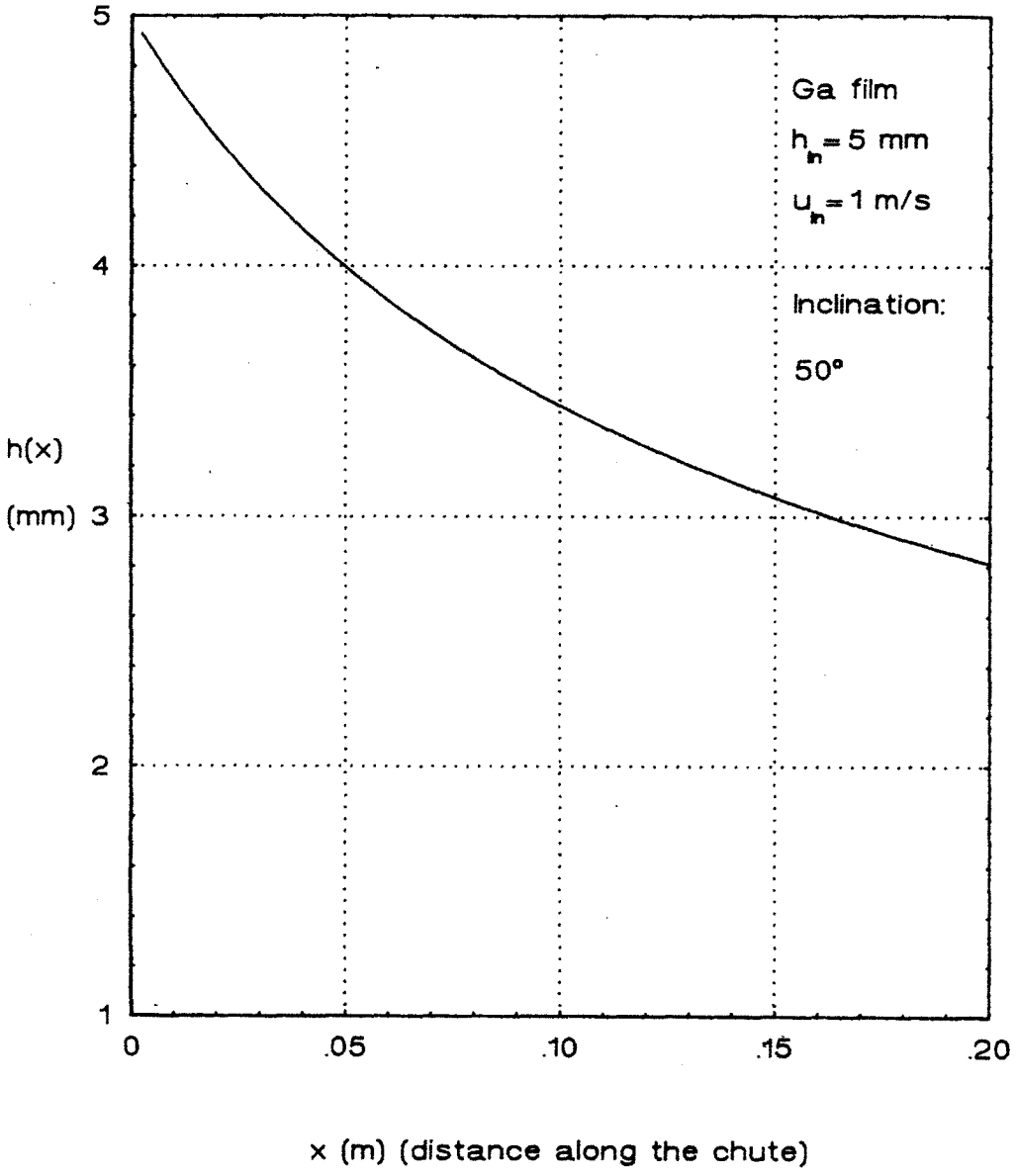

Figure VI.1: Liquid Ga film thickness evolution along the chute

Equation (VI.30) suggests the introduction of a "stream function" $\bar{\psi}_1$, i.e., $\bar{\psi}_1 = \bar{\phi}_1(\bar{y})\exp[i\bar{k}(\bar{x} - \bar{v_p}\bar{t})]$, such that $\bar{u}_1 = \frac{\partial}{\partial \bar{y}}\bar{\psi}_1$ and $\bar{v}_1 = -\frac{\partial}{\partial \bar{x}}\bar{\psi}_1 = -i\bar{k}\bar{\psi}_1$, where $i = \sqrt{-1}$, $\bar{v_p} \equiv \bar{\omega}/\bar{k}$ is the normalized phase velocity of the perturbing wave, and ω is its frequency (in general a complex variable).

$\bar{h}_1$ in equation (VI.29) can be eliminated by applying the full time derivative on $\bar{y} = \bar{h}(\bar{x}, \bar{t})$ at the film surface such that

$$\bar{v}_1(\bar{y} = \bar{h}_0) = i\bar{k}\bar{u}_0\bar{h}_1 - i\bar{k}\bar{v_p}\bar{h}_1$$

or

$$\bar{h}_1 = \frac{\bar{v}_1(\bar{y} = \bar{h}_0)}{i\bar{k}(\bar{u}_0(\bar{h}_0) - \bar{v_p})} = \frac{-\bar{\psi}_1(\bar{y} = \bar{h}_0)}{\bar{u}_0(\bar{h}_0) - \bar{v_p}} \qquad (VI.31)$$

Therefore, equation (VI.29) becomes,

$$\begin{aligned} &i\bar{k}(\bar{u}_0(\bar{y}) - \bar{v_p})\bar{\phi}_1' - i\bar{k}\bar{\phi}_1 \cdot [\bar{u}_0'] \\ &\qquad = \frac{\cos\theta}{Fr^2}\frac{i\bar{k}\phi_1(\bar{h}_0)}{\bar{u}_0(\bar{h}_0) - \bar{v_p}} + i\bar{k}^3\frac{We}{Fr^2}\frac{\bar{\phi}_1(\bar{h}_0)}{\bar{u}_0(\bar{h}_0) - \bar{v_p}} \\ &\qquad + \frac{1}{Re}\bar{\phi}_1''' - \bar{\Lambda}\bar{\phi}_1' \end{aligned} \qquad (VI.32)$$

where the prime stands for $\frac{\partial}{\partial \bar{y}}$.

The boundary condition at the chute bottom (equation (VI.23)) gives

$$\bar{\phi}_1'(0) = \bar{\phi}_1(0) = 0 \qquad (VI.33)$$

While substituting $\bar{u} \approx \bar{u}_0 + \bar{h}_1\frac{\partial}{\partial \bar{y}}\bar{u}_0 + \bar{u}_1$ into the surface shear stress balance equation (VI.24), we have

$$\bar{\phi}_1''(\bar{h}_0) + \frac{3}{\bar{h}_0^3(\bar{x})} \frac{1}{(\bar{u}_0(\bar{h}_0) - \bar{v}_p)} \bar{\phi}_1(\bar{h}_0) + \bar{k}^2 \bar{\phi}_1(\bar{h}_0) = 0 \qquad (VI.34)$$

Equations (VI.32), (VI.33), and (VI.34) are the formulas that the following successive expansion technique will be applied upon to search for the stable operational regime for the pumped liquid metal film divertors. That is, for a given perturbation wave number $\bar{k}$ (real number), the unstable operational conditions can be identified when the resultant $\bar{v}_p$ has possible positive imaginery part.

The coplanar magnetic field tends to suppress the buildup of perturbing waves. Since it has been proven that short wavelength (comparable to the film thickness) perturbations are stabilized by the liquid metal surface tensile force alone, the following analysis will be aimed at the long wavelength case, i.e., $\bar{k} \equiv k h_{in} = 2\pi \frac{h_{in}}{\lambda} \to 0$, where λ is the perturbation wavelength along the flow direction.

Thus $\bar{\phi}_1$ can be expanded over the powers of $\bar{k}$,

$$\bar{\phi}_1(\bar{y}) = \bar{\phi}_{10} + \bar{k}\bar{\phi}_{11} + \bar{k}^2 \bar{\phi}_{12} + \cdots \qquad (VI.35)$$

which then is substituted in equations (VI.32), (VI.33), and (VI.34) to examine the stability problem order by order.

$\bar{k}^0$ Order

The resulting equations are given by:

$$\bar{\phi}_{10}'''(\bar{y}) - M^2 \bar{\phi}_{10}'(\bar{y}) = 0 \qquad (VI.36)$$

$$\bar{\phi}_{10}'(0) = \bar{\phi}_{10}(0) = 0 \qquad (VI.37)$$

$$\bar{\phi}''_{10}(\bar{h}_0) + \frac{3}{\bar{h}_0^3(\bar{x})(\bar{u}_0(\bar{h}_0) - \bar{v}_{p0})}\bar{\phi}_{10}(\bar{h}_0) = 0 \qquad (VI.38)$$

where $M^2 = \bar{\Lambda}Re = 2Ha(h_{in}/b)^2$ stands for the magnetic field effect.

The solution is,

$$\bar{\phi}_{10}(\bar{y}) = \frac{A_0}{M^2}[\cosh(M\bar{y}) - 1] \qquad (VI.39)$$

$$\bar{v}_{p0} = \frac{3}{2\bar{h}_0} + \frac{3[\cosh(M\bar{h}_0) - 1]}{\bar{h}_0(\bar{x})^3 M^2 \cosh(M\bar{h}_0)} \qquad (VI.40)$$

where A_0 is an arbitrary constant. The correctness of the above solution can be justified by its reducing to the unmagnetized results $\bar{\phi}_{10}(\bar{y}) = A_0\bar{y}^2$, $\bar{v}_{p0} = 3$ [Benjamin, 1957], after removing the magnetic effect, (i.e., setting $M = 0$), and using conditions consistent with the gravity-driven flow, that is $\bar{h}_0 = 1$ (i.e., h_0 is uniform along the chute), $Fr^2 = (Re\sin\theta/3)$ (where $Re =< u_0 > h_0/\nu$, $< u_0 >= (1/h_0)\int_0^{h_0} u_0(y)dy$). Since on this order the solution is a simple propagating wave, the next order needs to be explored to locate the instability origin.

$\bar{k}^1$ Order

The resultant equations are:

$$\begin{aligned}\bar{\phi}'''_{11}(\bar{y}) - M^2\bar{\phi}'_{11} =& iRe\,[(\bar{u}_0(\bar{y}) - \bar{v}_{p0})\bar{\phi}'_{10}(\bar{y}) \\ &- \bar{\phi}_{10}(\bar{y})\frac{\partial}{\partial\bar{y}}\bar{u}_0(\bar{y}) - \frac{\cos\theta}{Fr^2}\frac{\bar{\phi}_{10}(\bar{h}_0)}{\bar{u}_0(\bar{h}_0) - \bar{v}_{p0}}]\end{aligned} \qquad (VI.41)$$

$$\bar{\phi}'_{11}(0) = \bar{\phi}_{11}(0) = 0 \qquad (VI.42)$$

$$\frac{\bar{h}_0(\bar{x})^3}{3}(\bar{u}_0(\bar{h}_0) - \bar{v}_{p0})\bar{\phi}''_{11}(\bar{h}_0) - \frac{\bar{h}_0(\bar{x})^3}{3}\bar{v}_{p1}\bar{\phi}''_{10}(\bar{h}_0) + \bar{\phi}_{11}(\bar{h}_0) = 0 \qquad (VI.43)$$

The general solution $\bar{\phi}_{11}(\bar{y})$ to equation (VI.41) is the sum of the homogenous solution $A\sinh(M\bar{y}) + B\cosh(M\bar{y}) + C$ plus any particular solution. After considerable algebra the exact solution of the $\bar{k}^1$-th order is found,

$$\begin{aligned}
\bar{\phi}_1 = iA_0Re\ \{\ & [\ -\frac{5\bar{h}_0}{8M^2} + \frac{3}{M^4\bar{h}_0} + \frac{3}{M^6\bar{h}_0^3}\ ](\cosh(M\bar{y}) - 1) \\
& + [\ \frac{1}{3}\frac{\cos\theta\ \bar{h}_0^3}{Fr^2M^3}\cosh(M\bar{h}_0) + \frac{27}{4M^5\bar{h}_0^2}\ ]\ \sinh(M\bar{y}) \\
& + (-\frac{1}{4M^3\bar{h}_0^3})(\bar{y}^3 - 3\bar{h}_0\bar{y}^2 + 3\bar{h}_0^2\bar{y})\ \sinh(M\bar{y}) \\
& + [\ \frac{-3\ (\cosh(M\bar{h}_0) - 1)}{2M^5\bar{h}_0^3\cosh(M\bar{h}_0)} + \frac{-39}{8M^5\bar{h}_0^3}\ ]\ \bar{y}\sinh(M\bar{y}) \\
& + [\ (\frac{15}{8M^4\bar{h}_0^3})(\cosh(M\bar{y}) - 1) + \frac{27}{8M^4\bar{h}_0^3}\ ]\ (\bar{y}^2 - 2\bar{h}_0\bar{y}) \\
& + [\ -\frac{1}{3}\frac{\cos\theta\ \bar{h}_0^3}{Fr^2M^2}\cosh(M\bar{h}_0)\ ]\ \bar{y}\ \ \}
\end{aligned} \tag{VI.44}$$

where A_0 is the same arbitrary constant as that in equation (VI.39).

$$\begin{aligned}
\bar{v}_{p1} = iRe\ \{\ & \frac{\cos\theta}{Fr^2M^3}\ (\frac{\sinh(M\bar{h}_0)}{\cosh(M\bar{h}_0)} - M\bar{h}_0) \\
& + \frac{9}{M^6\bar{h}_0^6}\ (3 - \frac{5}{\cosh(M\bar{h}_0)} + \frac{2}{\cosh^2(M\bar{h}_0)}) \\
& + \frac{9}{8M^5\bar{h}_0^5}\ \frac{\sinh(M\bar{h}_0)}{\cosh^2(M\bar{h}_0)}\ (1 + \frac{4}{\cosh(M\bar{h}_0)}) \\
& - \frac{81}{8M^4\bar{h}_0^4\ \cosh(M\bar{h}_0)} - \frac{3\sinh(M\bar{h}_0)}{4M^3\bar{h}_0^3\ \cosh^2(M\bar{h}_0)}\ \ \}
\end{aligned} \tag{VI.45}$$

Direct confirmation of the above results can be made by the fact that equation (VI.45) reduces to $\bar{v}_{p1} = iRe(-\frac{\cot\theta}{Re} + \frac{6}{5})$, the known result in the unmagnetized, gravity-driven film flow limit [Benjamin, 1957; Yih, 1963]. Note also that surface tension does not affect the order of the perturbed wave number, as compared with the results of Aitov et al [1988].

The fact that $\bar{v_{p_1}}$ is purely imaginary implies that either the propagating perturbing wave (of wave number k) will damp away or grow exponentially immediately after the onset of this wave. That is, the film flow system is linearly stable to the build-up of long wavelength perturbations within the liquid metal film if $\bar{v_p}/i < 0$, and is linearly unstable when $\bar{v_p}/i > 0$.

It is linearly stable for the above chute flow with $h_{in} = 5\ mm$, $u_{in} = 1.0\ m/s$, $\theta = 50°$, $b = 12.5\ cm$, and $L \sim 20\ cm$ (which meets the heat transfer requirement), since the corresponding $M = 7.5$ is greater than $M_{crit} = 5.5$ for marginal stability obtained from numerical calculation of equation (VI.45). It is also found that at moderate flow speed, e.g., $u_{in} = 1.0\ m/s$, the increase in h_{in} or decrease in b would lead to the desired decrease of M_{crit} for stable film divertor operation. Therefore, a self-cooling film with very small thickness (e.g., tens to hundreds of μm) and large chute width b is unstable with respect to instabilities analyzed here. In addition, it is clear that for a conducting chute, even though increasing b significantly can reduce the equilibrium film to the desired thickness (since $\Lambda_\epsilon \propto \epsilon_w \propto 1/b$), the resultant b will be too large to be favored in the divertor system.

If for some other reasons, e.g., to avoid blistering erosion, a higher liquid metal inlet speed is required (i.e., $u_{in} \approx 10\ m/s$) then the film divertor system is always linearly unstable unless chutes of very narrow widths are employed, which may not be desirable. This tendency is further illustrated by example cases in Figures VI.2-4.

Note that liquid metal film divertors can only be applied at the lower null point of the ITER plasma, not the upper one. This is because for $\theta > 90°$ there is no attracting equilibrium point for the film thickness evolution (see equation (VI.27)), and also at each location along the chute, the film is MHD unstable

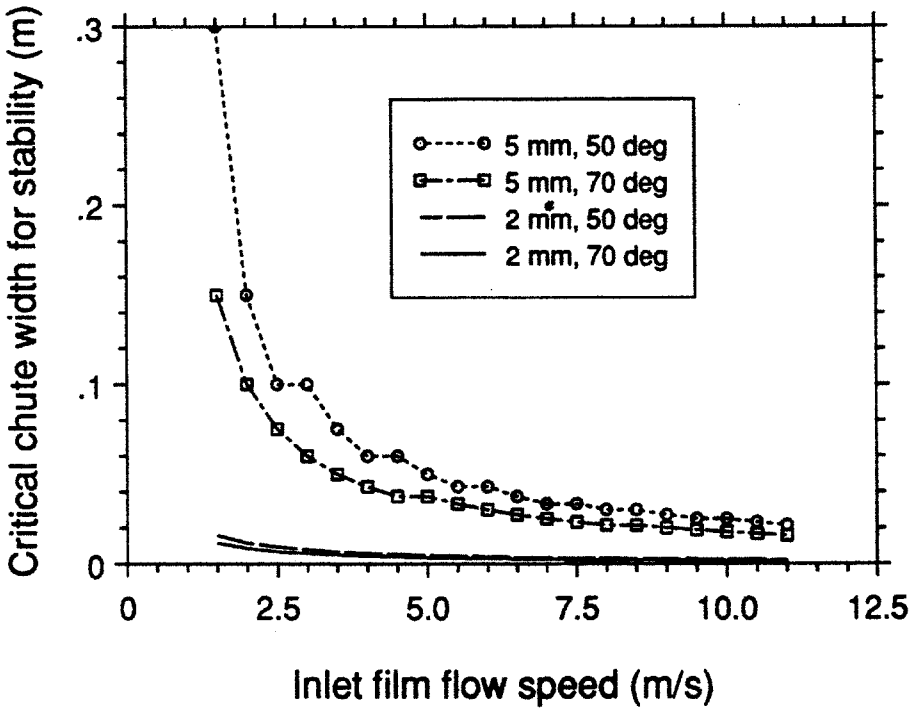

Figure VI.2: Critical chute width for stability vs inlet speed under $B = 3.6\,T$; $b < b_{crit}$ is needed for film MHD stability

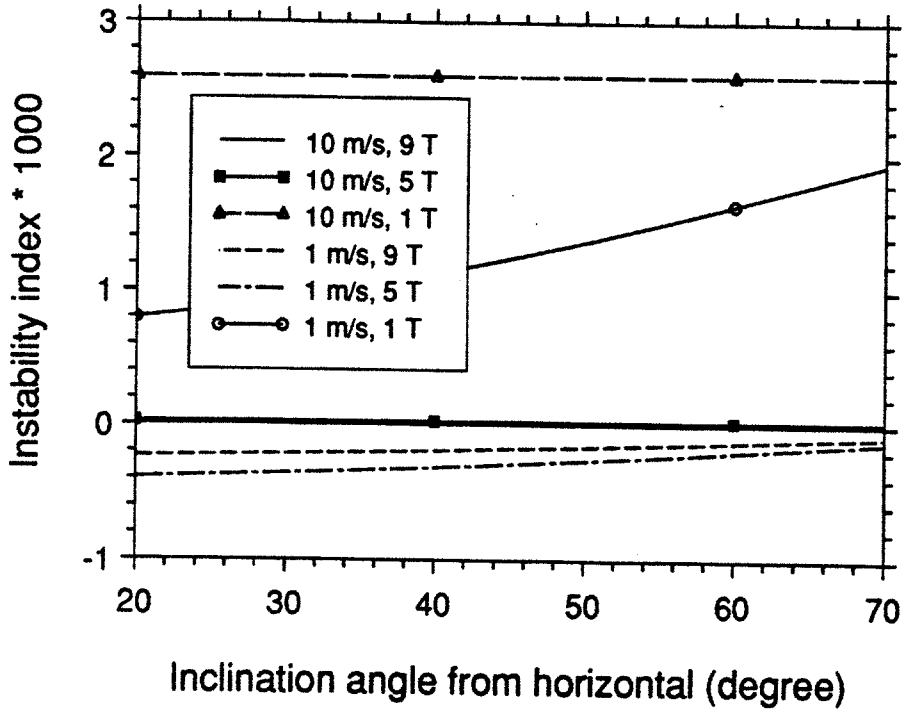

Figure VI.3: MHD instability index $\bar{v}_{p_1}/iRe$ vs the chute inclination angle;
region with $\bar{v}_{p_1}/iRe > 0$ is MHD unstable

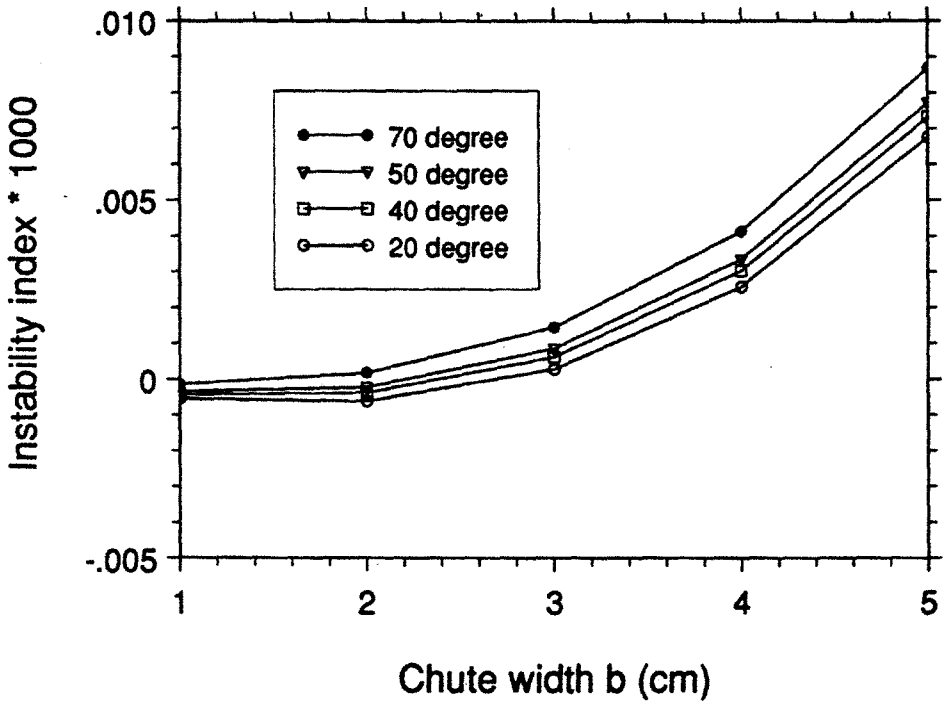

Figure VI.4: MHD instability index $\bar{v_{p_1}}/iRe$ vs the chute width,
with $h_{in} = 5\ mm$, $u_{in} = 10\ m/s$, $B = 3.6\ T$,
and variation of the chute inclination angle

(see equation (VI.45)).

VI.E. Heat Transfer and MHD Effects of Droplet Shower Divertor

VI.E.a. Heat transfer

The original Russian design of the Ga droplet curtain divertor was based on an overestimated heat transfer requirement, namely, the heat load on each divertor (two divertors for each null point) was set to be 100 MW (rather than 35 MW), hence the required jet droplet speed is about 10 m/s if the Ga operational temperature window is about 300°C [Murav'ev, 1989]. They have now realized this aspect [Murav'ev, private communication, 1991].

Nevertheless, the Russian ITER divertor project is not fully clear in treatments of different divertor engineering issues. For example, the most important parameter in divertor plasma operation, i.e., the recycling coefficient R, was not addressed, which makes their calculations in various aspects of the divertor performance ambiguous. Thus, effort was spent on the examination of these calculations based on the plasma simulation results of Chapter II as well as the evaluation of different engineering aspects in a more consistent manner.

In the proposed Ga droplet curtain divertor design, each layer of curtain is designed to have 100 % opaqueness to the grazingly incident charged particles (see Chapter III for details). For engineering redundancy, three layers are proposed. In the following heat transfer calculation, however, only one layer of droplet curtain will be used for simplicity. The number of droplets in one curtain layer is

$$N_d = 2\pi R_c L_{he}/(t_l t_t) \qquad (VI.46)$$

where R_c is the major radius of the divertor position, $L_{he} \approx 10\ cm$ is the effective exposed length of the curtain to the edge plasma bombardment, $t_l = 2.38\ d = 5.95\ mm$ is the distance between two falling droplets (center to center), $d = 2.5\ mm$ is the droplet diameter, and $t_t = (5/4)d = 3.1\ mm$ is the distance between adjacent (in toroidal direction) droplet jets (see Figure VI.5). Thus, $N_d = 1.7 \cdot 10^5$. The total heated surface in one curtain layer is thus (assuming only one hemisphere is heated for each droplet),

$$S = N_d \left[2\pi \left(\frac{d}{2} \right)^2 \right] \qquad (VI.47)$$

Thus, $S = 1.67\ m^2$.

If it is assumed that the heat deposited on a droplet hemisphere is immediately spread uniformly within the whole droplet volume, the heat balance equation is,

$$P_d \left(\frac{L_{he}}{u_d} \right) = N_d \rho c_p \frac{4}{3} \pi \left(\frac{d}{2} \right)^3 \Delta T \qquad (VI.48)$$

where P_d is 35 MW, u_d is the droplet speed to be evaluated, c_p is the Ga heat capacity, ΔT is the Ga operational temperature window width. If $\Delta T = 600°C$ is used, then the droplet speed is found to be only $u_d = 2\ m/s$. Thus, the heat transfer requirement for the droplet speed can be met without difficulty. Thus, it is for avoiding blistering erosion (see Chapter V) that the droplet speed is adjusted to about 10 m/s, which accordingly reduces the width of the Ga operational temperature window to $100°C$. This is desirable since the resultant

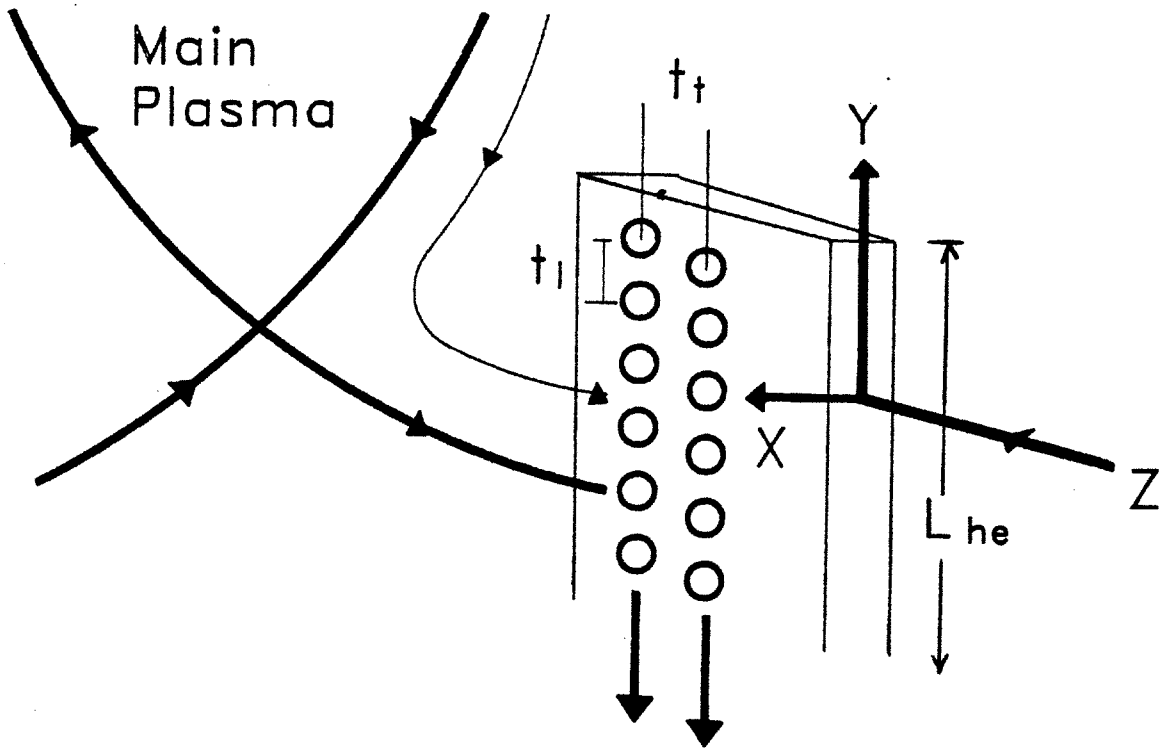

Figure VI.5: Topology of the liquid Ga curtain divertor

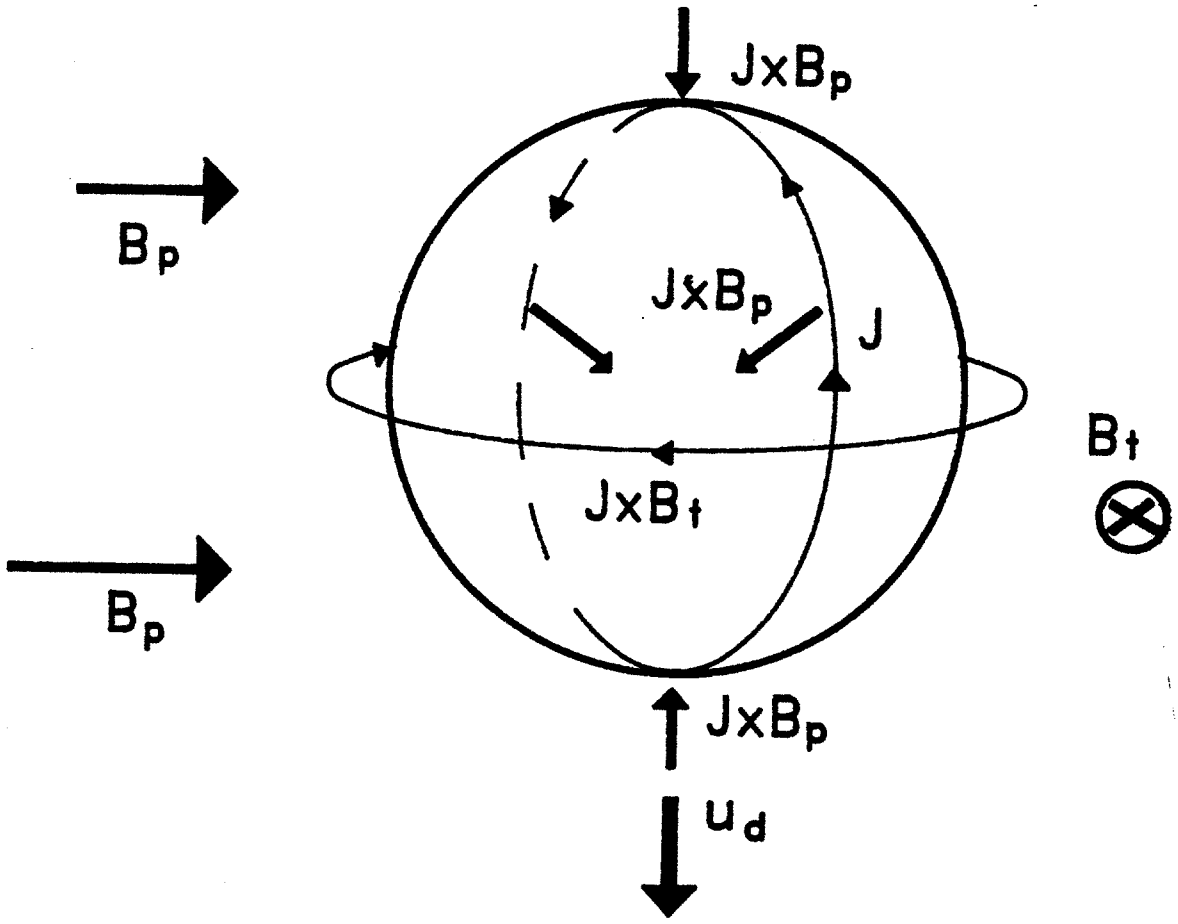

Figure VI.6: MHD effects on the flying liquid Ga droplet

operational temperature range ($100°C \sim 200°C$) will alleviate the compatibility problem between gallium and many structural materials. The decomposition of Ga jets into droplets at this speed has been proven feasible experimentally [Murav'ev, 1989].

VI.E.b. Droplet stability in non-uniform B field

When a Ga droplet is falling down it experiences gradual increase in the strength of the poloidal magnetic field. Therefore, there is some concern about the possible slowing-down of the Ga droplet as well as the deformation or even splitting of the droplet. A relevant MHD analysis based on a solid sphere rather than a liquid metal droplet was carried out by Murav'ev [1981]. When a metal sphere is dropping down, a current is generated within it to counter-balance the increased poloidal magnetic field (assuming the toroidal magnetic field remains constant) (see Figure VI.6). This current in turn interacts with the poloidal magnetic field to create a $j \times B$ force acting in the direction toward the sphere center. This creates three effects on the sphere in the case of liquid droplet, one is to change the shape of the droplet longitudinally; the other is to slow down the droplet due to the fact that the poloidal magnetic field strength at the droplet bottom is larger than that at top of droplet; another is to cause the rotation of the sphere owing to the interaction of the induced current and the toroidal magnetic field which may also lead to deformation of the droplet.

The net drag force slowing down the droplet was derived by Murav'ev [1981], i.e.,

$$F_{drag} = \frac{2\pi}{15}\sigma u_d \left(\frac{\partial}{\partial x}B_p\right)^2 \left(\frac{d}{2}\right)^5 \qquad (VI.49)$$

where B_p is the poloidal field strength, σ is the Ga electrical conductivity. For a change in B_p of about 0.01 T within 10 cm of the droplet flying distance, the drag force is found to be negligible, i.e., 10^{-8} N. It thus implies that both the droplet shape deformation and the retardation of the liquid Ga droplet can be ignored.

The rotational angular frequency ω_d (rad/s) was also derived by Murav'ev [1981] to be,

$$\omega_d = \frac{2\pi}{15}\sigma u_d \left(\frac{\partial}{\partial x}B_p\right) B_t \left(\frac{d}{2}\right)^5 \qquad (VI.50)$$

Calculation shows $\omega_d \approx 10^{-8}$ rad/s, and thus is negligible.

Therefore, the MHD effects on the liquid Ga droplet are essentially immaterial. This outcome also justifies the employment of the solid metal sphere analytic results derived by Murav'ev [1981].

VI.E.c. Plasma wind effect

The momenta (plasma wind) received by the droplet curtain from the grazingly incident charged particles consist of a component pushing the curtain radially outwards against the chamber wall as well as a component in toroidal direction.

Let us examine the toroidal component first. The pressure p_p exerted by the bombarding charged particles parallel to the toroidal field can be calculated through

$$p_p = m_{DT} v_{DT} \Gamma_p \qquad (VI.51)$$

where v_{DT} is the average charged particle speed obtained from the edge plasma simulation, and is about 40 km/s; Γ_p is the edge charged particle flux parallel to the toroidal magnetic field, and is about $10^{24}\ m^{-3}$ as obtained from the edge plasma simulation. Hence, p_p is found to be 150 Pa ($\sim 1\ Torr$). If the bending of particle trajectory by the sheath action is not included, for more conservative estimation of the plasma wind effect, the force exerted on each droplet can be approximated as $F_p \approx p_p(\pi d^2/4) = 7 \cdot 10^{-4}\ N$. The resultant droplet displacement in toroidal direction is $\Delta x_\phi = (1/2)(F_p/m_{DT})\Delta t^2 \approx 0.6\ mm$. The corresponding displacement in the radial direction is even smaller, i.e., 0.1 mm. It is thus clear that the plasma wind will have no effect on the Ga droplet curtain divertor.

VI.E.d. Electric charge accumulation effect

There is speculation that since the divertor plate is negatively charged, the accumulation of electrons on Ga droplets may cause repulsion between droplets to such an extent that deterioration of the the droplet curtain occurs. In addition, the motion of these negatively charged droplets across the toroidal magnetic field may result in the radially inward shift of the curtain [Murav'ev, 1989].

The number of electrons accumulated on one droplet can be estimated through the sheath floating potential ϕ_f (with respect to $\phi_{plasma} = 0$),

$$|\phi_f| = \frac{q_e}{4\pi\epsilon_0\left(\frac{d}{2}\right)} \approx \frac{3k_BT_e}{e} \qquad (VI.52)$$

For $T_e = 57\ eV$ (obtained in Chapter V), the accumulated negative charge is found to be $q_e = 1.7 \cdot 10^{-11}\ C$ per droplet (or $1.48 \cdot 10^8$ electrons).

Since the electric repelling force between toroidally adjacent droplets is $F_{es} = q_e^2/(4\pi\epsilon_0 t_t^2) \approx 5 \cdot 10^{-7}\ N$ (t_t is the distance between adjacent droplets), the total repulsion displacement can be calculated to be only about 0.3 μm, and hence is negligible.

While the radially inward displacement Δx_r can be estimated from,

$$\Delta x_r = \frac{1}{2}\left(\frac{u_d q_e B_t}{m_d}\right)\left(\frac{L_{he}}{u_d}\right)^2 \qquad (VI.53)$$

and Δx_r is found to be only about 1 nm. Therefore, the electric charge accumulation essentially has no effect on the droplet curtain.

VI.F. MHD Pressure Drop and Pumping Requirement

VI.F.a. Ga film divertor

The MHD pressure drop associated with the liquid Ga divertor film flow can be estimated through using rectangular conduits perpendicular to the toroidal magnetic field. In Figure VI.7, the liquid Ga flow with a velocity u is along the x direction across the toroidal magnetic field B_t (in z direction). The induced emf $\vec{E}^*$ ($=\vec{E} + \vec{v} \times \vec{B}_t$) forces the current density j_y to circulate mainly near the side walls (see Figure VI.7), i.e.,

$$\vec{j}_y = \sigma \vec{E}^* = -\sigma(E - uB)\vec{y} \qquad (VI.54)$$

The total current through the liquid Ga is then,

$$\begin{aligned} \vec{I}_c &\approx \vec{j}_y(2aL) = -\sigma(E - uB_t)2aL\vec{y} \\ &= \sigma(uB_t - E)2aL\vec{y} \end{aligned} \qquad (VI.55)$$

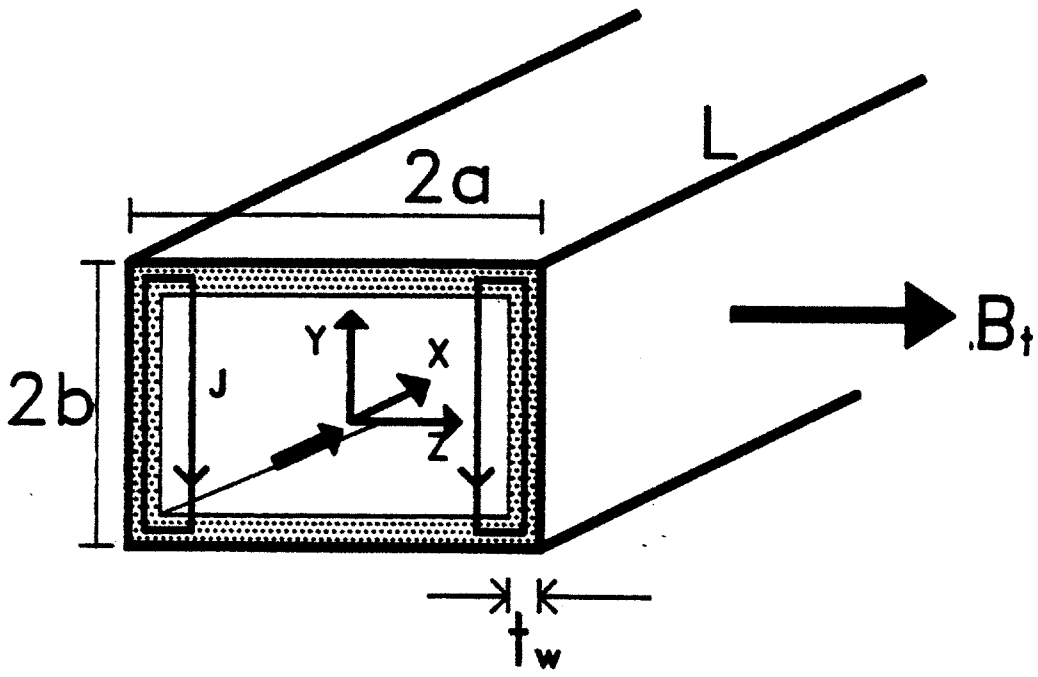

Figure VI.7: Duct flow crossing a magnetic field

If the duct walls have an electrical conductivity σ_w which is reasonably large, the current will return through the walls. The application of Ohm's law to the side walls gives (note $u = 0$ in the wall),

$$\vec{I}_c = \vec{I}_w = \sigma_w E \cdot 2t_w L\vec{y} \qquad (VI.56)$$

From equations (VI.55) and (VI.56), it can be obtained that

$$I_c = \sigma 2auLB_t \frac{C}{1+C} \qquad (VI.57)$$

where $C \equiv \sigma_w t_w/(\sigma a)$ is called the "wall conductance ratio". The MHD pressure drop Δp can thus be calculated through:

$$\begin{aligned} \Delta p &= \frac{I_c\, 2bB_t}{2a2b} = j_y B_t L \\ &= \left(\sigma u B_t \frac{C}{1+C}\right) B_t L \end{aligned} \qquad (VI.58)$$

The corresponding Ga pumping power is:

$$P_{pump} = Q\Delta p \qquad (VI.59)$$

where Q is the Ga volumetric flow rate (m^3/s).

If $2a = 2b = 10\ cm$, $L \approx 1\ m$, and the initial speed of the free surface Ga film (5 mm thickness) is 1 m/s, the needed liquid Ga flow speed u within the conduit is only 0.05 m/s. Thus the MHD pressure drop of each duct (total about 300 ducts toroidally) is 2.5 kPa, which leads to the total MHD part pumping power of around 400 W. Therefore, the MHD pressure losses associated with the film

divertor concept is not a concern. Even if the film speed is about 5 m/s, the total MHD pumping power of 10 kW is still easily manageable.

VI.F.b. Ga droplet shower divertor

Detailed calculations of the total pressure losses including the MHD pressure drop, frictional losses, and other minor losses have been carried out (see, [Murav'ev, 1989]). The total pressure loss for the four divertors associated with the two null operation of ITER fusion reactor is about 10 MPa. While the total liquid Ga volumetric flow rate is about 4 m^3/s. Thus, the total pumping power required is 40 MW, about 4 % of the steady state ITER thermal power.

VI.G. Summary and Conclusions of Chapter VI

This Chapter is devoted to the evaluation of the liquid gallium protective film divertor and the Ga droplet shower divertor on the heat transfer and MHD issues. The conducted liquid metal film MHD treatment may serve as an unification, and a correction, to the existing models. The treatment shows that the pressure exerted on the liquid metal film by the bombarding charged particles dominates that by the sheath pulling action, and therefore, there is no external free energy that can cause Rayleigh-Taylor type instabilities. However, this does not save the liquid metal film from the possible Helmholtz type instabilities, even under the stabilizing effect of the toroidal magnetic field.

The equilibrium solution is presented in a way consistent with the stability analysis and applied as an example to the film thickness evolution of a pumped Ga film divertor with non-conducting chute. Employment of metal chutes should not be considered due to the resultant large equilibrium film thickness. Also, the chute side walls are necessary to provide the appropriately thick film.

It is found that for a moderate chute inclination angle, say $50°C$, a film flow at about 1 m/s (with 12 cm width and 5 mm thickness, for example) can satisfy both the ITER heat transfer requirement and the stability criterion (under the assumption that liquid metal physical property does not change appreciably during the bombardment of charged particles). This is to be compared with another proposed "injection type" film divertor concept (see Figure III.1) which should be excluded since at such pumping speed the liquid metal (pumped up from the bottom) is likely to be injected into the plasma rather than being flown over the guiding substrate.

However, if a much higher film inlet speed is required, for instance, to avoid the blistering erosion (discussed in Chapter V), the film will be MHD-wise linearly unstable. Chute of very narrow width has to be used in order to achieve stability, which may not be structurally desirable. Note that in the above analysis, other more complicating and uncertain factors are not included such as the "halo current" (see, for example, [Post et al, 1991]) due to the developed electrical potential difference between the upper and lower (or inner and outer) divertors plates.

Even if the afore-mentioned problems related to the MHD effects never existed, there are other important engineering concerns with regards to the application of the liquid metal film divertor concept. One is the erosion of the exposed chute walls by the charged particle bombardment. A possible solution may be the one illustrated by Kirillov et al [1990] in which the shape of the chute are constructed in such a way that the side walls are not in the way of the grazingly incident charged particles (see Figure VI.8). The other engineering concern is that the non-conducting chute is not favorable in terms of heat transfer. Thus, it may seem desirable to use a metal chute which has non-

conducting coating on the side in contact with the liquid gallium. However, such insulator material needs to be found or developed.

For the liquid droplet curtain divertor, if only the heat transfer is of concern, then with Ga operational temperature range of about $600°C$, the necessary droplet (2.5 mm diameter) speed is less than 1 m/s (which may be undesirable in terms of the droplet formation). However, in order to avoid the blistering erosion caused by the hydrogen bubble eruptions, the droplet speed of about 10 m/s is preferred, which reduces the Ga operational temperature range to less than $200°C$. Since Ga is highly corrosive above about $400°C$ to many structural materials, this reduction of the maximum Ga operational temperature is much favorable.

MHD effects such as the plasma wind effect, the electric charge accumulation effect, and the droplet instability in nonuniform magnetic field are shown to have negligible influence on the liquid Ga droplet curtain divertor. While the total pressure drop (including MHD and frictional losses) for the four droplet divertors (two for each null point) associated with the ITER reactor design was calculated to be about 10 MPa [Murav'ev, 1989], and the corresponding pumping power is about 40 MW, i.e. 4 % of the ITER steady state fusion thermal power.

The major engineering uncertainty associated with the droplet curtain divertor concept is the possible spraying of the droplets into the plasma. In fact, when used as a limiter (under more than 10 MW/m^2 heat load of the Russian T-3M tokamak (major radius: 0.95 m, minor radius: 0.16 m, plasma current: 40 kA)) the liquid Ga-eutectic (67 % Ga, 20.5 % In, 12.5 % Sn) droplet curtain (with droplet speed of only $2 \sim 5$ m/s) tends to contaminate the main plasma [Vodyanyuk et al, 1988]. The reason is suspected by Russian scientists to be either the mechanical vibration of the droplet shower head (droplet shaper)

or the possible liquid metal-plasma interaction. It is not surprizing that at the limiter position any previously investigated liquid metal-plasma interactions (except MHD effects) can enhance the impurity level in the main plasma, such as the physical sputtering, the blistering erosion, etc. On the other hand, when used as a divertor, it is anticipated that the effect of this undesirable phenomenon will be significantly reduced. This point awaits verification by future experiments. If proven correct, then conclusion can be drawn that the liquid Ga droplet curtain divertor concept is preferred to the liquid Ga film divertor concept.

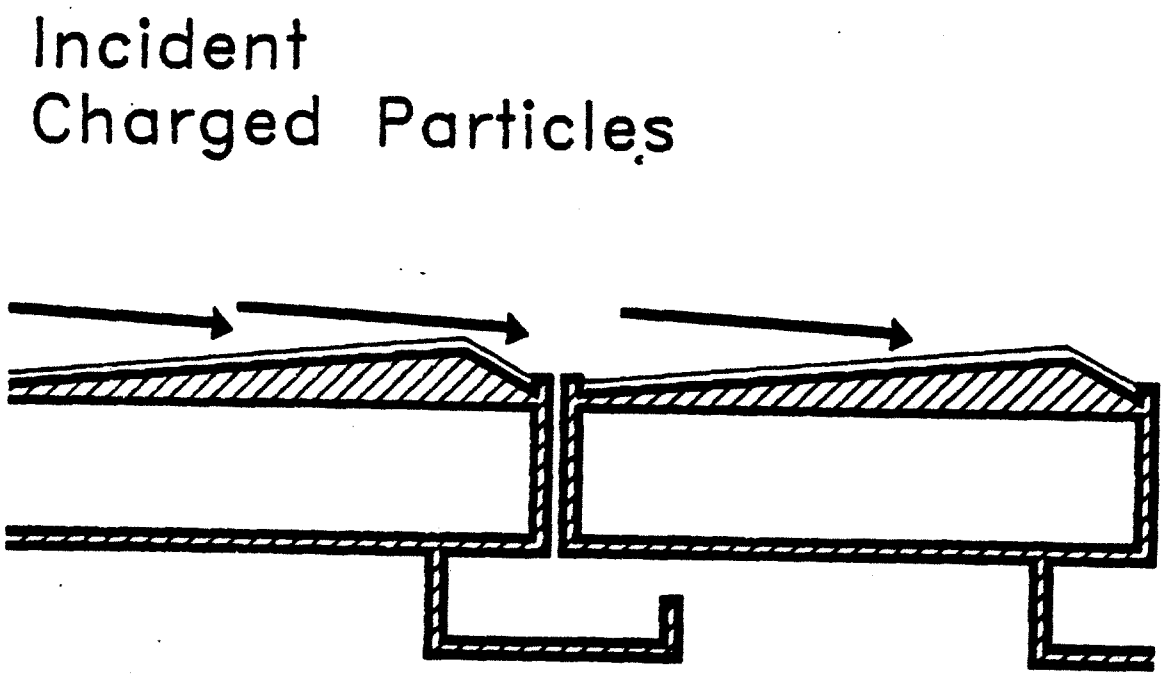

Figure VI.8: A chute design to avoid side wall erosion

CHAPTER VII. VACUUM PUMPING REQUIREMENT AND PROPOSED NEW DESIGN

VII.A. Potential Problem in Helium Ash Removal

A sufficient helium ash removal rate needs to be obtained in order to achieve steady state operation of a fusion tokamak reactor. Without sufficient helium pumping, the main plasma will quench in seconds due to increased radiation and fuel dilution. It may appear that by employing very efficient vacuum pumps this problem can in principle be overcomed. However, as mentioned in Chapter II, this is not the only requirement. The efficiency of helium (also deuterium and tritium) removal is mainly determined by the neutral helium atom escape probability from being ionized and recycled back into the plasma near the divertor plate. Even if the vacuum pumps have 100 % efficiency in removing neutral helium and hydrogen once they escape into the divertor plenum, there will be little or no helium or hydrogen exhaust if the average ionization mean free path is too short compared with the thickness of the plasma layer near a divertor plate. This concern is particularly obvious for an ITER-like reactor which is characterized by the high edge plasma temperature and hence short electron impact ionization mean free path of recycled neutrals.

VII.A.a. Vacuum pumping requirement

The required neutral particle (helium and hydrogen) pumping rate of an ITER-like reactor can be evaluated as follows. The number of helium (or alpha particle) created per second (or number of fusion reactions per second) is equal to the ratio of the fusion power (1000 MW) to the fusion reaction energy 17.6

MeV (i.e., 3.5 MeV alpha particle and 14.1 MeV neutron). Therefore, about $3.6 \cdot 10^{20}$ alpha particles are created per second. If the maximum permissible helium fraction within the main plasma is 10 % [Post et al, 1991], then a total of approximately $3.6 \cdot 10^{21}$ neutral particles (deuterons, tritons, helium) need to be pumped away from the main plasma per second. Thus, there exists an upper limit on the divertor recycling coefficient, R, in order to ensure sufficient helium ash removal.

The divertor recycling coefficient R is a complicated function of divertor throat conditions, scrape-off layer thickness, divertor plate material, orientation, and so on (see Chapter II). Thus, in reality, it self-evolves from the generated main and edge plasma conditions, rather than being simply specified externally. For an ITER-like reactor, the recycling coefficient is expected to be very large (i.e., close to unity) due to the high edge plasma temperature. Nevertheless, its exact value is unknown until future relevant ITER divertor experiments are conducted. This does not contradict or invalidate our previous use of $R = 0.99$ in the edge plasma modeling. The reason is that the simulation results for the edge plasma density, temperature, and most other derived quantities are not sensitive to the value of R. However, for sufficient neutral gas removal, an upper limit on the recycling coefficient is required.

The maximum permissible recycling coefficient for the liquid Ga droplet curtain divertors (4 divertors associated with 2 null points) can be evaluated through:

$$4 \cdot (1 - R)\Gamma_p A_c = 3.6 \cdot 10^{21}\ s^{-1} \qquad (VII.1)$$

where $\Gamma_p = 1.37 \cdot 10^{24}\ m^{-2}s^{-1}$ is the incident charged particle flux parallel

to the magnetic field (obtained in Chapter V), and $A_c = 0.35\ m^2$ is the divertor channel cross-sectional area perpendicular to the magnetic field. Thus, $R \leq 0.998$ is required for sufficient neutral gas pumping under the steady state ITER condition. Note that it is assumed that each of the 4 divertors shares the same amount of heat load and particle flux.

VII.A.b. Problem of the Ga droplet curtain divertor

The high edge plasma temperature ($\sim 57\ eV$) at the Ga droplet curtain divertor [Murav'ev, 1989] (4 divertors for two null points) associated with an ITER-like reactor may give rise to a neutral recycling coefficient R well above the upper limit 0.998. This is particularly true when the curtain divertor intercepts the divertor channel perpendicularly (viewed from the cross-sectional projection of the ITER tokamak) (see Figure III.5), since the corresponding probability for neutrals to escape being ionized is essentially zero. If, further, there is an abnormal increase of the divertor heat load due to certain thermal plasma instability or disruption, then the corresponding increase of the recycling coefficient is expected to aggravate the situation. Namely, the increase of the impurity level within the main plasma is expected to re-enforce the thermal plasma instability or disruption. Thus, an ITER-like main plasma with the original liquid Ga droplet curtain divertors constitute a system unstable to the impurity-induced plasma perturbations.

The maximum permissible neutral pressure of $10^{-4}\ Torr$ near the divertor plate required by the impurity level control (see Chapter IV) makes the vacuum pumping task more difficult. That is, in order to pump the the fairly low pressure neutral gases near the divertor plate, considerably large vacuum pumping duct area is required. An evaluation of the duct area can be performed as follows.

Let $Q = N_s k_B T$ be the pumping throughput (W) where N_s is the net number of neutral particles to be carried away by the pump per unit time, T is their average temperature and is assumed to be room temperature for the molecular flow, k_B is the Boltzmann constant. The relation between pressures and pumping speeds at the divertor chamber and at the vacuum pumps is described by [Chambers, Fitch, Halliday, 1989]:

$$Q = C(p_0 - p_0^*) = p_0 S_0 = p_0^* S_0^* \qquad (VII.2)$$

where p_0 (Pa) and S_0 (m^3/s) are the neutral pressure and the pumping speed in the divertor chamber; p_0^* and S_0^* are the neutral pressure and the pumping speed in the vacuum pump (see Figure VII.1). In our case, $p_0 \sim 10^{-4}\ Torr$ (or 13 mPa), and p_0^* has to be smaller than p_0. While C is the duct conductance, and is defined as [Lafferty, 1962] (valid for $D_m \ll L_{duct}$):

$$C = \frac{4}{3}\frac{\pi D_m^3}{12 L_{duct}} v_{th} \qquad (VII.3)$$

where D_m is the duct diameter, L_{duct} is the duct length, $v_{th} = (8k_B T/\pi m)$ is the thermal velocity of the neutral gas in the duct, and m is the mass of an average neutral particle.

Due to the fairly low gas pressure ($p_0 \sim 10^{-4}\ Torr$), the gas flow in the pumping duct is expected to be in the molecular flow regime. That is, there are no collisions among the neutral particles and hence there is no fluid behavior. Without the presence of the vacuum pump, the neutral particles have equal probability in going to either end of the duct after many bounces from the duct wall. The pump only serves as a trap to the entering particles. It is this

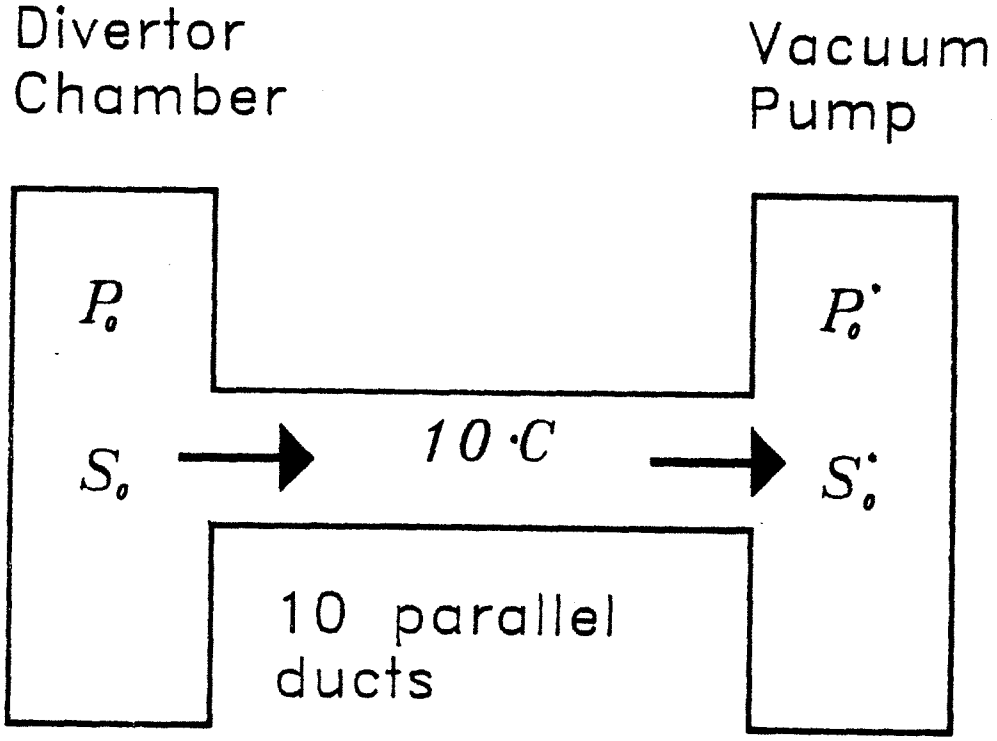

Figure VII.1: Definition of system pressures and pumping speeds

resultant particle number gradient that causes the migration of particles toward the vacuum pump. In the following calculations, all ducts will be assumed to be maintained at room temperature and consequently, neutral particles bouncing back and forth from the duct walls are expected to have the same temperature. Hence, $v_{th} = 1588\ m/s$ and $C = 416D^3/L_{duct}$.

Since $N_s = \frac{1}{4} \cdot 3.6 \cdot 10^{21}\ s^{-1}$ for one divertor, we have $Q = N_s k_B T = 3.73\ W$. If there are 10 ducts (toroidally) for each divertor, then under the conditions $p_0^* \ll p_0$ and $L_{duct} \approx 1\ m$, it is found that $C = 28\ m^3/s$, and the minimum required diameter for each duct can be calculated to be 0.4 m, according to equation (VII.2). Therefore, the required total pumping panel area for 4 divertors is at least 5 m^2 if the helium concentration in the main plasma is maintained at 10 %, and the divertor recycling coefficient R is low enough. Obviously, if a cleaner main plasma or longer duct length is preferred the duct diameter (and pumping panel area) needs to be increased.

In reality, however, the performance of this pumping system may be poor due to the non-uniformity in the spatial distribution of the neutral pressure $p_0(x)$ in the divertor chamber (see Figure VII.2). This is because the high edge plasma temperature causes the neutral ionization mean free path to be short compared with the pumping panel dimension, and thus a considerable fraction of the pumping panel area is not used properly. The needed duct diameter should be larger than 0.4 m (based on $p_0 = 10^{-4}\ Torr$) in order to meet the helium ash removal requirement. This may raise a problem from the engineering construction point of view.

Lastly, the molecular flow pumping formula [Lafferty, 1962] can be used to infer the molecular flow speed and the neutral particle number density near the divertor plate. Since $p_0^* \ll p_0$ in order to minimize the duct diameter, we have

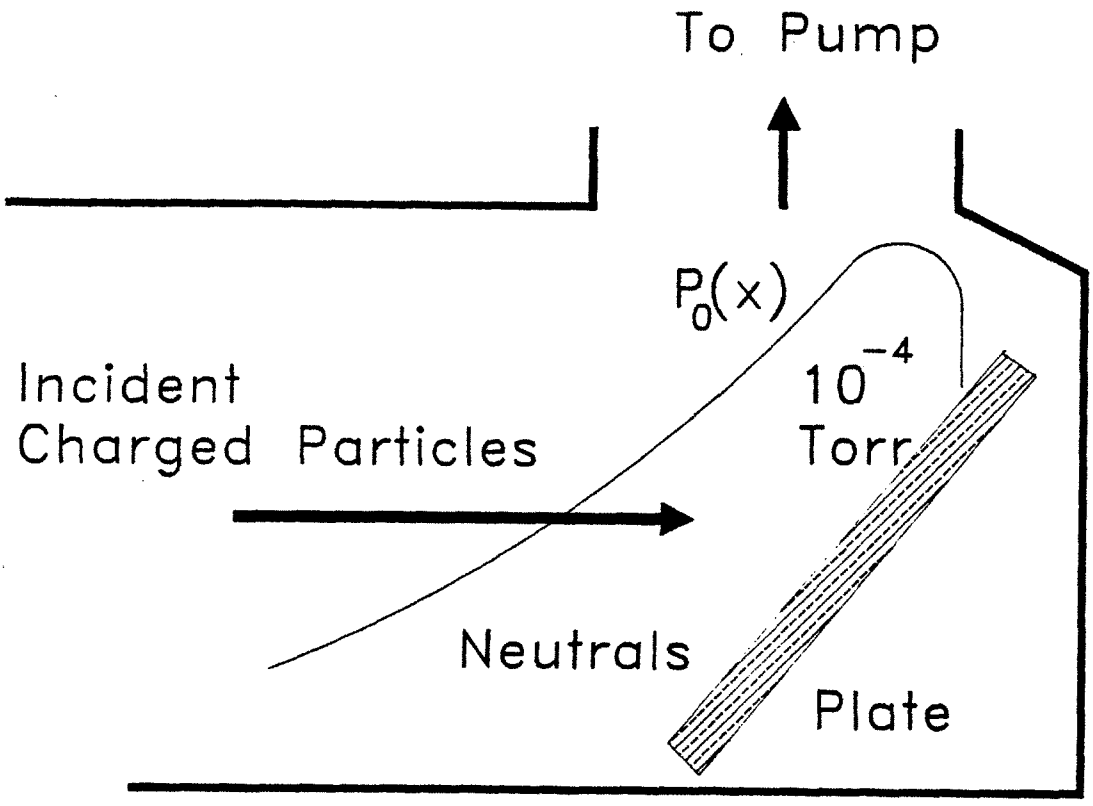

Figure VII.2: Neutral pressure distribution in front of the divertor plate

$S_0 \approx C$ (for each duct) according to equation (VII.2). Using $S_0 = \frac{\pi D^2}{4} v$ and $C = 28\ m^3/s$, the molecular flow velocity v toward pump can be calculated to be 223 m/s. This is much smaller than the thermal velocity 1558 m/s at room temperature as is characteristic of the molecular flow pumping. The neutral number density $\overline{n_0}$ in front of the divertor plate can also be evaluated as $1.6 \cdot 10^{16}\ m^{-3}$ by using $p_0 = 10^{-4}\ Torr$ and assuming each neutral particle has the Franck-Condon energy 5 eV [Dolan, 1982].

VII.B. New Concept for Vacuum Pumping

As is obvious from the above analyses, the problems with vacuum pumping of hydrogen and helium ashes are of two origins. One is the possible too high recycling coefficient, the other is the fairly low neutral pressure and hence the fairly large pumping duct area required to achieve the needed conductance C of the pumping ducts. It is thus desirable to have a design which eliminates these two origins of the pumping problem. In the following, an existing "Holy wall" concept [Downing, 1990] will first be illustrated and briefly discussed. Then, a new concept and the associated plasma simulation results will be presented. Finally, the proposed design will be revealed [LaBombard, private communication, 1991] and discussed.

VII.B.a. Holy wall concept

The large-area pump limiter concept [Downing, 1990] (hereafter referred to as the "Holy wall concept") is illustrated in Figure VII.3. The purpose of this design is to increase the pumping capability by allowing some charged particles to pass through the gaps between walls. However, when used at the limiter position, the magnetic field line topology does not facilitate this purpose. When

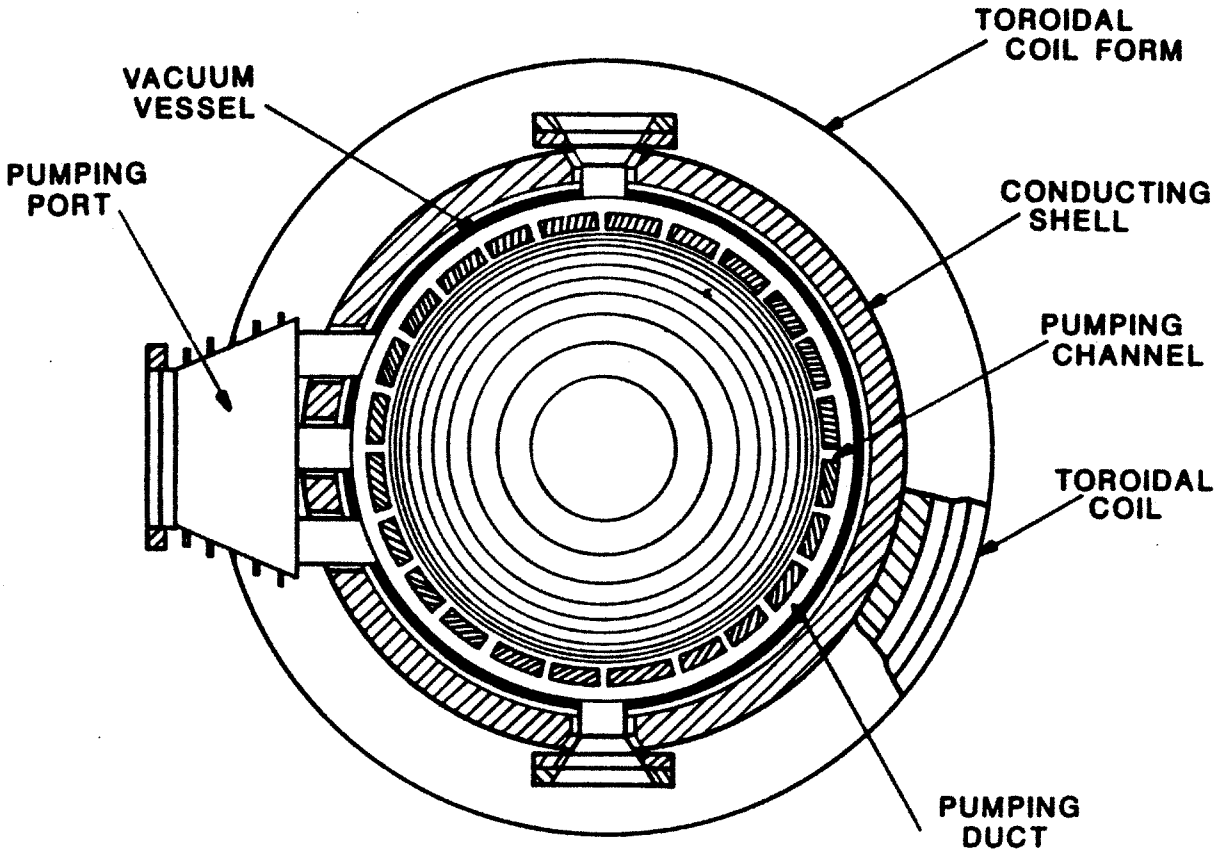

Figure VII.3: Holy wall concept to increase the vacuum pumping capability [Downing, 1990]

this concept is employed at the divertor position, charged particles may stream along the magnetic field and enter the pumping cavity behind the porous divertor plate. However, the difficulty is that the solid metal (or non-metal) Holy wall cannot sustain the heat flux and sputtering erosion (particularly at edges) under ITER steady state condition, as implied by the simulation results in Chapter II.

VII.B.b. New concept for vacuum pumping: semi-transparent liquid metal curtain

A new concept for better vacuum pumping is motivated by the gas pumping requirements and inspired by the Holy wall concept mentioned in the previous Subsection [LaBombard, private communication, 1991]. In this case the Holy wall is replaced by a semi-transparent liquid metal curtain made of moving Ga droplets. The droplet curtain divertor is made slightly transparent to the grazingly incident charged particles by properly synchronizing the Ga droplet jets, for example with the penetration probability f_t, say, 10 % (see Figure VII.4). The chamber behind the partially transparent curtain is made of tungsten. As compared with the stationary Holy wall concept, the new concept, if feasible, is expected to have the following advantages: 1) The concern about wall erosion is essentially immaterial to the liquid droplet curtain divertor; 2) The motion of the droplet curtain pattern facilitates the sweeping of the divertor heat load on the tungsten wall behind the curtain; 3) The neutral density within the chamber behind the curtain is expected to be at least one order of magnitude greater than that in front of the curtain, and is expected to be more uniformly distributed. This should significantly reduce the pumping duct diameter; 4) The capability of adjustment of the vacuum pumping panel area within the chamber offers another engineering control knob to the divertor

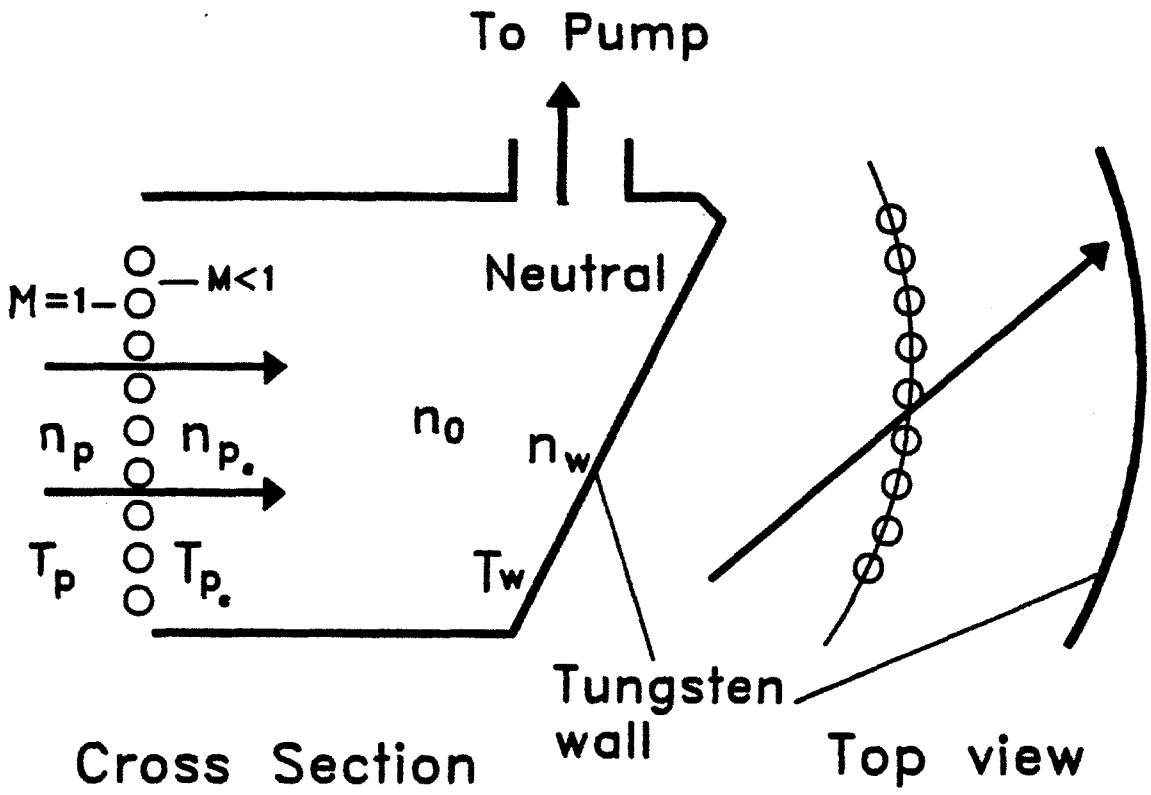

Figure VII.4: New concept for vacuum pumping

recycling coefficient R; 5) The variability of the droplet curtain pattern is expected to eliminate the problem of insufficient helium ash removal due to possibly too high divertor recycling coefficient;

VII.B.c. Simulation model of the new concept

To investigate the feasibility of the above new concept, plasma modeling within the pumping chamber behind the curtain divertor was done. There was a question, whether the back flow of the neutrals to the side in front of the curtain may make the neutral density behind the curtain too low to be pumped. A simple model was constructed by modifying the two-point model (see Chapter II) to have an estimate of the quantities of interest. Two assumptions were made for the simulation of the plasma condition behind the curtain: 1) Since the transparency of the curtain is about 10 % or 20 %, the penetrating energy flux is a perturbation to the total divertor heat load, and thus the conditions in front of the curtain is assumed to be the same as that obtained previously in Chapter V; 2) all neutrals behind the curtain have the Franck-Condon energy 5 eV and are uniformly distributed.

The neutral particle number N_0 balance behind the curtain at steady state is described by,

$$\begin{aligned}\frac{dN_0}{dt} &= 0 \\ &= n_{p_c} v_{p_c} (f_t A_c) - \frac{10C(p_0 - p_0^*)}{kT} - \frac{1}{4} n_0 v_0 A_b \\ &\approx n_{p_c} v_{p_c} (f_t A_c) - \frac{10 \cdot 416 D_m^3}{L_{duct}} n_0 \frac{T_0}{T} - \frac{1}{4} n_0 v_0 A_b\end{aligned} \qquad (VII.4)$$

where n_{p_c} and v_{p_c} are the plasma density and fluid velocity at the location between droplets of the curtain, $A_c = 0.35\ m^2$ is the divertor channel cross-

sectional area perpendicular to the magnetic field, D_m is the pumping duct diameter, $T = 300\ K$, $k_B T_0 = 5\ eV$ is the Franck-Condon energy and v_0 is the associated thermal velocity, n_0 is the neutral number density behind the curtain, $A_b \approx 2\ m^2$ is the transparent area on the curtain seen by the backflowing neutrals, and $L_{duct} \approx 1\ m$ is the length of each pumping duct (assuming 10 pumping ducts for each of the 4 divertors). Note that in equation (VII.4) p_0^* is set to be negligible compared with p_0 in order to have the minimum D_m. Note also that even helium neutral atoms (less than 10 % in number compared with hydrogen) do not possess Franck-Condon energy, their average ionization mean free path is calculated to be several centimeters and thus can be exhausted through the pumping system. In the following, calculations will be carried out in terms of the hydrogen neutrals for simplicity.

Thus, the steady state neutral number density n_0 is found to be,

$$n_0 = \frac{n_{p_c} v_{p_c} f_t A_c}{\left(\frac{1}{4} v_0 A_b + \frac{4160 D_m^3}{L_{duct}} \frac{T_0}{T}\right)} \qquad (VII.5)$$

The representation of the global divertor recycling coefficient R can be derived from the particle balance:

$$(1 - R)\Gamma_p A_c \approx \frac{\frac{4160 D_m^3}{L_{duct}} p_0}{kT} \qquad (VII.6)$$

where $\Gamma_p = 1.37 \cdot 10^{24}\ m^{-2} s^{-1}$ is the particle flux along the magnetic field obtained from the simulation in Chapter V. Thus,

$$R = 1 - \frac{4160 D_m^3 n_0}{L_{duct}} \left(\frac{T_0}{T}\right) \left(\frac{1}{\Gamma_p A_c}\right) \qquad (VII.7)$$

In order to obtain n_0 and R from equations (VII.5) and (VII.7), a plasma model behind the curtain needs to be constructed to obtain quantities such as n_{p_c} and v_{p_c}. A physical picture can also be obtained from this modeling effort. The modified two-point model for the plasma behind the divertor curtain is as follows: First, define an effective recycling coefficient, R_c, for the plasma fluxes behind the curtain,

$$R_c = \frac{(\Gamma_w - \Gamma_{p_c} f_t)}{\Gamma_w} \qquad (VII.8)$$

where Γ_w is the net D-T ion particle flux (parallel to the magnetic field) at the tungsten wall, Γ_{p_c} is that at the location between droplets of the curtain divertor. The plasma density near the tungsten wall, n_w, can then be written as:

$$n_w = \left[\left(\frac{n_w}{n_T}\right)^{\frac{7}{3}} + 1\right]^{\frac{2}{7}} \left[\frac{f_t n_{p_c}(1 + r_{p_c})(1 + M_{p_c}^2)}{[2 + (1 - R_N) f_{cxs} R_c + R_N f_{cxf} R_c](1 + r_w)}\right] \qquad (VII.9)$$

where r (= 1) is the ratio of ion temperature to electron temperature, the subscripts w and p_c refer to the values at the tungsten wall and at the location between droplets of the curtain, respectively; R_N is the particle reflection coefficient from the tungsten wall (see Chapter II for its empirical representation), M_{p_c} is the Mach number at the location between droplets of the curtain, and f_{cxf}, f_{cxs} are the ratios of fast and slow charge-exchange rate coefficients to that of the ionization process, respectively (see also Chapter II for details).

Also, similar to the two-point model for the plasma in front of the curtain,

$$T_w = \left[\left(f_t Q_t + \int_{p_c}^{w} S_E dx \right) \left(\frac{m^{\frac{1}{2}}}{n_w (1+r_w)^{\frac{1}{2}} (\delta_e + \delta_i)} \right) \right]^{\frac{2}{3}} \qquad (VII.10)$$

$$n_{p_c} = \frac{[2 + (1 - R_N) f_{cxs} R_c + R_N f_{cxf} R_c](1 + r_w)\, T_w\, n_w}{(1 + M_{p_c}^2)\,(1 + r_{p_c})\, f_t T_{p_c}} \qquad (VII.11)$$

with

$$n_T = \left(\frac{2\chi_0}{7 L_c u} \right)^{\frac{3}{7}} \cdot \frac{f_t Q_t^{\frac{4}{7}} (1 + \int_{p_c}^{w} S_E dx / f_t Q_t)}{(\delta_e + \delta_i)} \left(\frac{m}{1 + r_w} \right)^{\frac{1}{2}} \qquad (VII.12)$$

in which $L_c \approx 5\ m$ is the physical length of the straightened plasma channel behind curtain, and u is a measure of the fraction of energy input flux $f_t Q_t$ ($Q_t = 35\ MW/A_c$ per divertor) that is conveyed through thermal conduction in the chamber plasma channel, i.e., it is defined through

$$\frac{\left(\frac{2}{7}\right) \chi_0 \left(T_{p_c}^{7/2} - T_w^{7/2} \right)}{L_c} = u f_t Q_t \qquad (VII.13)$$

which results in

$$u = 1 + \frac{1}{f_t Q_t L_c} \int_{p_c}^{w} \left\{ \int_{p_c}^{x} S_E dx' - nv \left[\frac{1}{2} m v^2 + \frac{5}{2} T (1 + r) \right] \right\} dx \qquad (VII.14)$$

and is approximated as,

$$u \approx 1 + \frac{\int_{p_c}^{w} S_E dx}{2 f_t Q_t} - \frac{1}{f_t Q_t} \left[\frac{\phi_{p_c} + \phi_w}{2} \right] \qquad (VII.15)$$

where $\phi = nv\left(\frac{1}{2}mv^2 + \frac{5}{2}T(1+r)\right)$.

$$M_{p_c} \equiv \frac{v_{p_c}}{C_{sp_c}} = \left(\frac{a}{1-a}\right)^{\frac{1}{2}} \qquad (VII.16)$$

where $C_{sp_c} = \left(\frac{T_{p_c}(1+r_{p_c})}{m}\right)^{\frac{1}{2}}$ is the ion acoustic speed at location between droplets of the curtain.

$$a = \frac{f_t n_w}{n_{p_c}} \frac{(1-R_c)^2}{2\left[1 + \frac{(1-R_N)f_{cxs}R_c + R_N f_{cxf} R_c}{2}\right]} \qquad (VII.17)$$

Also, $v_w = C_{sw} \equiv \left(\frac{T_w(1+r_w)}{m}\right)^{\frac{1}{2}}$ is set as required by the Bohm sheath criterion [Stangeby, 1984]. And $\int_{p_c}^{w} S_E dx$ is the energy source flux whose detailed representation is similar to that in Chapter II.

VII.B.d. Simulation results

In order to evaluate the global divertor recycling coefficient R and the neutral density behind the curtain, n_0, the values of n_{p_c} and v_{p_c} need to be known. This can be accomplished by solving the chamber plasma model equations (VII.8) to (VII.17) if the value of the chamber recycling coefficient R_c is known. Unfortunately, it is not, even though the continuity of plasma pressure $(mnv^2 + nk(T_e + T_i))$ at the front and backside of the curtain transparent region should in principle facilitate the unique specification of R_c. This is because the value of plasma fluid speed in front of the hole of the curtain is not known. Therefore, different values of R_c needs to be used to see the variation of the modeling results. Note that smaller R_c implies more efficient vacuum pumping. In the plasma modeling, it is assumed that the plasma temperature at the backside of the curtain is the same as that in front of the curtain. Thus, the

input parameters are T_{p_c}, R_c, and the duct diameter D_m. The cases that meet the vacuum pumping requirement at the maximum R_c are illustrated in Table VII.1:

As revealed by results in Table VII.1, the applicability of the new concept for vacuum pumping seems positive. Namely, the neutral density behind the curtain divertor is in general greater than that in front of the curtain by more than an order of magnitude, and the pumping duct diameter D_m is much less than that in the case without the chamber behind curtain. Results also show that the Mach number on the backside of curtain is much less than unity (see Figure VII.4), which implies that there is slight stagnation of particle flow as soon as the charged particles penetrate the porous curtain divertor. This explains the fact that the obtained n_{p_c} is larger than n_p. The validity of the assumption of uniform neutral density behind the curtain can be confirmed by the obtained considerably long average mean free path in a chamber of ~ 1 m depth. Note also that there is no physical sputtering at the tungsten chamber wall.

VII.C. Proposed Design

The above new concept can be improved further [LaBombard, private communication, 1991], since as indicated by equation (VII.5), n_0 can be

Table VII.1

Simulation Results for New Concept of Vacuum Pumping

	Case 1	Case 2	Case 3
f_t given	0.1	0.2	0.2
R_c given	0.7	0.6	0.8
$D_m\ (m)$	0.4	0.2	0.2
R	0.99723	0.99303	0.99642
$n_{p_c}\ (m^{-3})$	$6.26{\cdot}10^{19}$	$5.98{\cdot}10^{19}$	$6.65{\cdot}10^{19}$
$n_w\ (m^{-3})$	$2.29{\cdot}10^{18}$	$4.60{\cdot}10^{18}$	$4.73{\cdot}10^{18}$
$n_0\ (m^{-3})$	$2.58{\cdot}10^{16}$	$5.20{\cdot}10^{17}$	$2.67{\cdot}10^{17}$
$T_{p_c}\ (eV)$ given	57.0	57.0	57.0
$T_w\ (eV)$	56.4	55.9	55.8
sputter yield Y	0.0	0.0	0.0
M_{p_c}	0.01	0.03	0.01
mean free path of neutrals (m)	0.28	0.14	0.13

increased significantly (and hence the neutral pressure) if A_b is made much smaller. This can be accomplished by orienting the droplet curtain in such a way that it intercepts the incident charged particles normally (rather than grazingly as in the afore-mentioned new concept) (see Figure VII.5). Thus, A_b becomes $f_t A_c = 0.035\ m^2$ (rather than $2\ m^2$). (Note that similar arrangement is not feasible for the conventional solid surface divertors since a large divertor plate area would be required to lower the heat deposition per unit area.) This can be achieved by employing many layers of Ga droplet curtains to ensure the selected transparency of the curtain divertor. In addition, by doing so the heat transfer can be handled as straightforward as in the case without a pumping chamber behind the curtain and thus, as before, no material compatibility problem is expected (see Chapter VI for details). The erosion problem of the tungsten wall edges at the backside of the curtain can be eliminated by making the curtain opaqueness 100 % at those locations (see Figure VII.5).

Simulation results for the proposed design are given in Table VII.2. Note that the imposed $T_{p_c} = 44\ eV$ is lower than $57\ eV$ in Table VII.1 in that there is no plasma momentum loss through the charge exchange between the neutrals and the fast incident charged particles. Several conclusions can be drawn from the simulation results. First, the neutral pressure behind the curtain can be brought up to $10^{19}\ m^{-3}$ (hence the neutral pressure in chamber to 0.5 $Torr$) , while the backflow flux $(1/4)n_0 v_0 A_b$ is smaller than the penetrating particle influx by one order of magnitude. (Note, however, the neutral particle flow in the pumping ducts maintained at room temperature is still in the molecular flow regime.) Thus, the required pumping duct diameter is much smaller than that associated with the original curtain divertor design (i.e., $0.4\ m$), in some cases nearly ten times. This implies that there can be a difference of nearly 100 times

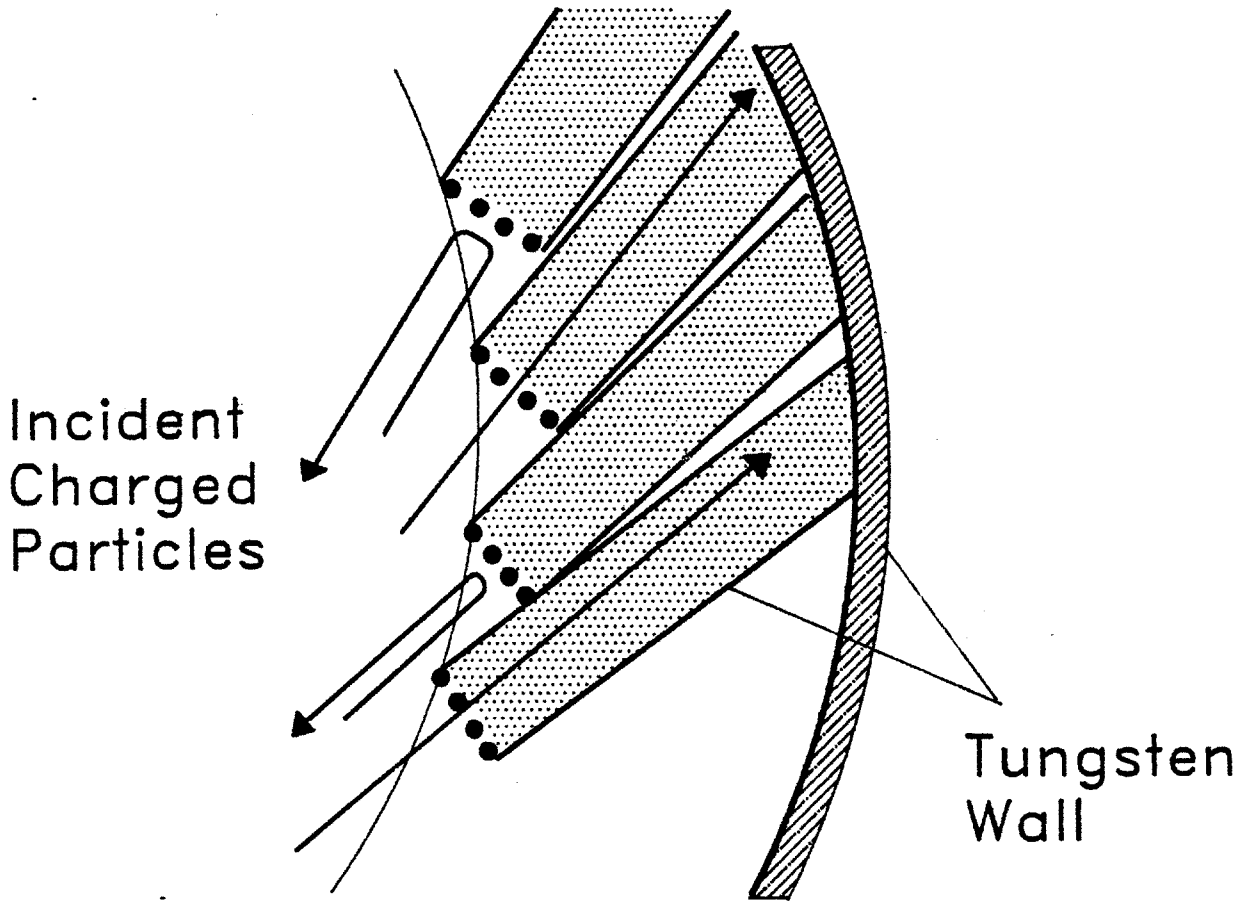

Figure VII.5: The proposed design to facilitate vacuum pumping

Table VII.2

Simulation Results for Proposed Design

	Case A	Case B	Case C	Case D
f_t given	0.1	0.2	0.1	0.2
R_c given	0.5	0.5	0.8	0.8
$D_m\ (m)$	0.05	0.05	0.10	0.05
R	0.9974	0.9934	0.9976	0.9972
$n_{p_c}\ (m^{-3})$	$8.43{\cdot}10^{19}$	$8.55{\cdot}10^{19}$	$9.93{\cdot}10^{19}$	$1.01{\cdot}10^{20}$
$n_w\ (m^{-3})$	$3.37{\cdot}10^{18}$	$7.00{\cdot}10^{18}$	$3.52{\cdot}10^{18}$	$7.40{\cdot}10^{18}$
$n_0\ (m^{-3})$	$1.25{\cdot}10^{19}$	$3.14{\cdot}10^{19}$	$1.45{\cdot}10^{18}$	$1.32{\cdot}10^{19}$
$T_{p_c}\ (eV)$ given	44.0	44.0	44.0	44.0
$T_w\ (eV)$	43.1	42.1	42.8	41.6
sputter yield Y	0.0	0.0	0.0	0.0
M_{p_c}	0.02	0.04	0.007	0.01
mean free path of neutrals (m)	0.21	0.10	0.20	0.10

in the total pumping panel area for a Ga droplet divertor with and without the proposed pumping design. Second, the plasma temperature near the tungsten chamber wall (T_w) is low enough such that the accelerated (by plasma sheath) charged particles have average energy below the tungsten sputtering threshold ($\sim 164\ eV$).

VII.D. Summary and Conclusions of Chapter VII

Potential vacuum pumping problems associated with the original liquid Ga droplet curtain divertors are pointed out. First, the possibly under-estimated recycling coefficient R under ITER high edge plasma temperature condition can lead to serious insufficiency in helium ash removal. This, in turn, can cause considerable radiation losses in the main plasma as well as excitation of plasma thermal instabilities (disruptions), and eventually quench the plasma. Second, the nonuniformity in neutral particle spatial distribution in front of the curtain is expected to make the required pumping duct diameter undesirably large. Hence, new schemes for vacuum pumping need to be considered.

A new concept is presented in which the Ga droplet curtain divertor is made slightly transparent (similar to a "Holy wall" concept previously proposed) to the grazingly incident charged particles which are then neutralized by the tungsten wall of the chamber behind the curtain. Simulation of the plasma within the chamber shows that the resultant neutral pressure is at least one order of magnitude greater than that in front of the curtain divertor (assuming each neutral has Franck-Condon energy $\sim 5\ eV$). Thus, with this new pumping scheme the sufficiency in helium ash removal can be ascertained, and further, the vacuum pumping panel area can be reduced. However, this new pumping scheme can be improved further.

One defect of the above pumping scheme is that the transparent area seen by the backflow neutrals A_b ($\sim 2\ m^2$) is much larger than that seen by the grazingly incident charged particles ($f_t \cdot 0.35\ m^2$), such that the desired chamber neutral pressure cannot be reached. Thus, it is proposed that the curtain be oriented so that it is facing normally to the incident charged particles, and that it achieve the slight transparency f_t by using about 10 (rather than 3) layers of the Ga droplet shower curtains. This not only brings A_b down to $f_t \cdot 0.35\ m^2$ but also takes care of the heat transfer requirement. Simulation results indicate that chamber neutral pressure of about 0.5 $Torr$ can be achieved with small pumping ducts ($\sim 5\ cm$ in diameter).

Finally, merits of the proposed pumping scheme are listed below:

1) The concern of porous wall erosion is essentially immaterial to the liquid droplet curtain divertor;

2) The motion of the droplet curtain pattern facilitates the sweeping of the divertor heat load on the chamber tungsten wall;

3) The neutral density within the chamber behind curtain is several orders of magnitude greater than that in front of the curtain, and is expected to be more uniformly distributed. This should significantly reduce the required pumping duct size;

4) The capability in adjustment of the vacuum pumping panel area within the chamber offers another engineering control knob to the divertor recycling coefficient R;

5) The variability of the droplet curtain pattern is expected to eliminate the problem of insufficient helium ash removal.

CHAPTER VIII. PLASMA DISRUPTIONS, MATERIAL COMPATIBILITY AND TRITIUM PERMEATION

VIII.A. Plasma Disruptions

Major plasma disruptions appear in all tokamaks under various conditions, which often result in catastrophic termination of the main plasma. Even with their physics far from being understood, they can roughly be classified according to cause (see, e.g., [Post et al, 1991]). Density limit disruptions are thought to be caused by a thermal instability of the edge plasma in machines with metal or carbon plasma-facing components. Impurity accumulation may also lead to disruptions by effectively lowering the density limit. While low-q_a disruptions usually occur when the main plasma operation has $q_a < 2$, where q_a is the "safety factor" defined as the ratio of the toroidal angle increment to that of the poloidal angle when following a magnetic field line at main plasma edge. Beta-limit disruptions occur near the Troyon β limit (i.e., $\beta \leq 0.03I(MA)/aB$ to avoid high n (internal) ballooning modes and low n (external) ballooning kink modes), where β is the ratio of the plasma pressure to the magnetic pressure, a is the plasma minor radius.

Disruptions also occur during transient phases of the plasma operation. Ramp-up disruptions occur during startup. Changes of plasma configuration (such as transition from limiter to separatrix-bounded plasma), large sawtooth crashes (particularly at low q), strong edge-localized wave mode (ELM) activity, and rampdown or termination of auxiliary heating can all give rise to serious plasma disruptions. Interested readers are referred to [Post et al, 1991] for more details.

VIII.A.a. Transient thermal load

The evolution of disruptions can be divided into four phases, which are most easily seen in density limit disruptions (for other disruptions, the pre-precursor and precursor phases sometimes do not appear explicitly). Major characteristics of these phases are as follows (see, e.g., [Post et al., 1991]):

1) Pre-precursor phase: This precedes a density limit disruption. A slow increase in radiation, up to a significant fraction of the input power during times up to 1 s, at the plasma edge, scrape-off layer, and divertor region.

2) Precursor phase: During this phase, MHD modes are frequently seen to be excited, particularly the m=2, n=1 mode (see, e.g., JET results in [ITER R& D, 1989]).

3) Thermal quench phase: This is the phase of most concern to the protection of divertor plates. A first stage of the thermal quench is often a redistribution of the electron temperature profile lasting for several ms (see, e.g. Tore Supra results in [Vallet et al, 1989]). Then, the plasma loses the major portion (50 % to 80 %) of its thermal energy in 100 to several hundred microseconds to the plasma-facing components; while the rest is presumably radiated away.

4) Current quench phase: After the energy quench, an increase of the total current, accompanied by a negative voltage spike, is observed and normally attributed to a flattening of the current profile [Post et al, 1991]. The duration of the current quench is variable, but the fastest quench times observed in various devices are 5 to 15 ms. During this phase, most (over 75 %) of the magnetic energy is lost by radiation. However, owing to the system's inductance, transient currents will be induced at the plasma-facing components which subsequently impose $J \times B$ body force on these components. For this reason, any liquid metal

divertor surface with large continuous area is not favored.

In the following, the performance of the Ga droplet curtain divertor will be evaluated against the major disruption heat load. The issues of the Ga vapor protection and the erosion of the Ga droplet curtain will be addressed.

VIII.A.b. Availability of Ga vapor protection

It has been predicted that for general fusion devices the liquid metal vapor generated through the evaporation of the liquid metal film divertor under the transient heat load can effectively protect the backing plate (see, e.g., [Hassanein and Smith, 1988]). It is thus interesting to inquire about the availability of such protection for the divertor chamber wall in the case of the liquid Ga droplet curtain divertor. The assumption is adopted that 80 % of the plasma thermal energy ($\sim 0.6\ GJ$) is lost to all plasma-facing components ($\frac{1}{2}$ to first wall, $\frac{1}{2}$ to divertors) in 0.1 ms [Nygren and Cohen, 1990]. If there are 4 divertors associated with the two-null main plasma, then the total thermal energy deposited onto each divertor is 60 MJ during the thermal quench phase (i.e., average deposited power $q_t = 6.0 \cdot 10^{11}\ W$). This means that for each shower curtain of effective (semi-sphere droplets) area of 1.67 m^2, the heat flux is $3.60 \cdot 10^{11}\ W/m^2$ in the 0.1 ms period.

The degree of liquid gallium evaporation can be roughly estimated by assuming that the liquid gallium boils immediately after the deposition of the transient heat load and that the whole spherical surface of each gallium droplet evaporates. In the following calculation, only one layer of the 3-layered droplet curtain will be employed for conservatism and also simplicity. The energy balance describing such a situation is given by:

$$P_{MD} = \rho \frac{dV}{dt} c_p \Delta T + \Gamma_v(T_b) A_{div} \left(\frac{h_{lg}}{N_A} + \epsilon_{ion} \right) \qquad (VIII.1)$$

where $P_{MD} = 6.0 \cdot 10^{11}\ W$ is the heat power deposited on each divertor, $\rho(T_b) \approx 4881\ kg/m^3$ is the gallium mass density at the boiling point ($T_b \approx 2478\ K$) under pressure of the order 1 atm, dV/dt is the liquid gallium volumetric flow rate, ΔT is the gallium temperature change from liquid phase to boiling, $\Gamma_v(T_b) = (1/4) n_{Ga} \overline{v}$ (n_{Ga} is the Ga vapor number density, $\overline{v} \approx 863\ m/s$ is the average speed of the evaporated Ga atom) is the evaporating gallium atomic flux, $A_{dia} = 3.34\ m^2$ is the effective curtain divertor area which evaporates, $h_{lg} = 272.5\ J/mole$ is the gallium evaporation heat, N_A is the Avagadro's number, and $\epsilon_{ion} = 5.999\ eV$ is the ionization energy of a gallium atom.

As can be easily proven that the heat power consumed in bringing the liquid Ga to boiling is negligible compared with the latter consumption by the evaporation and electron impact ionization. The calculated evaporating flux is thus $\Gamma_v(T_b) \approx 1.4 \cdot 10^{29}\ m^{-2} s^{-1}$ and accordingly, the gallium vapor number density is $n_{Ga} \approx 6.5 \cdot 10^{26}\ m^{-3}$.

The evaluation of the availability of Ga vapor protection can be accomplished by applying the appropriate stopping power ($-dE/dx$) formula. This is determined by the magnitude of the "Thomas-Fermi energy" ϵ_{TF} (see, e.g., [Langley et al, 1984]), which is defined as the ratio of the incident (D+T) particle energy to the normalization energy:

$$EL = \frac{(M_1 + M_2)(Z_1 Z_2)(Z_1^{2/3} + Z_2^{2/3})^{1/2}}{0.03255 M_2}\ eV \qquad (VIII.2)$$

Assuming the incident particle energy is about 10 keV during the major

disruption thermal quench phase, and using $EL = 3.25\ keV$ for the case of interest, the dimensionless Thomas-Fermi energy is obtained: $\epsilon_{TF} \approx 3.1$. In this regime the retardation of the energetic charged particle is through the electronic stopping of the gallium vapor atoms [Sigmund, 1981]. The appropriate stopping power equation is the Lindhard and Scharff formula [Sigmund, 1981] (in CGS unit),

$$\frac{-dE}{dx} = S_e n_{Ga}$$
$$S_e \approx Z_1^{1/6} 8\pi e^2 a_0 \frac{Z_1 Z_2}{\left(Z_1^{2/3} + Z_2^{2/3}\right)^{1/2}} \frac{2\pi v_1}{h} \qquad (VIII.3)$$

where S_e is the electronic stopping cross section, e is the statoelectic charge ($= 4.8 \cdot 10^{-10}\ esu$), $a_0 = 0.529 \cdot 10^{-8}\ cm$, v_1 is the average speed of the incident charged particle and is $8.7 \cdot 10^7\ cm/s$, and $h/(2\pi) = 1.05 \cdot 10^{-27}\ erg \cdot s$ is the barred Planck's constant. Thus, $S_e = 1.15 \cdot 10^{-25}\ erg \cdot cm^2$, and the stopping power is $-dE/dx = S_e n_{Ga} = 46.7\ MeV/cm$. For 10 keV incident charged particles during thermal quench phase, the average stopping range within the Ga vapor is about 2 μm. While the Ga vapor thickness in front of the curtain divertor can be estimated as roughly equal to the ionization mean free path l_{mfp} in the edge plasma with density say $n_e \sim 1 \cdot 10^{20}\ m^{-3}$,

$$l_{mfp} = \frac{\overline{v}}{n_e < \sigma v >_{ion}} \approx 520\ \mu m \qquad (VIII.4)$$

Therefore, the thickness of the Ga vapor is much larger than the stopping range of the 10 keV charged particles. The Ga vapor can thus effectively protect the tokamak wall as well as other structure behind the curtain divertor during the major disruptions of ITER-like reactors.

VIII.A.c. Erosion of the Ga droplet curtain divertor

Since, as implied in the last Subsection, the sputtering effect caused by the energetic incident particles on the Ga droplet curtain divertor is essentially immaterial due to the vapor shield, the erosion of the divertor can be attributed mainly to the evaporation depletion. The erosion rate dr_d/dt of each Ga droplet (2.5 mm diameter) can be estimated by

$$\Gamma_v(T_b)4\pi r_d^2 m_{Ga} = \frac{dr}{dt}4\pi r_d^2 \rho \qquad (VIII.5)$$

where $\Gamma_v(T_b) = 1.4 \cdot 10^{29}\ m^{-2}s^{-1}$ is the evaporation flux, $r_d = 1.25\ mm$ is the Ga droplet radius before being eroded, m_{Ga} is the mass of a Ga atom, $\rho = 4881\ kg/m^3$ is the Ga mass density at the boiling temperature ($T_b = 2478\ K$) under pressure of several atm. Thus dr/dt is calculated to be 3.4 m/s, and the total eroded droplet radius in the thermal quench phase (0.1 ms) is about 0.34 mm, which is much less than the original droplet radius 2.5 mm.

It is therefore concluded that during a major disruption event, the Ga droplet curtain divertor is far from being burnt out, and thus structures behind the curtain divertor are expected to be well protected.

VIII.B. Gallium Property and Material Compatibility

Unlike lithium, gallium does not interact in any noticeable way with oxygen and nitrogen. In fact, even pure and dry oxygen has no appreciable effect on gallium at temperature up to 260°C. And there is no reaction between nitrogen and gallium even at 1000°C [Sheka et al, 1966]. From the point of view of gallium handling and safety protection, this is very desirable.

However, when gallium is at high temperature (above $400°C$) it becomes very corrosive to many structural materials (both metals and nonmetals). Among metals, the greatest resistance to reaction with gallium is manifested by tungsten and tantalum, and an alloy which is 92.5 % tantalum and 7.5 % tungsten [Sze, 1991, private communication]. At temperatures above $400°C$, tantalum is only slightly attacked by gallium, while tungsten does not interact with gallium noticeable until $800°C$ [Sheka et al, 1966].

Vanadium reacts readily with gallium. The compound V_3Ga is known to be a superconductor material at 14.3 K. Niobium is stable till $400°C$ but is strongly attacked at $450°C$. Titanium, Zirconium, and Thorium are easily coroded by gallium at $540°C \sim 600°C$. Special alloys containing iron, chromium, molybdenum, nickel and certain stainless steels are all severely attacked by gallium at temperature around $600°C$. Gallium reacts readily with manganese above $600°C$. Pure iron, cobalt, and nickel react easily with gallium and form compounds or solid solutions. With cobalt, gallium forms GaCo; with nickel, gallium forms GaNi which melts at $1220°C$. Beryllium does not react with gallium below $500°C$, and remains stable up to $1000°C$. For nonmetals, graphite withstands the attack of gallium up to $800°C$, while quartz glass to $1160°C$ [Sheka et al, 1966] (see Figure VIII.1 for a comparison).

However, as pointed out in Chapter VI, the operational temperature range of the liquid Ga droplet curtain divertor should be from above the Ga melting point to about $200°C$, rather than to more than $400°C$ as originally presented by Russians [Murav'ev, 1989] owing to their application of the over-estimated divertor heat load. The identified low Ga operational temperature has significant importance to the material compatibility of gallium with structural materials, particularly for the portion of conduits connecting the acceptor of the heated

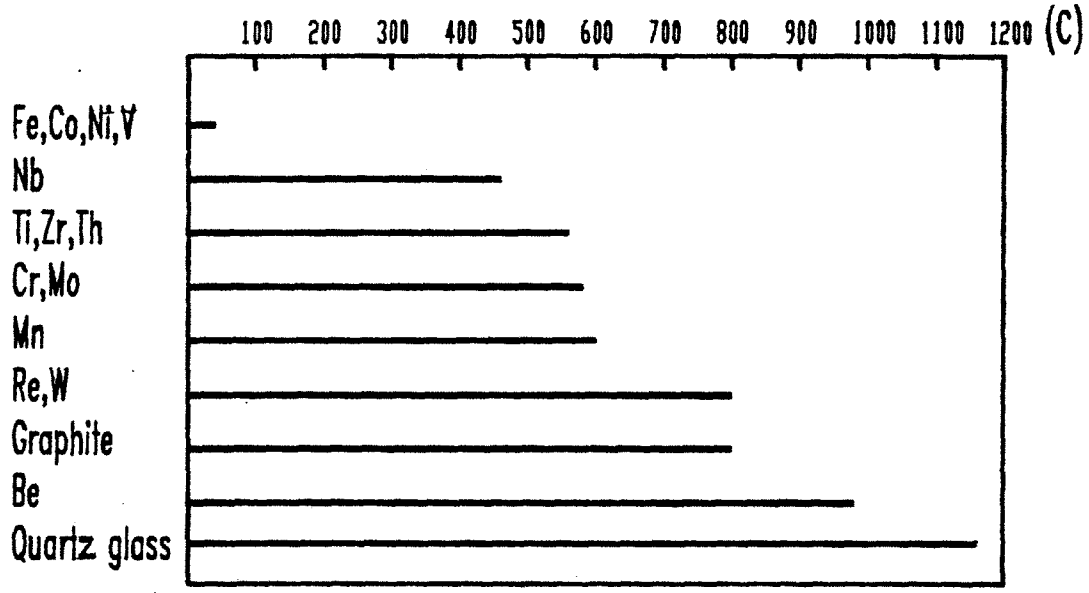

Figure VIII.1: Compatibility of Materials with gallium

Ga droplets.

For the operational temperature window of interest in the case of Ga droplet curtain divertor (i.e., about $100°C \sim 200°C$), the corrosion data for various materials are not available. Nevertheless, experimental data obtained by Russians [Murav'ev, 1989] at $250°C$ and $400°C$ can be useful for an evaluation of the material compatibility issue. It was discovered that (based on 500 hours testing time) at $250°C$, steels coated with chromium have corrosion rate of merely several $\mu m/yr$. In addition, other chromium alloyed steels, martensitic steels, ferritic steels, and austenitic steels all have corrosion rate less than 0.1 mm/yr [Murav'ev, 1989]. Thus, it is realized that the much concerned material compatibility problem is, in fact, not a serious one.

VIII.C. Tritium Permeation

One major concern in conveying liquid gallium through the piping system is the tritium permeation problem, particularly under the steady state operation of the Ga droplet curtain divertor. In addition, it should be ascertained that the hydrogen recombination coefficient on the inner side of the selected conduit material is large enough so that tritium inventory will not become a problem eventually. Therefore, the best solution is to employ a conduit made of a certain material which has much less hydrogen solubility than gallium. Since the data for the hydrogen solubility of Ga is unavailable, this option remains open. Nevertheless, beryllium seems to be one of the best among pure metals [Doyle and Brice, 1984] in this respect. Besides, it does not react with gallium at temperature of interest, and it has high thermal conductivity. Thus, beryllium coating is considered applicable on the inner side of the Ga-conveying pipes or conduits for Ga transport purpose.

VIII.D. Summary and Conclusions of Chapter VIII

It is shown that during the thermal quench phase of a major disruption, the evaporated gallium atom cloud in front of the Ga droplet curtain can serve as a protective shield to the divertor system. In addition, at the end of this phase the liquid Ga droplets are far from being burnt out. Hence, the liquid Ga droplet curtain divertor design is robust against off-normal situations.

Due to the realization in Chapter VI that the upper operational temperature for the liquid Ga is about $200°C$, the material compatibility concerns turn out not to be serious. Namely, chromium coated steels and other martensitic, ferritic, and austenitic steels all have very little reaction with gallium under the relevant conditions.

Even though the hydrogen solubility of the liquid Ga is very little (presumably similar to that of aluminum [Sze, 1991, private communication]) under the situation of interest, there can still be tritium permeation concern as the steady state ITER-like reactor is operated for a long period of time. Beryllium coating is proposed to be used as the tritium permeation barrier in the Ga-conveying conduits and in the heat exchanger, even though it is a toxic material. The choice is based not only on beryllium's low reaction crossection with Ga at temperature of interest (see, e.g., [Murav'ev, 1989]) but also on its much higher surface hydrogen recombination coefficient and much lower hydrogen diffusion coefficient (compared with those of aluminum) [Doyle and Brice, 1984]. In addition, beryllium has high thermal conductivity (better than tungsten, about half of that of copper) which is desirable in terms of heat transfer.

CHAPTER IX. SUMMARY AND CONCLUSIONS

The severe requirements imposed on divertors by the steady state operational conditions of the fusion reactors (such as conceived for the ITER tokamak) motivates another examination of the old idea of applying liquid metals as divertor neutralizer materials. For example, without accounting for redeposition (to be more conservative since it may not be spatially uniform) and self-sputtering, the physical sputtering erosion rate of a tungsten plate (the most sustaining among solid divertor plates) is 0.56 mm/day. The liquid metal divertors are appealing in part because of the self-cooling and self-annealing properties, thus eliminating the design conflict between the sputtering erosion and heat transfer limits associated with the solid surface divertors. They have also other possible more subtle merits, examples of which are:

1. providing a degree of capability in controlling the neutral particle recycling to the plasma, which may yield cleaner main plasma and, therefore, longer energy confinement time;

2. providing a liquid metal vapor cloud which which enhances the protection of the divertor system and may also block the flight of sputtered or evaporated liquid metal plate atoms into the main plasma (see, e.g., [Dolan, 1982]);

3. resulting in an expected lower edge plasma temperature compared with that of the most promising solid metal (tungsten) divertor plate.

Motivated by the afore-mentioned possible advantages of the liquid metal divertor, several reference designs were proposed. These include the liquid metal protective film divertor (Figure III.1 and III.2), the liquid metal pool divertor (Figure III.3), the lithium jet droplet beam divertor (Figure III.4), and the Ga

droplet curtain (shower) divertor (Figure III.5). The working fluids employed by the above reference designs are mostly lithium, gallium and Ga-eutectic (67 % Ga, 20.5 % In, 12.5 % Sn).

There are, however, some concerns about the liquid metal divertors. They include:

a. evaporation depletion and contamination of the main plasma
b. sputtering erosion and contamination of the main plasma
c. blistering erosion and contamination of the main plasma
d. heat transfer and pumping requirement
e. MHD equilibrium
f. MHD stability
g. tritium inventory and permeation
h. helium ash removal
i. liquid metal renewal (tritium separation)
j. material compatibility
k. major disruptions

This work investigates the feasibility issues of the afore-mentioned reference liquid metal divertor concepts based on both the potential merits and concerns. In the process of evaluation, if a certain reference concept cannot meet one requirement imposed by the steady state tokamak reactor conditions, this concept is considered infeasible. In addition, by the knowledge gained during this investigation, a new divertor pumping scheme and some suggestions for future experiments are provided. In the analyses, ITER parameters are used only for illustration purposes.

IX.A. Edge Plasma Modeling

It is widely recognized that results from divertor models can be quite sensitive to the boundary conditions that are assumed at the divertor neutralizer plate. However, some models in the past have assumed electron and ion heat transmission coefficients with little justification. In this work it is pointed out that energy and momentum fluxes from backscattered neutral deuterium and tritium atoms can significantly contribute to the energy and momentum balance of the divertor plasma and consequently affect the estimates of steady state plasma conditions.

A two point model similar in its structure to Galambos and Peng [1984] is derived, including momentum and energy sources from charge exchange and a self-consistent fluid treatment of the sheath heat transmission coefficients. This model is analytically simple, but accurate enough for engineering evaluation purposes and is applicable to all types of solid or liquid metal surface divertors. In Chapter II, divertor conditions associated with INTOR [IAEA, 1980] and ITER [Post et al, 1991] fusion reactors are estimated and the effects of including the backscattered fluxes are discussed.

It is shown that results from Harrison's INTOR edge plasma modeling [Harrison, 1983] are too optimistic in terms of the achieved edge plasma density and temperature. Namely, without taking into account the backscattered energy and the momentum loss due to the charge exchange process, dense and cool edge plasma is obtained, which makes the average energy of the accelerated charged particles (through sheath action) below the tungsten plate sputtering threshold. However, correct simulation indicates that dense and cool edge plasma cannot be achieved (under the same divertor throat plasma density), and that the

physical sputtering threshold of the tungsten divertor plate is exceeded. A surprising discovery is that the throat plasma density is not necessarily larger than that near the divertor plate (as always seen in small power fusion devices), particularly under INTOR or ITER-like steady state conditions. However, the throat plasma temperature is always larger than that near the divertor plate, as it should be, in order to convey the heat load through thermal conduction. In addition, the functional relation between the plasma densities at the divertor throat and near the divertor plate, as predicted by Ohyabu et al [1982], is confirmed numerically.

When the steady state ITER parameters (with tungsten divertor) are incorporated in the edge plasma model, the resultant plasma condition is rather pessimistic. That is, even without taking into account the peak-to-average factor 3.4 of divertor heat load [Post et al, 1991], the plasma temperature near the plate is predicted to exceed 100 eV, while the plasma density is always smaller than the throat plasma density (see Table II.3). Ignoring redeposition, the consequent physical sputter yield of about 0.01 may lead to the tungsten plate erosion rate of 20 cm per year (cf. about 70 cm per year for beryllium plate at 100 % duty cycle, agreed with the estimation of Nygren and Smith [1991]). Furthermore, other processes can also cause significant damage to the divertor plate. For example, the blistering erosion resulting from hydrogen bubble formation within the brittle tungsten plate may lead to eroded holes and exfoliation on the plate [Dolan, 1982]; unipolar-arc can deplete the divertor plate on a steady state basis by emitting ions and macroparticles from the moving arc spots. Thus, the applicability of any solid surface divertor plate is questionable.

IX.B. Feasibility of Droplet Beam Divertor

Among the various liquid metal divertor concepts, the feasibility of the lithium droplet beam divertor [Werley, 1989] is suspected. In this concept, the liquid lithium is intended to be used as an ion burial material in the hope that the sorption of both hydrogen and helium can significantly facilitate impurity removal. However, even with many merits, the concept suffers three major defects. First, in Werley's calculation, the assumed incident ITER edge plasma particle flux is three orders of magnitude smaller than what would be realistically expected (see, simulation results in Chapter II and [Post et al, 1991]). That is, the realistic incident flux would form about one mole of solid LiH per second in the liquid lithium divertor (if lithium is, as postulated, a hydrogen getter). Thus, the proposed capability for refreshing the liquid lithium is highly questionable, even with large-scale batch job arrangement (aside from tritium inventory problem).

Second, the employment of empirical relations for fluid jet atomization in air is inappropriate since lithium is not allowed to be exposed to air to avoid the fire hazard. Thus, there is uncertainty about the breakup length of the liquid lithium jet if it is in the vacuum environment. Besides, if two beam-confining tubes are to be built at the top and bottom of the tokamak, space related problems will materialize. Third, the reception of the high speed (160 m/s) droplet beam at the end tank can be a difficult task, as was pointed out by Werley [1989]. The splashing of the liquid lithium can contaminate the vacuum environment and subsequently poison the main plasma.

Therefore, the lithium droplet beam divertor concept is not ranked favorable by the authors.

IX.C. Liquid Metal-Hydrogen Interactions

In order to carry out engineering evaluations of the liquid metal divertors (particularly, those of lithium (Li) and gallium (Ga)), knowledge of the edge plasma conditions is required. One crucial physical quantity in the divertor plasma operation is the recycling coefficient R, which is closely related to the liquid metal-hydrogen interactions. (R is the probability that an ion incident on the divertor plate will be re-ionized in the plasma. For solid surface divertors R is close to unity under ITER-like conditions.) If the liquid metal is a hydrogen getter (or ion burial material) then the divertor will be operating in a low recycling mode until the liquid metal is nearly filled with hydrogen (if there is no tritium inventory concern). On the contrary, if the liquid metal is not a hydrogen getter, the divertor will be operating in a high recycling mode (i.e., one incident particle will cause immediately the emission of one implanted particle in the liquid metal).

The permissible operational temperature range for a specific liquid metal is determined by the impurity level control considerations, which set the upper limit for the neutral pressure near the divertor plate to be 10^{-5} to 10^{-4} $Torr$ (1.3 mPa to 13 mPa). The maximum operational temperatures for lithium (melting point 186°C) and gallium (melting point 29°C) are 325°C and 750°C, respectively.

The hydrogen release process from the liquid metal is controlled by both the hydrogen transport and the surface molecular recombination processes. Knowledge of the diffusion coefficient D and the surface recombination coefficient K_f will suffice for the estimation of the liquid metal divertor recycling coefficient R. However, such crucial data are not available for the case of interest,

particularly K_f. Therefore, K_f is indirectly inferred from the comparison of a theoretical model [Doyle and Brice, 1984] and the existing experimental data of deuterium bombardment on liquid lithium [McCracken and Erents, 1969].

The result indicates that liquid lithium is a very good hydrogen getter under ITER-like steady state conditions (as it forms solid lithium hydrides LiH (a white solid which melts at $680°C$)) and it takes tens of minutes to fill a liquid lithium film neutralizer of 5 mm thickness with hydrogen. However, by this stage the resultant tritium inventory will be too large (several tens of kilograms for the whole divertor system) and may not be accepted due to safety considerations. The proposed maximum tritium inventory in the divertor system is set to be 2 kg [Cohen, private communication, 1991]. Another option to operate the lithium divertor in a low recycling mode is to refresh the liquid lithium efficiently (i.e., removal of about one mole tritium per second per divertor). However, the availability and reliability of such technology is questionable. Therefore, another option may be to have a slowly flowing thin film (of hundreds of microns) as the lithium divertor, if the phase of liquid lithium is not changed appreciably by the formation of LiH's, and if the provision of a secondary coolant can be made acceptable.

Liquid gallium, on the contrary, does not have the tritium inventory problem due to its negligible hydrogen solubility in the temperature range of interest (i.e., about $50°C$ to $200°C$) [Galaktionowa, 1980], and the decomposition of its thermally most stable hydrides Ga_2H_6 (even its existence is controversial) beyond $130°C$. In other words, the liquid gallium is not a hydrogen getter. Thus, even though the data for D and K_f of hydrogen in gallium are not available, the liquid gallium divertor is expected to operate in a high recycling mode.

IX.D. Divertor Plate Erosion and Main Plasma Contamination

Based on the analytic edge plasma model developed in Chapter II, and the investigation of liquid metal-hydrogen interactions, a steady state edge plasma simulation is carried out for the liquid metal divertors in comparison with the tungsten divertor, under ITER steady state operational conditions. For a typical divertor recycling coefficient $R = 0.99$, the result indicates that denser and cooler (but still very high temperature $\sim$ 100 eV) edge plasmas can be achieved by liquid metal (Li and Ga) divertors than by the tungsten divertor. Note that, as a reminder, the Li divertor here refers to a very thin lithium layer (about hundreds of microns) slowly flowing over a coolant-cooled metal plate, since the thicker self-cooled Li divertor has tritium inventory problem. Note also that if $R > 0.99$ then there are expected problems due to insufficient helium ash removal. However, since the edge plasma modeling results are found not to be sensitive to the value of R within the range from 0.80 to 0.99, the engineering evaluations based on the $R = 0.99$ edge plasma simulation results are appropriate.

From the modeling results it is realized that in order to reduce the edge plasma temperature, the droplet curtain divertor design [Murav'ev, 1989] is most desirable. That is, instead of using a single long divertor (about 1 m long in the tokamak toroidal cross-sectional view) for each null point (ITER is proposed to have two nulls, one on top, one at bottom), two shorter divertors (about 10 cm long each) are employed. This, according to the simulation results, can reduce the edge plasma temperature to about 57 eV.

The most important questions about the feasibility of applying liquid metals

as divertor plate materials, i.e., evaporation and sputtering, turn out not to be serious ones. The liquid metal vapor pressures at temperatures of interest are far below the maximum permissible neutral pressure in the divertor chamber limited by the impurity level control. For this same reason, it also implies that there is no vapor shield in front of the divertor plate at steady state. Under the plasma sheath action (different from the unipolar arc sheath), the physical sputter yields of the liquid metals (~ 0.8) are several times larger than that associated with the tungsten, according to Smith et al's empirical formula [Smith et al, 1981] under the simulated steady state ITER edge plasma conditions. However, it is expected that most of the sputtered atoms suffer from either electron impact ionization or charge exchange upon leaving the plate and are recycled back to the self-annealing liquid metal plate. Therefore, the resultant neutral pressures are estimated to be at most on the order of the maximum permissible neutral pressure ($\sim 10^{-4}\ Torr$), and these sputtered atoms are considered well confined near the liquid metal divertor plate. Even if some fraction of these sputtered atoms is transported to the main plasma, the resultant negative effects are not expected to be as serious as those caused by the tungsten divertor.

The large bombarding charged particle flux of a fusion reactor poses severe threat for the lifetime of solid surface divertors through blistering erosion, embrittlement and subsequent exfoliation. The concern relevant to the liquid metal divertors is the blistering erosion and divertor chamber contamination which result from the hydrogen bubble formation and eruptions within the liquid metals. It is found that if this phenomenon is to be avoided, the pumping speed of liquid metals will be very hard to achieve (i.e., on the order of 100 m/s), for a single long divertor at each null point. If, like the Russian droplet shower design, two short divertors (about 10 cm long each) are employed at each null point,

then the pumping speed of about 10 m/s can be achieved without difficulty, especially for the droplet curtain divertor concept.

From this investigation, it is obvious that the slowly flowing Li thin film divertor concept is not desirable. For this same reason, any (stationary) pool type liquid metal divertors are considered inappropriate. Therefore, only moving Ga divertors are discussed in the following.

Unipolar arc erosion appears to be a concern for the liquid metal divertors, particularly for the liquid Ga which is characterized by the low thermal conductivity (only about a quarter of that of the tungsten). Indeed, it is estimated that this phenomenon will very likely occur at all plasma facing components of an ITER-like fusion reactor, especially the divertors. Even though experimental data for the arc erosion rate of Ga is unavailable, it is expected that these emitted Ga atoms should have very short range under the high edge temperature environment and are recycled back to the self-recovering Ga plate. In case there is some emission of macroscopic particles, it is anticipated that even if the divertor chamber may be polluted by Ga droplets, the rendered detrimental effects on the main plasma may not be serious, since this does not occur close to the main plasma. However, this point needs to be confirmed in the future experiments.

On the other hand, it may appear ironic that the occurrence of the unipolar arc phenomena may be beneficial for the suppression of the physical sputtering on the divertor plates. Namely, when the unipolar arc is initiated, the divertor plate voltage drops from about 150 V (under steady state ITER conditions) to 10 V. In other words, the normal plasma sheath is now replaced by the so-called "unipolar arc sheath". If this is proven to be true in future experiments, then the concern associated with the physical sputtering of divertor plates is essentially

immaterial, for now the sputter threshold is no longer achieved by the average charged particles. As a comparison with the conventional solid surface divertors, even if this can be beneficial for the liquid Ga divertor, this is not the case for the tungsten divertor, since the latter still suffers severe threats from other physical processes such as the arc erosion and the blistering erosion.

It is concluded in Chapter V that the Ga droplet curtain divertor design is more favorable than the protective Ga film divertor, as far as the divertor erosion is concerned.

IX. E. MHD Flow and Heat Transfer

Evaluation of both the liquid Ga protective film divertor and the Ga droplet shower divertor in the heat transfer and MHD aspects is carried out in Chapter VI. A consistent liquid metal film MHD analysis was performed on a liquid metal film flowing down a chute across the toroidal magnetic field. The treatment shows that the pressure exerted on the liquid metal film by the bombarding charged particles dominates that by the sheath pulling action, and therefore, there is no external free energy that can cause Rayleigh-Taylor type instabilities. However, the free energy responsible for the possible Helmholtz type instabilities was proven to come from the equilibrium velocity profile within the liquid metal film.

Existing equilibrium solution [Aitov et al, 1987] implies that only non-conducting chute can be used for a pumped Ga film neutralizer since employment of any metal chute would result in too large equilibrium film thickness ($\sim O(10\ cm)$). Also, the chute side walls are necessary to provide the appropriately thick film. It is found that a 5 mm thick Ga film with inlet flow speed 1 m/s and with 50° inclination angle, the heat transfer requirement of ITER (even

one divertor for each null point) on the liquid Ga flow pumping speed can be met without difficulty. This is to be compared with another proposed "injection type" film divertor concept (see Figure III.1) which should be excluded since at such pumping speed the liquid metal pumped up from bottom is likely to be injected into the plasma rather than being flown over the guiding substrate.

Based on the equilibrium results, a stability analysis is performed. It is realized that for a moderate chute inclination angle, say 50°, it is not difficult for the film flow to satisfy both the ITER heat transfer requirement and the stability criterion (under the assumption that liquid metal physical property does not change appreciably during the bombardment of charged particles). However, if much higher film inlet speed is required, for instance, to avoid the blistering erosion (discussed in Chapter V), the film will be MHD-wise (linearly) unstable. Note that in the above analysis, other more complicating and uncertain factors are not included such as the "halo current" (see, for example, [Post et al, 1991]) resulting from the developed electrical potential difference between the upper and lower (or inner and outer) divertors plates. Note also that the blistering erosion is avoided by making the time period during which the circulating Ga plate is exposed to the charged particle bombardment short enough, and as soon as the Ga fluid flows out of the exposure region, stirring or other separation procedure should be employed to enforce the liberation of hydrogen gas bubbles.

Even if the afore-mentioned problems related to the MHD effects can be resolved, there are other important engineering concerns with regards to the application of the liquid metal film divertor concept. One is the erosion of the exposed chute walls by the charged particle bombardment. A possible solution may be the one illustrated by Kirillov et al [1990] in which the shape of the chute are constructed in such a way that the side walls are not in the way of the

grazingly incident charged particles (see Figure VI.8). The other engineering concern is that the non-conducting chute is not favorable in terms of heat transfer. Thus, it may seem desirable to use a metal chute which has non-conducting coating on the side in contact with the liquid gallium. However, such insulator coating material (which should also be compatible with gallium) needs to be found or developed.

For the liquid droplet curtain divertor, if only the heat transfer is of concern, then with Ga operational temperature range of about $600°C$, the necessary droplet (2.5 mm diameter) speed is less than 1 m/s, which may be undesirable in terms of the droplet formation. However, in order to avoid the blistering erosion caused by the hydrogen bubble eruptions, droplet speed of about 10 m/s is preferred, which reduces the Ga operational temperature range to only about $200°C$. Since Ga (melting point $29°C$) is highly corrosive above about $400°C$ with respect to many structural materials, this reduction of the maximum Ga operational temperature is of significant consequences.

MHD effects such as the plasma wind effect, the electric charge accumulation effect, and the droplet instability in the nonuniform magnetic field are shown to have negligible influence on the liquid Ga droplet curtain divertor. While the total pressure drop (including MHD and frictional losses) for the four droplet divertors (two for each null point) associated with the ITER reactor design was calculated to be about 10 MPa [Murav'ev, 1989], and the corresponding pumping power is about 40 MW, i.e. 4 % of the ITER steady state fusion thermal power.

The major engineering uncertainty associated with the droplet curtain divertor concept is the possible spraying of the droplets into the plasma. In fact, when used as a limiter (under more than 10 MW/m^2 heat load of the

Russian T-3M tokamak (major radius: 0.95 m, minor radius: 0.16 m, plasma current: 40 kA)) the liquid Ga-eutectic (67 % Ga, 20.5 % In, 12.5 % Sn) droplet curtain (with droplet speed of only $2 \sim 5$ m/s) tends to contaminate the main plasma [Vodyanyuk et al, 1988]. The cause is suspected by Russian scientists to be either the mechanical vibration of the droplet shower head (droplet shaper) or the possible liquid metal-plasma interaction. If the real cause is the former, then in principle this problem should be solvable. If it is the latter, the problem is more involved.

However, the above experimental result is not surprising. This is because at the limiter position any previously investigated liquid metal-plasma interactions can enhance the impurity level in the main plasma, such as physical sputtering, blistering erosion, etc. On the other hand, when used as a divertor, it is anticipated that the effect of this undesirable phenomenon will be significantly reduced. This point would await verification by future experiments. If it is indeed the case, then the conclusion can be drawn from the conducted analyses that the liquid Ga droplet curtain divertor concept is more appealing than the liquid Ga film divertor concept, and that future efforts in the development of liquid Ga divertors should be focused on the former.

IX.F. Vacuum Pumping Requirement and Proposed New Design

Potential vacuum pumping problems associated with the original liquid Ga droplet curtain divertors are pointed out in Chapter VII. First, the possibly under-estimated recycling coefficient R under ITER high edge plasma temperature condition can lead to insufficiency in helium ash removal. This, in turn, can cause considerable radiation losses in the main plasma as well

as excitation of plasma thermal instabilities (disruptions), and eventually termination of the main plasma. Second, the nonuniformity in neutral particle spatial distribution in front of the curtain is expected to make the required pumping duct diameter undesirably large (on the order of 1 m). Hence, new schemes for more efficient vacuum pumping are motivated.

An existing solid Holy wall divertor concept is shown to be infeasible due to the serious sputtering erosion under the steady state ITER-like conditions. Then, a new concept is presented in which the Ga droplet curtain divertor is made slightly transparent (like Holy wall) to the grazingly incident charged particles which are then neutralized by the tungsten wall of the chamber behind the curtain. Simulation of the plasma within the chamber shows that the resultant neutral pressure is at least one order of magnitude greater than that in front of the curtain divertor (assuming each neutral has Franck-Condon energy $\sim 5\ eV$). Thus, with this new pumping scheme the sufficiency in helium ash removal can be ascertained, and further, the vacuum pumping panel area can be reduced. However, this is still not good enough and thus is not the proposed design.

One defect of the above new pumping scheme is that the transparent area seen by the backflowing neutrals A_b ($\sim 2\ m^2$) is much larger than that seen by the grazingly incident charged particles ($f_t \cdot 0.35\ m^2$, where f_t is the transparency of the curtain divertor), such that the desired high chamber neutral pressure cannot be reached. Thus, the proposed design is to further orient the curtain divertor so that it is facing normally to the incident charged particles, and to achieve the slight transparency f_t by using about 10 (rather than 3) layers of the Ga droplet shower curtains. This not only brings A_b down to $f_t \cdot 0.35\ m^2$ but also takes care of the heat transfer requirement under the now more intense heat

load per unit area. Simulation results indicate that chamber neutral pressure of about 0.5 $Torr$ can be achieved with much smaller pumping ducts ($\sim$ 5 cm in diameter).

To conclude, characteristics of the proposed pumping scheme associated with the liquid Ga droplet curtain divertors are listed below:

1) The concern of wall erosion is essentially immaterial to the liquid droplet curtain divertor;

2) The motion of the droplet curtain pattern facilitates the sweeping of the divertor heat load on the chamber tungsten wall;

3) The neutral density within the chamber behind curtain is several orders of magnitude greater than that in front of the curtain, and is expected to be more uniformly distributed. This should significantly reduce the required pumping duct size;

4) The capability in adjustment of the vacuum pumping panel area within the chamber offers another engineering control knob to the divertor recycling coefficient R;

5) The variability of the droplet curtain pattern is expected to eliminate the problem of insufficient helium ash removal due to possible too high divertor recycling coefficient;

IX.G. Plasma Disruptions, Material Compatibility and Tritium Permeation

During the thermal quench phase of a major disruption (in which about half of 0.6 GJ energy is expected to be dumped on the ITER divertors in 1 ms [Post

et al, 1991]), the evaporated gallium atom cloud (with density $\sim 10^{25}\ m^{-3}$) in front of the Ga droplet curtain can serve as a protective shield to the divertor system. The range of a deuterium ion within the approximately 500 μm thick Ga vapor is estimated to be about several μm's, using electronic stopping theory [Sigmund, 1981]. In addition, at the end of this phase, only about 0.3 mm of the droplet radius (1.25 mm) is calculated to evaporate, and hence, the liquid Ga droplets will be far from being burnt out. Therefore, the liquid Ga droplet curtain divertor design is robust against off-normal situations.

IX.H. Final Conclusions and Suggestions for Future Experiments

It is found that the liquid lithium should not be used as a liquid metal divertor material owing to the resultant large tritium inventory that may develop. A comparison of Li and Ga as materials for liquid metal divertors is given in Table IX.1. The price of regular gallium is about $ 400 for 250 grams [AESAR company, 1991].

From the evaluation of this work, the liquid gallium droplet curtain divertor design together with the proposed vacuum pumping scheme is the best among existing liquid metal divertor concepts. The liquid Ga curtain divertor can be described as a more robust design compared to the solid surface divertors in terms of the scrape-off characteristics, MHD effects, and abnormal situations. While the other popular option – the protective Ga film divertor concept, suffers from mainly the MHD instability problem if the blistering erosion is to be avoided. Other divertor concepts such as the separately cooled slowly flowing very thin film and pool type divertors are considered inappropriate due to the blistering erosion concern. A comparison among different liquid metal divertor concepts is summarized in Table IX.2.

This work is conducted under the circumstances of dearth of relevant data for the fusion purposes. Therefore, the evaluation results should be considered tentative. Experimental efforts are necessary in the future in order to gain more precise knowledge of the engineering details to ensure the success of a divertor system associated with ITER as well as an electricity producing large tokamak. Also, other liquid metal options such as indium, tin, and lead (which are not hydrogen getters according to Galaktionowa, 1980] and [Hurd, 1952]) may also need to be explored experimentally.

Table IX.1

Comparison of Li and Ga as Liquid Metal Divertor Materials

	Lithium (Li)	Gallium (Ga)
Interaction with Hydrogen	Hydride Formation	No Hydride
Surface H-Release Process	Recombination-Limited	Diffusion-Limited
Divertor Operation	Low Recycling	High Recycling
Tritium Inventory Concern	Yes	No
Compatibility with Structure	Not Corrosive	Corrosive ≥ 400°C

*Except the slowly flowing thin Li film divertor

Table IX.2

Comparison of Different Steady State Divertor Concepts

	Solid	Lithium		Gallium		
	Solid Plate	Li drplt beam	Li Thin Film	Ga Pool	Ga Film	Ga Drplt Curtain
Sputtering erosion	yes	no	no	no	no	no
Insufficient heat removal	no	no	no	no	no	no
Design conflict in erosion and heat transfer	yes	no	no	no	no	no
H embrittlement and exfoliation	yes	yes*	yes	no	no	no
Tritium inventory concern	no	yes*	no	no	no	no
Blistering erosion	yes	yes*	yes	yes	no**	no
Detrimental MHD effects	no	no	no	no	yes	no
Detrimental disruption effects	yes	no	maybe	no	no	no
Limited to lower divertor	no	maybe+	yes	yes	yes	no

* Assuming the efficient Li renewal technology is not available
** Assuming it is a short film divertor (0.1 *m* long) flowing at 10 m/s
\+ Depending on the availability of tokamak space

REFERENCES

AESAR company, Ward Hill, Massachusetts, catalogue, 1991.

Aitov T. N., Ivanov A. B., Tananaev A. V., "Flow of Liquid Metal in A Coplanar Magnetic Field," *Magnetohydrodynamics*, **2**, 78, 1987.

Aitov T. N., Kirillina E. M., Tananaev A. V., "Stability of the Flow of A Thin Layer of Liquid Metal in A Coplanar Magnetic Field," *Magnetohydrodynamics*, 5, 1988.

Alire R. M., "Transport of Hydrogen in Liquid Lithium," *J. Chem. Phys.*, **65**, 1134, 1976.

Baehre M. D., Steiner D., "A Simple One-dimensional Personal Computer-based Plasma-edge Engineering Model for Divertor Design Calculations," *Fusion Tech.*, **17**, 412, 1990.

Baskes M. I., "A Calculation of the Surface Recombination Rate Constant for Hydrogen Isotopes on Metals," *J. Nucl. Mater.*, **92**, 318, 1980.

Begrambekov L. B. et al, "Emission of Material From the Surface of a Liquid Metal Under Irradiation in a Plasma," *Magnetohydrodynamics*, **23**, 263, 1987.

Behrisch R. (Eds.), *Sputtering by Particle Bombardment-I*, p.24, Springer-Verlag, New York, 1981.

Benjamin T. B., "Wave Formation in Laminar Flow Down An Inclined Plane," *J. Fluid Mech.*, **2**, 554, 1957.

Borgstedt H. U. and Mathews C. K., *Applied Chemistry of the Alkali Metals*,

Plenum Press, New York, p. 136, 1987.

Brooks J. N., "Erosion/Redeposition Analysis of the International Thermonuclear Experimental Reactor Divertor," *Fusion Technology*, **18**, 239, 1990.

Chambers A., Fitch R. K., Halliday B. S., *Basic Vacuum Technology*, p. 20, Adam Hilger, New York, 1989.

Chen T. F. and Davis J. R., "Disintegration of A Water Jet," *ASCE J. Hyd. Div.*, **90**, 182, 1964.

Cohen S., at Princeton Plasma Physics Lab, private communication, 1991.

Dolan T. J., *Fusion Research*, Pergamon Press, New York, 1982.

Downing J. N., "A Large-Area Pump Limiter Concept," in *Workshop on Innovative Technologies for Impurity Control*, Princeton Plasma Physics Lab, 1990.

Doyle B. L., "A Simple Theory for Maximum H Inventory and Release: A New Transport Parameter," *J. Nucl. Mater.*, **111 & 112**, 628, 1982.

Doyle B. L. and Brice D. K., "Steady State Hydrogen Transport in Solids Exposed to Fusion Reactor Plasmas, Part II: Application of Theory," *J. Nucl. Mater.*, **122/123**, 1523, 1984.

Dylla H. F. et al, "Conditioning of the Graphite Bumper Limiter for Enhanced Confinement Discharges in TFTR," *Nuclear Fusion*, **27**, 1221, 1987.

Erents S. K. and McCracken G. M., "Trapping and Re-emission of Fast Deuterium Ions From Nickel," *J. Phys.*, **D2**, 1397, 1969.

Finn P. A., "Lithium Test Module on ITER/TIBER: Engineering Design of the Tritium Recovery System," *Fusion Technology*, **14**, 798, 1988.

Galaktionowa N. A., *Hydrogen-Metal Systems Databook*, Ordentlich Press, Holon, Israel, 1980.

Galambos J. D., Peng Y. M., "Two Point Model for Divertor Transport," *J. Nucl. Mater.*, **121**, 205, 1984.

Harrison M. F. A. et al, "Plasma Characteristics and Gas Transport in the Single-null Poloidal Divertor of the International Tokamak Reactor," *Nuclear Technology/Fusion*, **3**, 432, 1983.

Hassanein A. M. and Smith D. L., "Evaluation of Liquid Metal Protection of A Limiter/Divertor in Fusion Reactors," Argonne National Lab Report, Conf-881031-66, 1988.

Hurd D. T., *Chemistry of the Hydrides*, John Wiley & Son, Inc., New York, p. 27, 1952.

"INTOR Tokamak Concept Innovation, Vienna", IAEA-TEC-DOC-373, 13-17 Jan. 1986.

ITER Physics R& D Reports (contribution by DIII-D team), Task PH07, Disruptions, ITER-TN-PH-9-7-PH07-U3, 1989.

Jensen R. V., Post D. E., and Jassby D. L., "Critical Impurity Concentrations for Power Multiplication in Beam-Heated Toroidal Fusion Reactors," *Nuclear Science and Engineering*, **65**, 282, 1978.

Keilhacker M. and Lackner K., "Divertors and Impurity Control, Where We Stand, Where We Have to Go," *J. Nucl. Mater.*, **111 & 112**, 370, 1982 a.

Keilhacker M. et al, "Plasma Boundary-Layer in Limiter and Divertor Tokamaks," *Physica Scripta*, **T2(SI)**, 443, 1982 b.

Kirillov I. R., Mazul I. V., Murav'ev E. V., "Alternative Concepts of the Divertor Targets," Working Materials to the ITER October 1990 Session, 1990.

LaBombard B., Plasma Fusion Center of MIT, private communication, 1991.

Lafferty D., *Scientific Foundations of Vacuum Technique*, p. 87, John Wiley and Sons, New York, 1962.

Langley R. A. et al, "Data Compendium for Plasma-Surface Interactions," *Nuclear Fusion*, Special Issue, 1984.

Lavrent'ev I. V., "Liquid Metal Blanket and Contact Devices for ITER/OTR." presented at 1989 USSR/US Exchange II.5 Topical Meeting on Comparison of Liquid Metal Blanket Approaches and Experiments, November 1989.

Mazul I. V.,"USSR Contribution to Session 14 of INTOR Workshop Phase II.A. (Part 3), Vienna", Leningrad, 1986.

McCracken G. M., Erents S. K., "Ion Burial in the Divertor of a Fusion Reactor," *B.N.E.S. Nuclear Fusion Reactor Conference*, at Culham Lab., September 1969.

McCracken G. M. and Stott P. E., "Plasma-Surface Interactions in Tokamaks", *Nuclear Fusion*, **19**, 889, 1979.

Morley N. B., Tillack M. S., Abdou M. A., "Analysis of Thin Film Liquid Metal

Protection of Fusion Reactor Limiter/Divertor Surfaces," *Fusion Technology*, **19**, 1765, 1991.

Murav'ev E. V., "Motion of Conductive Spherical Particles in A Nonuniform Magnetic Field," *Magnetohydrodynamics*, 255, 1981.

Murav'ev E. V., "Film MHD Flows Under Conditions of A Thermonuclear Reactor," *Magnetohydrodynamics*, **1**, 115, 1988.

Murav'ev E. V., "Liquid Metal Droplet Heat Removal System for ITER Divertor," Working Material to ITER June-October 1989 Session, Garching, Germany, 1989.

Nygren R. E. and Cohen S. A., *Workshop on Innovative Technologies for Impurity Control*, Princeton Plasma Physics Lab, 11-12 January 1990.

Nygren R. E. and Smith M. F., "Beryllium, An Alternative Material for Plasma-facing Components," *Fusion Tech.*, **19**, 2092, 1991.

Ohyabu N., DeBOO J. C., and A. Mahdavi, "Radiative Cooling in the Magnetically Expanded Boundary," *General Atomic Report*, GA-A16434, 1982.

Phinney R. E., "The Breakup of A Turbulent Liquid Jet in A Gaseous Atmosphere," *J. Fluid Mech.*, **679**, 1973.

Post D. E. et al, "ITER PHYSICS," ITER documentation series no. 21, *IAEA*, 1991.

Raeder J. et al, "ITER SAFETY," *IAEA*, ITER Documentation Series, No. 36, 1991.

Rayleigh F. R. S., "On the Instability of Jets," *Proc. London Math. Soc.*, **10**, 4, 1878.

Reed C. B., "An Assessment of Soviet Liquid Metal Technology in the Area of LMMHD for Fusion Reactors," *Argonne National Lab Report*, uncoded, June 1989.

Robson A. E. and Thonemann P. C., "An Arc Maintained on An Isolated Metal Plate Exposed to A Plasma," *Proc. Phys. Soc., London*, **73**, 508, 1959.

Roth J., "Physical Sputtering of Solids at Ion Bombardment," in *Physics of Plasma-Wall Interactions in Controlled Fusion*, p.351, Plenum Press, New York, 1984.

Roth J., Eckstein W., and Bohdansky J., "Beryllium Self-Sputtering: An Interpolation of Data for D, He, Ne and Ar," *J. Nucl. Mater.*, **165**, 199, 1989.

Sheka I. A. et al, *The Chemistry of Gallium*, Elsevier Publishing Company, New York, 1966.

Shercliff J. A., *A Textbook of Magnetohydrodynamics*, Pergamon Press, New York, 1965.

Sigmund P., in *Sputtering by Particle Bombardment I*, Behrisch R. eds., Springer-Verlag, p. 24, 1981.

Smith D. L. et al, Proc. 9th symp. on engineering problems of fusion research (Chicago, 1981), Institute of Electrical and Electronics Engineers, N. Y., p. 719, (1982).

Stangeby P. C., "The Plasma Sheath," in *Physics of Plasma-wall Interactions in Controlled Fusion*, p. 41, Plenum Press, New York, 1984.

Sze D. K., Argonne National Lab, private communication, 1991.

Tachon J., "Plasma Wall Interactions in Heated Plasmas," in *Physics of Plasma-Wall Interactions in Controlled Fusion*, p. 1005, Plenum Press, New York, 1984.

Vallet J. et al, "First Results on Disruptions in Tore Supra," presented at ITER Specialists' Meeting on Disruptions, Garching, Sept. 1989.

Vladimirov V. V., "Collective Phenomena in Plasma Interaction with Metal Surface," *1987 International Conference on Plasma Physics*, Sitenko A. G. eds., **1**, 169, World Scientific, Singapore, 1987.

Vodyanyuk V. O. et al, "Liquid-Metal Tokamak Limiter: Statement of the Problem and First Results," *Sov. J. Plasma Phys.*, **14**, 1988.

Wark I. W., "The Physical Chemistry of Flotation. I," *J. Phys. Chem.*, **37**, 623, 1933.

Werley K., "A Lithium-Droplet Beam (LDB) for Collecting Diverted Energy Particles in ITER," *Los Alamos Report*, LA-UR-89-962, 1989.

Yang T. F. et al, "A Compact Poloidal Divertor Reference Design for TNS," *Westinghouse Electric Corporation Report*, WFPS-TME-055, 1977.

Yih C. S., "Stability of Liquid Flow Down An Inclined Plane," *Phys. Fluids*, **6**, 321, 1963.

NOMENCLATURE

A_c = divertor channel area parallel to the magnetic field (m^{-3})

A_b = transparent area on the curtain divertor seen by the back-flowing neutral particles behind the curtain (m^2)

B_t = toroidal magnetic field (T)

b = width of the chute

b_w = thickness of the conducting chute side wall

C_b = implanted hydrogen concentration at the back side of liquid metal divertor plate

C_f = implanted hydrogen concentration at the plasma side of liquid metal divertor plate

C_p = implanted hydrogen concentration at stopping depth (m^{-3})

C_s = ion acoustic speed (m/s)

C_Y = coefficient in the Smith's sputter yield formula

$C_{1/2}$ = hydrogen concentration within lithium when

D = hydrogen diffusion coefficient within liquid metals (m^2/s)

D_m = the pumping duct diameter (10 ducts for each of the 4 divertors)

E_0 = incident charged particle energy

EL = reduced energy for the incident charged particle on the liquid metal vapor

E_{th} = physical sputter threshold energy of the divertor plate

f = pumping fraction

f_t = the transparency of the liquid Ga droplet curtain divertor

Fr^2 = $\frac{u_{in}^2}{gh_{in}}$ square of Froude number

$G(\vec{v})$ = ion probability density distribution function in velocity space after charge-exchange with recycled neutrals

h = thickness of liquid metal film

Ha = $Bb\sqrt{\frac{\sigma}{\rho\nu}}$ Hartmann number

h_{in} = inlet liquid metal film thickness on chute

$h(\vec{v})$ = electron probability density distribution function in velocity space after collision

J_{im} = implanted hydrogen ion particle flux $(m^{-2}s^{-1})$

J_{reem} = re-emitted hydrogen neutral particle flux $(m^{-2}s^{-1})$

K_b = hydrogen molecular recombination coefficient at back side of the liquid metal divertor plate (m^4/s)

K_f = hydrogen molecular recombination coefficient at the plasma side of the liquid metal divertor plate (m^4/s)

L = length of the chute in the flow direction

M^2 = $2Ha(\frac{h_{in}}{b})^2$

M_p = plasma fluid Mach number in front of the divertor plate

M_t = plasma fluid Mach number at the divertor throat

M_{p_c} = plasma fluid Mach number on the backside of the porous gallium droplet divertor curtain

n = plasma density $(n_e = n_i = n)$ (m^{-3})

n_p = plasma density near divertor plate (m^{-3})

n_t = plasma density at divertor throat (m^{-3})

n_0 = neutral number density (m^{-3})

$\overline{p}$ = neutral escape probability into divertor plenum

q = $u_{in}h_{in}$ constant liquid metal flow rate per unit chute width

Q_t = input parallel energy flux at the divertor throat (W/m^2)

Q_{back} = backscattered energy flux from the divertor plate (W/m^2)

r = T_i/T_e

r_c = critical radius of the hydrogen bubble with the liquid metal before eruption

r_e = secondary emission coefficient of the divertor plate

R = recycling coefficient, typically 0.99 for ITER reactor design

R_a = the stopping range of the implanting D+T particle flux in the liquid metal neutralizer

R_c = major radius of the divertor position (m)

Re = $\frac{q}{\nu}$ Reynolds number

R_N = ion particle reflection coefficient

R_{Ei} = ion energy reflection coefficient

R_{Ee} = electron energy reflection coefficient

S_n = plasma birth rate per unit volume per second through ionization of the recycled neutrals

t_l = distance between two down falling droplets of curtain divertor (m)

t_t = distance between toroidally adjacent droplets of curtain divertor (m)

T = temperature at which the pumping duct is maintained (i.e., room temperature)

T_0 = the temperature associated with the 5 eV neutrals

u = thermal conduction fraction

u_d = droplet speed of the curtain divertor (m/s)

u_{in} = inlet liquid metal film speed on chute

v = $(K_b/J_{im})^{1/2}C_b$

$\bar{v}_0$ = normalized phase velocity (wrt u_{in}) of the perturbation wave on the $\bar{k}^0$ order

$\bar{v}_1$ = normalized phase velocity (wrt u_{in}) of the perturbation wave on the $\bar{k}^1$ order

v_p = plasma speed near divertor plate (m/s)

v_t = plasma speed at divertor throat (m/s)

v_0 = the thermal velocity of the neutrals with Franck-Condon energy 5 eV

v_{p_c} = plasma fluid velocity on the back side of the curtain divertor (m/s)

W = $\frac{R_a(J_{im}K_f)^{\frac{1}{2}}}{D}$ a dimensionless parameter in hydrogen transport model

W_e = $(\sigma_s/\rho g h_{in})$ Weber number

x_0 = thickness of the liquid metal divertor plate

Y = physical sputter yield of the divertor plate

Γ = plasma particle flux $(= nv)$

$\delta_{i,e}$ = ion/electron energy transmission coefficients across the sheath

ϵ = energy carried by each backscattered neutral

ϵ_{in} = incident charged particle energy (eV)

ϵ_T = $\frac{\epsilon_{in}}{EL}$ Thomas-Fermi energy (dimensionless)

ϵ_w = $\sigma_w b_w/\sigma b$ wall conductance ratio

$< \sigma v >_q$ = rate coefficient for process q

χ_0 = Spitzer thermal conductivity coefficient $(W(eV)^{-7/2}m^{-1})$

$\eta(t)$ = hydrogen trapping efficiency of liquid metals at time t

γ = $(K_f/K_b)^{1/2}$

α = R_a/x_0

ϕ_f = floating potential of the divertor plate with respect to the edge plasma

σ = electrical conductivity of liquid metal $(1/\Omega - m)$

σ_s = surface tension of the liquid metal (N/m)

σ_w = electrical conductivity of the chute $(1/\Omega - m)$

n_{p_c} = plasma number density on the back side of the curtain divertor (m^{-3})

ν = kinematic viscosity

θ = chute inclination angle with respect to horizontal

Λ = $(2B/b)(\sigma\nu/\rho)^{1/2}$ a measure of the resistance to liquid metal film motion due to the developed Hartmann layers at chute side walls

Λ_ϵ = $2\epsilon B^2\sigma/\rho$ resistance to liquid metal film motion due to conducting chute effect

$\bar{\phi}$ = stream function from which the perturbed fluid velocities $\bar{u}_1$ and $\bar{v}_1$ are derived

<u>subscripts</u>

p = at plate condition

t = at throat condition

i = ion

e = electron

1 = of incident charged particle

2 = of bombarded divertor plate